Layered Nanocomposites For Neural Prosthetic Devices

by

Huanan Zhang

A dissertation submitted in partial fulfillment

of the requirement for the degree of

Doctor of Philosophy

(Chemical Engineering)

In The University of Michigan

2014

Doctoral Committee:

Professor Nicholas A. Kotov, Chair

Professor Cynthia A. Chestek

Professor Joerg Lahann

Professor Michael J. Solomon

Dedication

To my family, my mentors and my friends

ACKNOWLEDGMENTS

This dissertation would not have been possible without the support and contribution of many individuals. I would like to express my sincere gratitude to all of them.

First, I would like to express my appreciation to Professor Nicholas A. Kotov as my Ph.D advisor. He has been a tremendous mentor for me. He always supported and encouraged me for my intellectual curiosity. He always gave me enlightened feedback and suggestions when I faced challenges in my Ph.D study. His perseverance, knowledge, creativity, intelligence, and kindness will always inspire me in my future career.

I would also like to express my gratitude to my committee members, Professor Joerg Lahann, Professor Michael J. Solomon, and Professor Cynthia A. Chestek to discuss my research, offer me advice, and review my thesis.

I would like to thank the current and past member of the Kotov group for their friendship and scientific discussions. Especially, Dr. Jian Zhu, Dr. Christine Andres, Dr. Bongjun Yeom, Asish Misra and Terry Shyu have given me tremendous amount of scientific feedback and technical assistance. I would also like to thank my undergraduate students, Jimmy Shin, Betsy Gast, Samantha Rahmani for their assistance with my experiments.

I also deeply appreciate many collaborators I have worked with over the years. I would like to thank Dr. Takashi D. Yoshida Kozai and Paras Patel for their insightful advice and assistance. I would also like to thank Dr. Xueding Wang and Dr. Scott Swanson for mentoring me on the neuroimaging project.

Lastly, I would like to thank my parents for their unconditional love and care. I would also like to thank my friends for their companionship and support over the years.

TABLE OF CONTENTS

LIST OF FIGURES

electrochemical properties of the nanocomposite electrodes. Eight electrodes were tested for each size.

Figure 2.5 Schematic of the electrode/shuttle system

Figure 2.6 (A) Schematic of the photoacoustic microscopy (PAM) setup. (B) PAM image of two electrodes inserted into the brain. (C) MRI image of the implant in the y-z plane (Sagittal plane) (D) Zoom in MRI image of the y-z plane (Sagittal plane). (E) MRI image of the x-y plane (transverse plane). (F) Confocal microscopy of brain tissue and inserted electrode. Electrode was stained with FITC (green color) and cells were stained with toluidine blue (red color). (G) Cross-section SEM image of the electrode after brain insertion. There are three distinct layers as labeled in the graph.

Figure 2.7 (A) Harvested animal brain after recording experiment. (B) Low frequency signal recorded from the brain with the 10 μm wide nanocomposite electrode (100μm^2 recording site) (C) Power spectrum of the low frequency signal recording, signal peak at 5 Hz. . Blank recording experiment in phosphate buffered saline (PBS) (D) Local field potential recorded from PBS. (E) Power Spectrum of the recorded local field potential.

Figure 3.1. (A) AFM image of 15 bilayers of Au NP LBL film. (B) AFM image of 25 bilayers of CNT LBL film. (C) First bilayer of Au NP LBL film. (D) Ellipsometric thickness of Au NP LBL films for different number of bilayers.

Figure 3.2 SEM images of Au NP film and CNT film. (A, B) SEM images of Au NP film at different magnifications. (C) Cross-section image of Au NP film. (D, E) SEM images of CNT film at different magnifications. (F) Cross-section image of CNT film.

Figure 3.3 (A) Fabrication process of the microelectrodes with LBL films of Au NPs and CNTs (1) deposition and development of the positive photoresist; (2) E-beam deposition of the metal gold; (3) lift-off of the metal gold layer; (4) deposition and development of the positive photoresist (5) deposition of the LBL film (6) lift-off of LBL film and deposition/development of insulating photo-resist layer. (B) Optical image of Au NP LBL film coated electrode. (C) Optical image of CNT LBL film coated electrode.

Figure 3.4 EDAX spectra of CNT (A, C) and Au NPs (B, D) LBL films before (A, B) and after (C, D) microfabrication on silicon substrates.

Figure 3.6 Circuit analog of the impedance data

ABSTRACT

The motivation of this dissertation is developing neural prosthetic devices for chronic brain-computer interface. To maintain a chronically sustainable brain-computer interface, implantable devices should have minimal chronic inflammation, mechanically compliance with neural tissue, and long term durability under physiological conditions. Traditional neural prosthetic devices can seldom fulfill these requirements. This dissertation presents a nanocomposite approach to design the next generation neural prosthetic devices. The rationally designed nanocomposite can achieve the combination of the desired material properties for neural prosthetic devices, currently unattainable by traditional materials. In this dissertation, we first fabricated a mechanically compliant neural electrode from carbon nanotubes. The seamless integration of carbon nanotubes and polymer offered both mechanical flexibility and electrical conductivity for neural prosthetic devices. Then we explored other nanomaterials to design more exceptional nanocomposites. The gold nanoparticle nanocomposite developed in this research outperformed carbon nanotube composite in term of electrochemical performance. Additionally, we utilized the nanocomposite approach to design flexible insulation material for implantable electronic. By combining aramid nanofibers and epoxy resin, the composite material has outstanding adhesion and biocompatibility. Lastly, we designed a microfabrication process to combine gold nanoparticle composite and aramid

nanofiber composite to create tissue compliant and high performance neural electrodes.

Chapter 1

Introduction

1.1 Motivation

Neurological disorders and trauma injuries are among some of the most challenging medical problems we face today. These conditions often have devastating effects on patients and their familes. Neural prosthetic devices (NPDs) are a class of medical devices that have the potential to revolutionize the diagnosis and treatments of these neurological conditions. Generally, there are two classes of NPDs, one interacts with the central nerve system and the other communicates with the peripheral nerve system. Due to the large dissimilarity between the two biological systems, the design parameters for each class of NPDs are distinctive from each other.[1] For peripheral system , cochlear implants[2, 3] and pacemakers[4, 5] are highly developed and commercialized devices that utilized for restoring neural functionality

or regulating neural activity. For central nerve system, chronic deep brain stimulation[6] (DBS) demonstrated the ability to relieve symptoms of Parkinson's[7-9] and even Alzheimer's disease.[10] NPDs have also allowed patients of ayomyotrophic lateral sclerosis to regain motor control.[11] Recently, advances in brain-computer interface have received increasing attention due to the possibility of using multi-site recording NPD platforms for abstracting neural signals and controlling external devices.[12-15]

Despite the initial clinical success, most of the NPDs for central nerve system cannot retain a functional interface with neurons in the brain over a long period of time.[16-19] Chronic device failure is a complex problem related to inflammatory response, low electrochemical performance, charge transport resistance at tissue/electrode interface, and chemical stability of the electrode materials, etc.[20, 21] To resolve these issues, it would require innovative design approach to tailor the materials properties.

Nanomaterials offer possibilities to design the next generation NPDs[22]. Nanomaterials have been utilized in many area of biomedical research, exemplified by the tremendous amount of research on drug delivery[23, 24] and tissue engineering[24, 25]. By combining nanomaterials with other traditional materials, we can create nanocomposite with a combination of the desirable properties for NPDs to resolve aforementioned issues in neural interface applications.

This dissertation will mainly discuss the issues and possible solutions for NPDs interfacing with the cerebral cortex. First we will systematically evaluate the current issues with NPDs, particularly materials challenges and investigate possible nanocomposite materials to resolve these issues. We will also demonstrate that nanocomposite materials from layer-by-layer (LBL) assembly can be fabricated into functional devices.

Neural engineering is an interdisciplinary field, involves material science, biomedical engineering, biology, and chemistry etc. In this introductory chapter, we will first survey the development of current NPD designs, which include the manufacturing technology, shapes, sizes, materials, and layouts of current NPDs. Then we will examine more details related to the tissue responses of current NPD. We then follow up by reviewing the different material components in the NPDs, the methodologies to measure the material performance, and some current approaches in material design to improve performance and mitigate tissue response. Lastly, we will discuss on layer-by-layer (LbL) assembled nanocomposite as an excellent choice for the next generation NPDs.

1.2 Current Design of Neural Electrodes for Interfacing the Central Nervous System

Typically, there are two ways for NPDs to communicate with the nervous system, and this is through electrical stimulation and recording.[21] During electrical

stimulation, the neural electrode delivers charges to activate the targeted neurons, thus facilitating electrical signal transduction of the damaged or defective neural circuits. For example, muscle contraction can be stimulated externally by delivering electrical charges to the related nervous system.[26] Instead of electrical stimulation, electrical recording is the detection of the neural signal in the nervous system. In this system, the neural electrode serves as a passive device that extracts information from the neural system to the external devices. Neural recording technology has been the essential development for brain-computer interface, where electrodes can extract electrical signals from the brain to the external electronics, and the information can be decoded and understood for the control of external devices.[27]

Metal wires have been traditionally used as electrodes for fundamental and clinical neuroscience due to their excellent electrical conductivity. By using metal wires, Hodgkin and Huxley conducted experiments on a single neuronal fiber to understand signal transduction in neurons, which became the foundation of modern neuroscience.[28] The next revolution in neural electrode technology came from the advances in micromachining. Advanced micromachining technology allows for the fabrication of smaller wires and the assembly of microwire array. Today, one of the most common electrodes in clinical neuroscience are metal microwire arrays made of gold, platinum, tungsten, iridium, and stainless steel, which are coated with insulating materials to expose specific functional site.[16, 29, 30] For clinical applications, a large number of microwires arrange in an array to record from many neurons (Figure 1.1A). The typical dimension of the metal wires range from 50 μm to 200 μm in diameter.

These multielectrode arrays allow the researchers to acquire single neural signals from a large area of the motor cortex for precise prosthetic control, and eventually led to the demonstration of close-looped brain-computer interface in monkeys.[31]

The next revolution in NPDs also originated from another advanced manufacturing technique. Silicon based microfabrication technology has been the main driving force for advanced neural electrode design for the past 30 years.[32-34] It offers us unprecedented control over the size, shape, and spacing of the neural electrodes and functional sites[35]. In addition, one could also integrate other electronic components, such as signal processing units[36, 37] and wireless transmitting units[38] with the neural electrode to achieve other functionalities. The advancement in silicon microfabrication technology allows increasingly smaller electrodes and higher density electrode arrays, which further leads to better spatial resolution and signal-to-noise ratio. The electrode design includes planar configuration and 3D configuration. (Figure 1.1B and 1.1C). The original planar array was fabricated from a single thin sheet of silicon that is 100um wide and 15um thick with several recording sites along the shank.[35] The silicon 3D array was first developed at the University of Utah.[34] A block of silicon was etched,doped and heat-treated to create an array of microneedle-like structures, which is very similar to the microwire arrays.

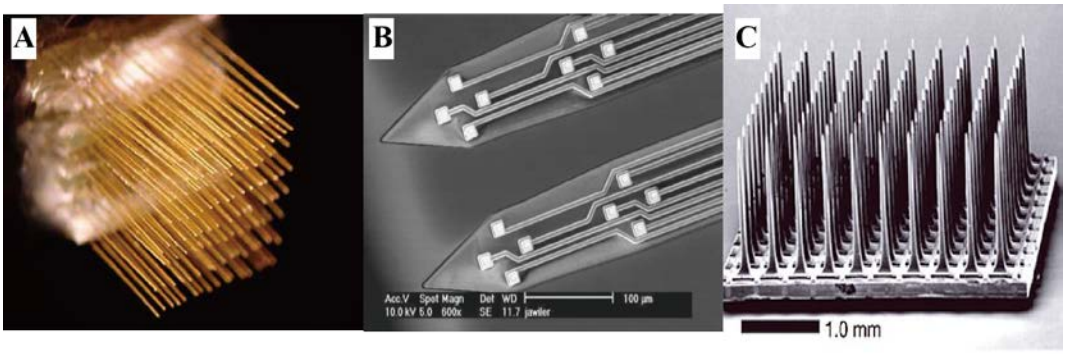

Figure 1.1 Common types of NPD devices (A) Metal microarray electrodes[16] (B) Planar silicon electrode[39] (C) 3D silicon electrode array[40]

1.3 Brain Tissue Response to Chronically Implanted Electrodes

1.3.1 The Invasive Nature of NPDs and Cellular Responses from Brain Tissue

Although significant progress has been made in the past several decades in terms of electrode design, the current devices are uable to retain their functionalities over a long period. The longest functional recording device sustained its functionality *in vivo* over a year.[41] This is still much farther from the targeted lifetime for chronic neural implants, which should retain their functionality over decades. Many studies suggest that one of the main causes for decreasing recording ability is the inflammatory response of the brain tissue toward implanted devices.[20] In order to design better chronic neural implants, we should first understand the cells responsible for the inflammatory response and the key elements that trigger inflammatory responses. This would allow us to design better electrodes to mitigate these issues.

Although the main functional cell type for communication in the brain is the neuron, it constitutes less than 25% of the total cells in the brain. Other majorities of the brain cells include glial cells (oligodendrocytes, astrocytes, and microglia) and vascular cells. Astrocytes and microglia are the cells responsible for inflammatory response and other regulatory functions of the brain.[42] Upon activation of astrocytes and microglia, both cells produce neural toxins and highly reactive chemical species, as a part of defense mechanism in the brain.[42]

From previous simulation and experiment studies, we can conclude that the electrodes need to be in close proximity to the targeted neuron for single unit recording (between 50 um to 100um).[43, 44] Therefore, all electrodes for single unit recording are invasive and inevitably create trauma injuries during initial insertion to the brain. Studies related to initial trauma injuries have shown that indeed, initial trauma injuries activate both astrocytes and microglia.[45, 46] However, as soon as six days after initial injury, the study observed a significant reduction of excess fluids and damages to cellular components.[47] After several week and months, the initial trauma wound will heal and no tracks of the initial electrode insertion can be observed.[48, 49] This indicates that the chronic existence of the electrodes contribute to the long-term inflammatory response, not the initial trauma injuries.

Long-term inflammatory responses in the brain around electrodes is exemplified by glial scar formations around the electrode after weeks of the implantation (Figure 1.2A).[50] The process is very similar to foreign body

encapsulation in other parts of the body. Evidently, the glial scar creates an insulating barrier between the electrodes and neurons, and prevents the successful recording of the neurons. An immune staining study revealed that the main component of the glial scar is reactive astrocytes, which further suggests that glial scar formation is closely related to inflammatory responses.[46, 51] time course studies also suggested that the reactive astrocyte extended several hundred of microns away from the electrodes.[46, 50] The exact mechanism and purpose of the glial scar are uncertain in the scientific community. However, for the last decade, much research has been devoted to designing optimal electrodes for minimizing the glial scar formation. Empirical studies have unveiled several possible routes of electrode design to reduce inflammation.

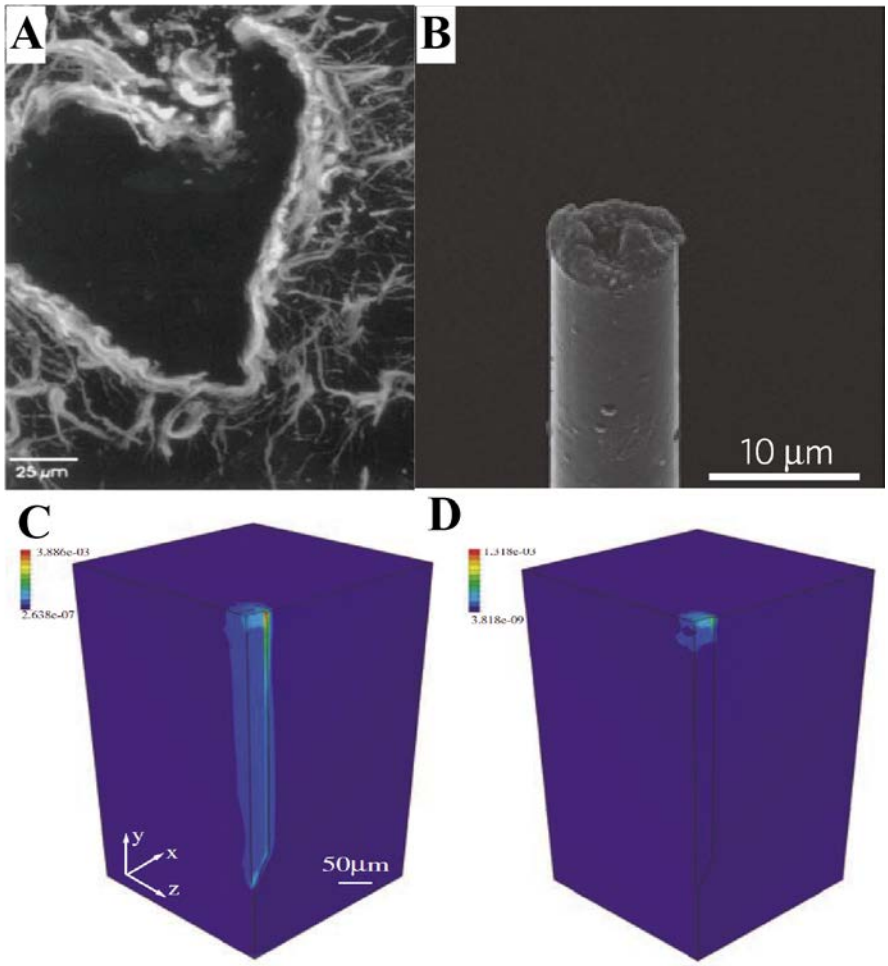

Figure 1.2 Tissue response to NPDs (A) Glial scar formation around the implanted silicon electrode[20] (B) ultrasmall carbon fiber electrode to minimize tissue response[52] (C) Magnitude of strain around implanted silicon electrode[53] (D) Magnitude of strain around implanted polyimide electrodes[53]

1.3.2 Electrode Size Related Inflammation Responses

Numerous studies have demonstrated that the physical characteristics, such as size, shape, and tip geometry etc. are very important for the degree of inflammation induced around the electrodes in the initial stage of the implantation. Here we will examine the case of the electrode size closely. Szarowki et al. conducted a similar

study with silicon-based electrodes. Time course histology study was conducted with electrodes of different sizes (100um by 15um and 200um by 130um).[46] No noticeable difference in the inflammatory response was observed after 12 weeks. Sanders et al. implanted single polymer fibers of different diameters *in vivo* to examine the effect of the fiber diameter on glial scar encapsulation and macrophage density. The results showed a reduction of the encapsulation diameter and the macrophage density as the polymer fibers became smaller.[54] Combining the results from the two studies, it suggests that the electrode size should be around 10 um in diameter or smaller in order to reduce the inflammatory response. In a recent study by Kozai et al., the researcher implanted a single carbon fiber electrode (8 um in diameter) into the brain.[55] (Figure1.2B) A significant reduction of activated astrocytes was observed when compared to silicon devices after six weeks of implantation. This result further demonstrated the importance of size reduction in electrode design. Initial impressions on size reduction strategies seem very feasible because silicon microfabrication technology has achieved submicron resolution today. However, as we significantly reduce the size of the electrodes, we encounter a fundamental material challenge: the drastic reduction in the electrochemical performance of the electrodes. Thus, advanced materials are required to overcome this challenge, which will be illustrated in detail later.

1.3.3 Mechanical Properties Related Inflammatory Responses

Besides the many studies related to electrode size, mechanical properties of neural electrodes were also investigated extensively to uncover their relationship with chronic inflammation. The initial hypothesis suggests inflammation and mechanical properties originated from the observation that there is a tremendous amount of mechanical mismatch at the electrode/brain tissue interface. For example, the Young's modulus of brain tissue is on the order of kPa range.[56] On the other hand, the Young's modulus of silicon and gold are 130 GPa and 78 GPa, respectively. Due to its soft and gel-like mechanical properties, the brain is constantly under dynamic motion, also called micromotion.[57] Due to large mechanic mismatch and constant micromotion, the implanted electrodes will consistently create damages to the brain tissue and the brain-blood barrier.[58] It will ultimately lead to chronic inflammation. Brain micromotions around stationary implants have been quantified in rodents.[57] The study showed that the displacement of the brain tissue largely correlates to the respiration rate of the animals. The displacement of 10 um to 60 um has been observed.[57] With the finite-element analysis method, researchers further understood the shear strain in the tissue/electrode interface.[59] The study showed that radial and tangential tethering forces could significantly elevate the strain at the electrode tip and the shearing along the electrode shank/tissue interface. A softer electrode than silicon would reduce the tissue strain by two orders of magnitude (Figure1.3C and D). These results suggest that more mechanically compliant electrodes are indeed beneficial toward a chronically functional neural interface. Nonetheless, most of the common electrical conductive materials have a large mechanical mismatch with brain

tissue. This imposes another material challenge to NPD design: engineering of flexible and soft electrical conductors.

1.4 Material Components for Neural Prosthetic Devices

Based on the previous studies on the tissue response of the chronic implants, we can conclude that the next generation of neural prosthetic devices requires a complete redesign of the material components. All neural electrodes primarily consist of two major material components: electrical components and insulation components. Both components are equally important in terms of electrode engineering as both components contribute to the mechanical properties of the electrode, the size of the electrodes, and the functionality of the electrodes. Electrical components are electrically conductive materials of the electrodes that sense the flux of the ions during neuron activation; and sequentially transduce the signal to the processing unit. The insulation components are typically dielectric materials that protect the electrical components of the electrodes and define the specific recording site of the electrodes. They are the materials have the most contact with the brain tissue.

1.4.1 Electrical Components of Neural Prosthetic Devices

As mentioned previously, electronically conductive materials like metal and doped silicon have been used as the electrical components of the electrodes for obvious reasons: electrical conductors are exceptional for transducing the electrical

field change to the signal-processing unit in solid-state electronics. An electrical conductor is an excellent choice if the main conduction mechanism is based on electrons. However, neural tissues mostly consist of fluids with ions instead of electrons. Ions are also the main signal transduction carrier for neurons. The electrodes operate at the interface between the ion transport to the electron transport, where the majority of the resistance comes from (Figure 13A).[21] Therefore, an excellent neural electrode is defined by its low resistance at the electrode/tissue interface, not the electrical conductivity.[60] The main parameter to characterize the resistance at the electrode/tissue interface is electrochemical impedance (Z). Electrochemical impedance is typically measured by electrochemical impedance spectroscopy. The measurement is conducted over a large frequency range (1 Hz to 10^5 Hz) with a very small amount of current. With the voltage response data, one can reconstruct a circuit model with basic electrical components, such as resistors and capacitors. It is a valuable tool to investigate the interfacial properties. In the electrode/tissue case, we can model the interface as a resistor and a capacitor in parallel with each other (Figure 1.3B). [61] The magnitude of the impedance in this case represents the overall resistance at the interface and the amount of charge stored at the interface. Impedance data is arguably the most important parameter to estimate the recording ability of the electrodes. A high impedance value normally correlates a decrease in electrode functionality; given no other malfunction occurs at the same time.[21]

Cyclic voltammetry (CV) is another common technique used to characterize electrodes. CV experiments typically scan a voltage window at a specific scan rate. The instrument will record voltage vs. current. From the CV scan, charge storage capacity (CSC) can be calculated. CSC indicates the interfacial capacitance at the electrode/tissue interface, which is also a component in the impedance measurement. In addition, the interfacial chemical reactions can also be probed by the CV experiments, which offer information on the chemical stability of the interface.[26]

Studies have shown that the Z and CSC of the metals diminish significantly as the size of the electrode reduces. Therefore, there is a major challenge to reducing electrode size while retaining electrode functionality. The Z and CSC value have a close relationship with the conductivity and the surface area of the electrodes. The perfect smooth surface of the metals could have contributed to the reduction of the Z and CSC value. Therefore, many materials have been developed to enhance the Z and CSC values, include Iridium oxide (IrO), conducting polymers, and carbon nanotubes (CNTs) etc.

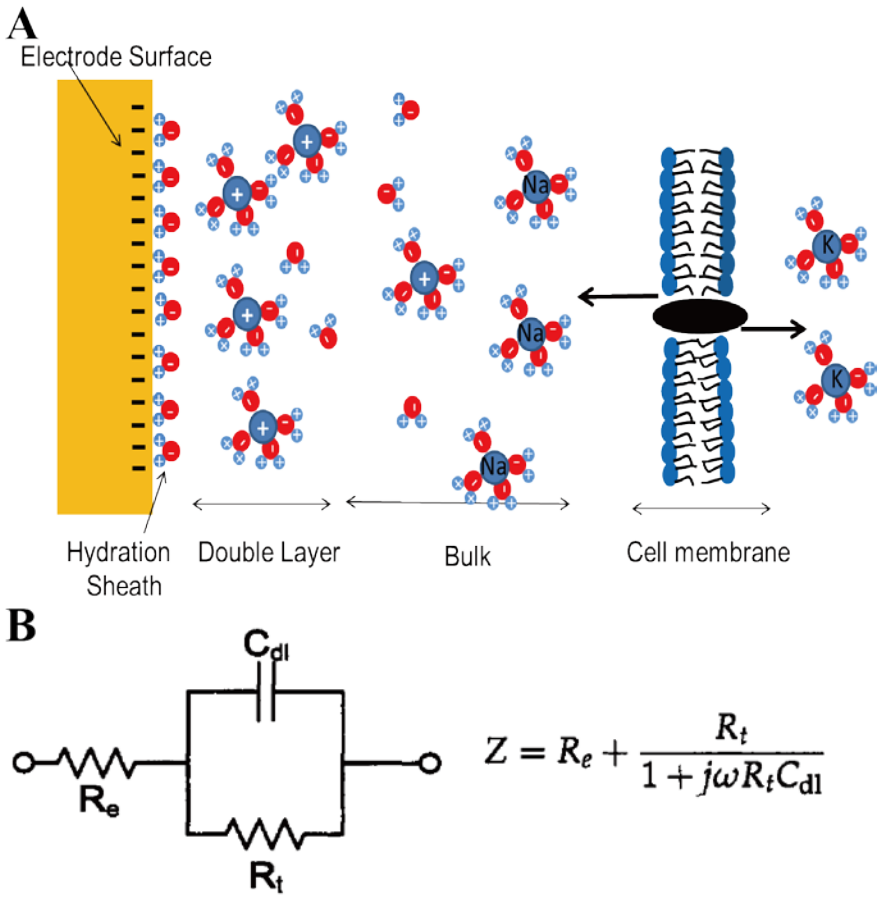

Figure 1.3 Mode of electrode/tissue interface (A)Simplified schematic of the electrode/tissue interface (B) Circuit analog of the electrode/tissue interface

1.4.2 Advanced Materials for Neural Interfacing

Metal oxides like IrO[62] were one of the first advanced materials that developed for neural electrodes. Typically, IrO films were formed by the electrochemical activation of Ir metal, so called AIROF. The activation process will create a high surface area and hydrated oxide film with improved Z and CSC value.[63] IrO can also be produced by reactive sputtering from iridium in oxidizing plasma.[64, 65]

However, delamination of IrO on metals have been observed in some studies. This will induce reduction of the CSC and Z over time and affect the efficiency of the devices.[63, 66, 67]

The common conducting polymers for NPDs are polypyrrole and polythiophene. Poly(3,4 - ethylenedixoythiophene) (PEDOT), which is a polythiophene based polymer, has attracted a lot of attention due to its biocompatibility and chemical stability.[68-70] There are several advantages of using conductive polymers in NPDs, including biocompatibility, limited toxic effects, and easy functionalization. Through electrochemical deposition, polymers can be localized in a specific site with controlled thickness. Conductive polymers may also act as delivery agents for biologically active molecules and drugs that could be released in response to electrical stimulation.[71-73]

Carbon nanotubes (CNTs) are another emerging material that have been investigated extensively over the past decade for neural interface applications.[74-79] Metallic CNTs are highly conductive and with a current density of two or three magnitudes higher than metals, like aluminum and copper.[80] Their high conductivity and unique 1D structure offer opportunities to engineer high performance neural interface devices. The biocompatibility of the CNT has been evaluated with different types of cell liness. Patterned CNTs can support neural adhesion and growth. Study has demonstrated that the CNT coating can improve the recording quality in

primates.[79] CNT based layer-by-layer composites have also been investigated for neural interface applications. They will be discussed in greater detail later.

Although great efforts have been invested in developing materials with improved Z and CSC, all of the aforementioned materials have been utilized as a coating for the tradition style of the electrodes. They can improve the electrochemical parameters of the smaller silicon or metal electrode. Nevertheless, they do not resolve the issue of mechanical mismatch. In order to resolve both issues (size and mechanical properties) simultaneously, other material design strategies are required to develop both flexible, electrically conductive, and high electrochemical performance materials. This issue will be addressed specifically in this dissertation.

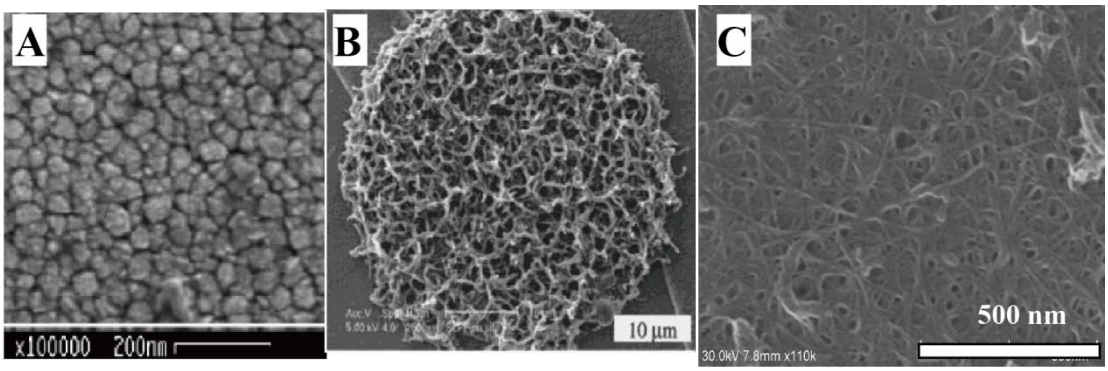

Figure 1.4 Advanced materials for neural interface (A) SEM image of sputtered IrO[81] (B) SEM image of electrodeposited PEDOT[70] (C) SEM image of LBL assembled CNT

1.4.3 Insulation Components for Neural Prosthetic Devices

Although insulation components of the NPDs do not participate in signal transduction, they still play a key role in device functionality. First, insulation components protect the electrical wires of the electrodes from corrosion and degradation of environmental chemicals. Second, insulation components also isolate individual electrodes in the array configuration to prevent short circuit and cross talk between electrodes. Third, insulating components define the specific recording sites of the electrode. The size of the recording site determines the quality and the specificity of neural recordings. All of these functionalities largely depend on the strong adhesion between the insulation components and the electrical components of the electrodes.[82, 83] Delamination of the insulating components will result in device failure. In silicon-based devices, silicon oxide and silicon nitride are commonly used as an insulating layer. However, the mechanical properties of the silicon oxide and silicon nitride also have a large mismatch with the brain tissue. Therefore, many polymeric materials were considered as an insulating layer. Teflon, polyester, epoxy basin, polyimide, and parylene have all been utilized in electrode fabrication.[20] Many flexible electrodes have been developed by combining polymer-based insulation materials with metals in order to reduce the mechanical mismatch at the electrode/tissue interface.[84-87] This strategy further improves the mechanical mismatch. However, it still relies on metals as the electrical components, which still has a large mechanical mismatch with brain tissue. Furthermore, many polymeric insulating layers have adhesion and delamination issues, due to the large surface energy difference between the insulation layer and the electrical layer. This

significantly hinders the long term functionality of the devices.[82] For instance, parylene is an emerging material as insulating layer for neural electrodes. It is FDA approved, chemically inert, and has low oxygen/water permeability. Nevertheless, the hydrophobic nature of the material leads to poor adhesion on metals and affect the device performance.[82]

The insulating components protect the electrical components of the electrode. Therefore, it has the most interaction with the surrounding brain tissue. Its surface properties and mechanical properties have directly effect on how the surrounding brain tissue reacts to the neural electrode. Nonetheless, this close interaction also offers opportunities to engineering the surface morphology and bioactivity of the insulating component, which could possibly lead to improved inflammatory responses. Using bioconjugation techniques, anti-inflammatory coating can be attached to electrode surfaces. Dexamethasone, an anti-inflammatory coating on neural electrodes showed a reduction in microglia and macrophages around the electrodes.[88, 89] Other anti-inflammatory drug coatings and neural adhesion coatings also resulted in a decreasing amount of activated astrocytes.[90-96] Together, these demonstrated the importance of modulating the surface bioactivity of insulating layers.

1.5 Layer-by-Layer (LbL) Assembled Nanocomposite and its Applications in Neural Interface

1.5.1 Fundamentals of LbL Assembly

Layer-by-layer (LbL) assembled thin film composites are tightly alternating monolayers of oppositely charged materials. The assembly is based on the principle of charge-interaction, which was originally introduced for polyelectrolytes by Decher et al. in 1992[97] independently of the earlier version of the same technique introduced by Iler.[98] All material surfaces have a net charge once immersed in the solution due to oxidation, hydrolysis, and preferential adsorption of ions.[99] When a negatively charged surface is immersed in a solution of positive polyelectrolyte, such as poly(dimethyldiallylammonium chloride) (PDDA), the positive electrolyte absorbs onto the surface. After rinsing with water to remove all of the loosely bound polyelectrolytes, the net charge on the surface would be positively charged from the remaining monolayer of polyelectrolyte. This surface could then be immersed in a solution with a negative polyelectrolyte and the net charge on the surface would reverse to negative. With a cyclic process, a multilayer film of alternating polyelectrolyte monolayers can be deposited on the surface with controlled structure and thickness. This process is not limited to polyelectrolytes. Many nanomaterials are dispersed in a solution with a net charge and could be used as a component in the LbL assembly process creating textures and nanostructures based on the nanomaterial. (Figure 1.5A) However, because of the multilayer nature of the LbL process, it allows a homogenous high loading of nanoscale components in the material matrix. With simple instruments, LbL assembly can also easily control coating thickness with nanoscale accuracy, incorporating different material components, and adjusting other relevant properties to achieve multiple functionalities. It is especially relevant for

biological applications where tailored mechanical, electrical, and biological properties are required. Therefore, LbL assembly is one of the most versatile methods for the preparation of nanostructures on various surfaces.

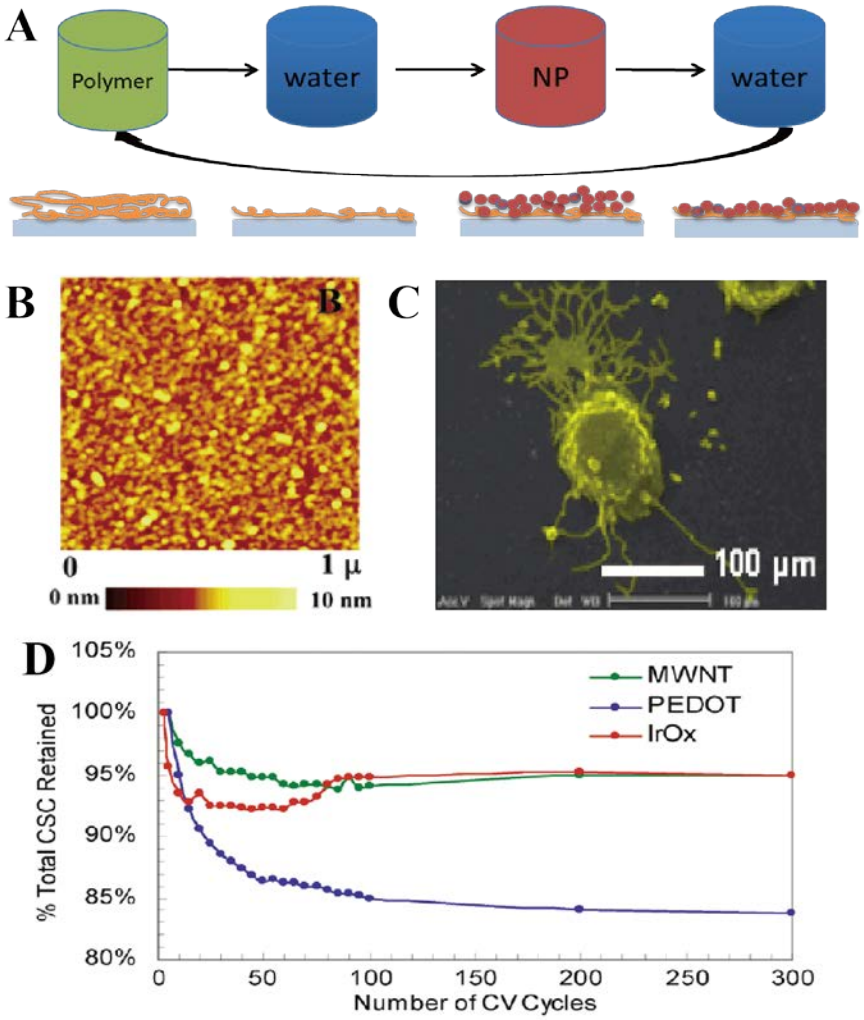

Figure 1.5 LBL assembled Nanostrutures and its applications (A) Illustration of the LBL deposition process (B) AFM image of LBL assembled HgTe nanoparticles with PDDA[100] (C) Neural stem cell differentiation on LBL assembled CNT film[75] (D) Stability test of different advanced neural interface materials[101]

1.5.2 The LbL Assembled Nanostructure for Neural Interface Applications

LbL-assembled nanostructures have many electrochemical advantages for neural stimulation by significantly increasing the electrochemical surface area of the stimulating electrode, thus enhancing the charge-transport capability.[21] Since LbL assembly is a bottom up fabrication method, it can be applied to a variety of electrode surfaces. The versatility of the LbL system offers opportunities to fabricate nanostructures with various nanocomposites of the most diverse composition and nanoscale organization incorporating metal nanoparticles (NPs), semiconductor NPs also known as quantum dots (QDs), and carbon nanotubes (CNTs). Selecting nanomaterials based on unique electrical and optical properties allow for flexibility in different modes of neural stimulation (direct current or photostimulation). Free standing film from LbL assembly cannot only retain excellent electrochemical properties, but also offers mechanical flexibility and high mechnical strength.[102] As mentioned previously, flexible neural electrodes are believed to play an important role in improving chronic *in vivo* tissue integration and reducing chronic inflammation. Recent work indicates that LbL-assembled film can be successfully patterned with lithography techniques opening new opportunities for designing neural electrodes[103]

Semiconductor nanoparticles or quantum dots (QDs) are a unique class of nanomaterials that are both optically and electrically active. Thus, photocurrents can be generated and utilized for neural stimulation by QDs. Moreover, due to the

quantum confinement effect, QDs can be tailored to respond to specific wavelengths of light when compared with bulk semiconductor materials. By combining both the photoelectric and quantum confinement effect, nanostructures can be engineered to stimulate neurons with specific spectral and electrical responses. By applying LbL assembly of mercury telluride (HgTe) nanoparticles and PDDA, polyelectrolyte-nanostructured films have been created with photostimulation capabilities.[104] The nanoscale features can be clearly observed under an atomic force microscopy (Figure 5.1B). Neuroblastoma/glioma hybrid cells (NG108) were successfully cultured and differentiated on the HgTe/PDDA film. While stimulating with a 532 nm laser, depolarization of the differentiated cells on HgTe/PDDA surface was observed, as measured with a standard patch-clamp setup.

CNTs have electrical properties, chemical stability and desirable dimensions to create nanostructures suitable for neural modulation. They have drawn much attention for neural interface applications over the past decade. LbL-assembled CNT nanostructures combine excellent electrical conductivity, biocompatibility, and strength to advance neural interface applications. A single-walled carbon nanotube (SWNT)/polyelectrolyte LbL film successfully supported and stimulated neuroblastoma/glioma hybrid cells (NG108)[75, 105]. In a systemic comparison study, LbL-assembled CNTs showed lower impedance and higher CSC compared to electrochemically deposited PEDOT and iridium oxide.[101] After 300 fast charging cycles, the CNT film retained 95% of its CSC without any surface cracks compared to PEDOT and iridium oxide, which showed minor or major cracks, respectively

(Figure 1.6D). The structural stability of the LbL CNT nanostructures is related to the homogenous high loading of CNT in the polymer matrix and the close interaction between each nanoscale layer. The homogenous loading of CNT in the polymer matrix enables the development of materials that are mechanically strong and flexible. Flexibility of the implantable neural electrode is believed to be a critical parameter for *in vivo* implantation, and prevents glial encapsulation of the nanostructure electrode site.

LbL-assembled nanostructures have demonstrated superior electrochemical performance over other materials. Nevertheless, next generation devices for neural stimulation require not only outstanding electrical performance, but also the ability to facilitate and promote cell growth. One of the advantages of LbL-assembled nanostructures is their ability to control composition and surface properties to promote cell growth and enhance biocompatibility, while maintaining electrical performance.

To illustrate the biocompatibility of the LbL-assembled nanostructure, previous work indicates that LbL-assembled SWNT nanostructures support the growth and differentiation of neural stem cells.[75] Unlike common model cell lines, neural stem cells are very sensitive to their culture environment and other physical and chemical signals. Here, the SWNT nanostructures did not alter the progression of neural stem cell differentiation. To demonstrate the versatility of the LbL method further, an extracellular matrix protein (laminin) was incorporated as a

complementary layer into the LbL film with SWNTs to create biocompatible nanostructures. By creating a laminin/SWNT composite, cell adhesion was enhanced through the adhesion-promoting nature of laminin and the nanoscale features of the SWNTs (Figure 1.6C).[106] This example demonstrated the successful differentiation of neural stem cells and the ability to stimulate the neural cells. It also illustrates how LbL-assembled nanostructures could be an excellent tool for the multifunctional engineering of nanostructures.

Other than improving cell adhesion and biocompatibility, one can further incorporate other functional components into the LbL-assembled nanostructures. With this approach, it is possible to prepare biologically active neural modulation devices.[107] To demonstrate this concept, a plasmid DNA layer was deposited on top of an electrically active LbL CNT nanostructure. The plasmid DNA on the CNT nanostructure transfected neural cells with greater efficiency compared to traditional solution-based methods.

1.6 Overview

Through close examination of the current NPD technology and tissue responses to the current NPDs, we can conclude that material innovation is necessary in order to develop the next generation of NPDs. There are several requirements for the new materials to be utilized in NPDs. In terms of the electrical component: (1) excellent electronic conductors for electrical signal transduction to the signal

processing unit (2) exceptional electrochemical performance for enhancing the ability to interface with ions in the physiological condition and minimizing the footprint of the devices and, (3) the mechanic properties should match with the brain tissue as close as possible to minimize any damages from mechanic strain. In terms of the insulation component: (1) superb adhesion properties to the electrical component of the NPD (2) chemically and biologically inert (3) low oxygen and water permeability and, (4) has the ability to be functionalized at the surface to modulate biological activities.

Nevertheless, it is very difficult for traditional materials to acquire all of the necessary requirements for neural interface applications. LbL assembled nanocomposites offer unique opportunities to revolutionize the field of NPDs. LbL assembled nanocomposites have demonstrated both mechanically flexible and excellent electrical conductivity in previous studies. Furthermore, the LbL assembly method offers us the ability to fine-tune the material properties for specific applications. We can modulate among mechanical properties, electrical properties, electrochemical performance, biocompatibility, etc.

This dissertation is focused on the design and fabrication of LbL nanocomposites for fully functional NPDs. Chapter 2 further examines the mechanical compliance of the electrodes with brain tissue and establishes the formal concept of tissue compliant neural electrodes. Then it demonstrates the tissue compliance of the LbL assembled CNT composite and its ability to be integrated into

fully functional devices *in vivo* . Chapter 3 looks beyond CNT as a fundamental nanomaterial for neural interface. It explores the ability of other nanomaterials to create nanocomposites with superior electrical and electrochemical properties to that of CNT. Chapter 4 examines the current insulation materials utilized in the field and proposes a nanocomposite approach to fabricate insulation materials with outstanding adhesion properties and the ability to be functionalized on the surface. Lastly, Chapter 5 will collectively utilize the innovations in nanocomposite research from previous chapters to design an all nanocomposite neural electrode.

1.7 References

1. Grill, W. M.; Norman, S. E.; Bellamkonda, R. V., Implanted Neural Interfaces: Biochallenges and Engineered Solutions. *Annual review of biomedical engineering* 2009, 11, 1-24.

2. Spelman, F. A., The Past, Present, and Future of Cochlear Prostheses. *Engineering in Medicine and Biology Magazine, IEEE* 1999, 18, 27-33.

3. Spelman, F. A., Cochlear Electrode Arrays: Past, Present and Future. *Audiology and Neurotology* 2006, 11, 77-85.

4. Bayer, G.; Borck, A. Implantable Stimulation Electrode with a Hyaluronate Coating for Increasing Tissue Compatibility. 2004-EP5550

2004112891, 20040521., 2004.

5. Libbus, I.; Moffitt, J. Stimulator for Auricular Branch of Vagus Nerve. 2004-5703

2006122675, 20041207., 2006.

6. Perlmutter, J. S.; Mink, J. W., Deep Brain Stimulation. *Annu. Rev. Neurosci.* 2006, 29, 229-257.

7. Chang, J.-Y., Brain Stimulation for Neurological and Psychiatric Disorders, Current Status and Future Direction. *J. Pharmacol. Exp. Ther*. 2004, 309, 1-7.

8. Benabid, A. L., Deep Brain Stimulation for Parkinson's Disease. *Current Opinion in Neurobiology* 2003, 13, 696-706.

9. Haberler, C.; Alesch, F.; Mazal, P. R.; Pilz, P.; Jellinger, K.; Pinter, M. M.; Hainfellner, J. A.; Budka, H., No Tissue Damage by Chronic Deep Brain Stimulation in Parkinson's Disease. *Annals of neurology* 2000, 48, 372-376.

10. Laxton, A. W.; Tang-Wai, D. F.; McAndrews, M. P.; Zumsteg, D.; Wennberg, R.; Keren, R.; Wherrett, J.; Naglie, G.; Hamani, C.; Smith, G. S.; Lozano, A. M., A Phase I Trial of Deep Brain Stimulation of Memory Circuits in Alzheimer's Disease. *Annals of neurology* 2010, 68, 521-34.

11. Hochberg, L. R.; Serruya, M. D.; Friehs, G. M.; Mukand, J. A.; Saleh, M.; Caplan, A. H.; Branner, A.; Chen, D.; Penn, R. D.; Donoghue, J. P., Neuronal Ensemble Control of Prosthetic Devices by a Human with Tetraplegia. *Nature* 2006, 442, 164-71.

12. Velliste, M.; Perel, S.; Spalding, M. C.; Whitford, A. S.; Schwartz, A. B., Cortical Control of a Prosthetic Arm for Self-Feeding. *Nature* 2008, 453, 1098-101.

13. Collinger, J. L.; Wodlinger, B.; Downey, J. E.; Wang, W.; Tyler-Kabara, E. C.; Weber, D. J.; McMorland, A. J.; Velliste, M.; Boninger, M. L.; Schwartz, A. B., High-Performance Neuroprosthetic Control by an Individual with Tetraplegia. *Lancet* 2013, 381, 557-64.

14. Nicolelis, M. A., Actions from Thoughts. *Nature* 2001, 409, 403-7.

15. Wessberg, J.; Stambaugh, C. R.; Kralik, J. D.; Beck, P. D.; Laubach, M.; Chapin, J. K.; Kim, J.; Biggs, S. J.; Srinivasan, M. A.; Nicolelis, M. A., Real-Time Prediction of Hand Trajectory by Ensembles of Cortical Neurons in Primates. *Nature* 2000, 408, 361-5.

16. Nicolelis, M. A.; Dimitrov, D.; Carmena, J. M.; Crist, R.; Lehew, G.; Kralik, J. D.; Wise, S. P., Chronic, Multisite, Multielectrode Recordings in Macaque Monkeys. *Proceedings of the National Academy of Sciences of the United States of America* 2003, 100, 11041-6.

17. Rousche, P. J.; Normann, R. A., Chronic Recording Capability of the Utah Intracortical Electrode Array in Cat Sensory Cortex. *Journal of neuroscience methods* 1998, 82, 1-15.

18. Suner, S.; Fellows, M. R.; Vargas-Irwin, C.; Nakata, G. K.; Donoghue, J. P., Reliability of Signals from a Chronically Implanted, Silicon-Based Electrode Array in Non-Human Primate Primary Motor Cortex. *IEEE transactions on neural systems and rehabilitation engineering : a publication of the IEEE Engineering in Medicine and Biology Society* 2005, 13, 524-41.

19. Vetter, R. J.; Williams, J. C.; Hetke, J. F.; Nunamaker, E. A.; Kipke, D. R., Chronic Neural Recording Using Silicon-Substrate Microelectrode Arrays Implanted in Cerebral Cortex. *Ieee T Bio-Med Eng* 2004, 51, 896-904.

20. Polikov, V. S.; Tresco, P. A.; Reichert, W. M., Response of Brain Tissue to Chronically Implanted Neural Electrodes. *J Neurosci Meth* 2005, 148, 1-18.

21. Cogan, S. F., Neural Stimulation and Recording Electrodes. *Annu. Rev. Biomed. Eng.* 2008, 10, 275-309.

22. Kotov, N. A.; Winter, J. O.; Clements, I. P.; Jan, E.; Timko, B. P.; Campidelli, S.; Pathak, S.; Mazzatenta, A.; Lieber, C. M.; Prato, M.; Bellamkonda, R. V.; Silva, G. A.; Kam, N. W. S.; Patolsky, F.; Ballerini, L., Nanomaterials for Neural Interfaces. *Adv Mater* 2009, 21, 3970-4004.

23. Douglas, S. J.; Davis, S. S.; Illum, L., Nanoparticles in Drug Delivery. *Critical reviews in therapeutic drug carrier systems* 1987, 3, 233-61.

24. Cho, K.; Wang, X.; Nie, S.; Chen, Z. G.; Shin, D. M., Therapeutic Nanoparticles for Drug Delivery in Cancer. *Clinical cancer research : an official journal of the American Association for Cancer Research* 2008, 14, 1310-6.

25. Goldberg, M.; Langer, R.; Jia, X., Nanostructured Materials for Applications in Drug Delivery and Tissue Engineering. *Journal of biomaterials science. Polymer edition* 2007, 18, 241-68.

26. Merrill, D. R.; Bikson, M.; Jefferys, J. G., Electrical Stimulation of Excitable Tissue: Design of Efficacious and Safe Protocols. *J Neurosci Methods* 2005, 141, 171-98.

27. Hatsopoulos, N. G.; Donoghue, J. P., The Science of Neural Interface Systems. *Annual review of neuroscience* 2009, 32, 249-66.

28. Hodgkin, A. L.; Huxley, A. F., Action Potentials Recorded from inside a Nerve Fibre. *Nature* 1939, 144, 710-711.

29. Williams, J. C.; Rennaker, R. L.; Kipke, D. R., Long-Term Neural Recording Characteristics of Wire Microelectrode Arrays Implanted in Cerebral Cortex. *Brain research. Brain research protocols* 1999, 4, 303-13.

30. Jackson, A.; Fetz, E. E., Compact Movable Microwire Array for Long-Term Chronic Unit Recording in Cerebral Cortex of Primates. *J Neurophysiol* 2007, 98, 3109-18.

31. Laubach, M.; Wessberg, J.; Nicolelis, M. A. L., Cortical Ensemble Activity Increasingly Predicts Behaviour Outcomes During Learning of a Motor Task. *Nature* 2000, 405, 567-571.

32. Wise, K. D.; Angell, J. B.; Starr, A., An Integrated-Circuit Approach to Extracellular Microelectrodes. *Biomedical Engineering, IEEE Transactions on* 1970, BME-17, 238-247.

33. Wise, K. D.; Angell, J. B., A Low-Capacitance Multielectrode Probe for Use in Extracellular Neurophysiology. *Biomedical Engineering, IEEE Transactions on* 1975, BME-22, 212-219.

34. Campbell, P. K.; Jones, K. E.; Huber, R. J.; Horch, K. W.; Normann, R. A., A Silicon-Based, Three-Dimensional Neural Interface: Manufacturing Processes for an

Intracortical Electrode Array. *IEEE transactions on bio-medical engineering* 1991, 38, 758-68.

35. Wise, K. D., Silicon Microsystems for Neuroscience and Neural Prostheses. *Engineering in Medicine and Biology Magazine, IEEE* 2005, 24, 22-29.

36. Changhyun, K.; Wise, K. D., A 64-Site Multishank Cmos Low-Profile Neural Stimulating Probe. *Solid-State Circuits, IEEE Journal of* 1996, 31, 1230-1238.

37. Najafi, K.; Wise, K. D., An Implantable Multielectrode Array with on-Chip Signal Processing. *Solid-State Circuits, IEEE Journal of* 1986, 21, 1035-1044.

38. Wise, K. D.; Anderson, D. J.; Hetke, J. F.; Kipke, D. R.; Najafi, K., Wireless Implantable Microsystems: High-Density Electronic Interfaces to the Nervous System. *Proc. IEEE.* 2004, 92, 76-97.

39. Finn, W. E.; LoPresti, P. G., *Handbook of Neuroprosthetic Methods*. CRC Press: Boca Raton, 2003; p 437 p.

40. Maynard, E. M.; Nordhausen, C. T.; Normann, R. A., The Utah Intracortical Electrode Array: A Recording Structure for Potential Brain-Computer Interfaces. *Electroencephalography and clinical neurophysiology* 1997, 102, 228-39.

41. Alivisatos, A. P.; Chun, M. Y.; Church, G. M.; Greenspan, R. J.; Roukes, M. L.; Yuste, R., The Brain Activity Map Project and the Challenge of Functional Connectomics. *Neuron* 2012, 74, 970-974.

42. Schultz, S. K., Principles of Neural Science, 4th Edition. *Am J Psychiat* 2001, 158, 662-662.

43. Eaton, K. P.; Henriquez, C. S., Confounded Spikes Generated by Synchrony within Neural Tissue Models. *Neurocomputing* 2005, 65, 851-857.

44. Henze, D. A.; Borhegyi, Z.; Csicsvari, J.; Mamiya, A.; Harris, K. D.; Buzsaki, G., Intracellular Features Predicted by Extracellular Recordings in the Hippocampus in Vivo. *J Neurophysiol* 2000, 84, 390-400.

45. Fujita, T.; Yoshimine, T.; Maruno, M.; Hayakawa, T., Cellular Dynamics of Macrophages and Microglial Cells in Reaction to Stab Wounds in Rat Cerebral Cortex. *Acta Neurochir* 1998, 140, 275-279.

46. Szarowski, D. H.; Andersen, M. D.; Retterer, S.; Spence, A. J.; Isaacson, M.; Craighead, H. G.; Turner, J. N.; Shain, W., Brain Responses to Micro-Machined Silicon Devices. *Brain research* 2003, 983, 23-35.

47. Stensaas, S. S.; Stensaas, L. J., The Reaction of the Cerebral Cortex to Chronically Implanted Plastic Needles. *Acta neuropathologica* 1976, 35, 187-203.

48. Yuen, T. G.; Agnew, W. F., Histological Evaluation of Polyesterimide-Insulated Gold Wires in Brain. *Biomaterials* 1995, 16, 951-6.

49. Biran, R.; Martin, D. C.; Tresco, P. A., The Brain Tissue Response to Implanted Silicon Microelectrode Arrays Is Increased When the Device Is Tethered to the Skull. *J. Biomed. Mater. Res., Part A* 2007, 82A, 169-178.

50. Turner, J. N.; Shain, W.; Szarowski, D. H.; Andersen, M.; Martins, S.; Isaacson, M.; Craighead, H., Cerebral Astrocyte Response to Micromachined Silicon Implants. *Experimental neurology* 1999, 156, 33-49.

51. Schmidt, E. M.; Bak, M. J.; McIntosh, J. S., Long-Term Chronic Recording from Cortical Neurons. *Experimental neurology* 1976, 52, 496-506.

52. Kozai, T. D.; Langhals, N. B.; Patel, P. R.; Deng, X.; Zhang, H.; Smith, K. L.; Lahann, J.; Kotov, N. A.; Kipke, D. R., Ultrasmall Implantable Composite Microelectrodes with Bioactive Surfaces for Chronic Neural Interfaces. *Nat Mater* 2012, 11, 1065-73.

53. Subbaroyan, J.; Martin David, C.; Kipke Daryl, R., A Finite-Element Model of the Mechanical Effects of Implantable Microelectrodes in the Cerebral Cortex. *J Neural Eng.* 2005, 2, 103-13.

54. Sanders, J. E.; Stiles, C. E.; Hayes, C. L., Tissue Response to Single-Polymer Fibers of Varying Diameters: Evaluation of Fibrous Encapsulation and Macrophage Density. *Journal of biomedical materials research* 2000, 52, 231-237.

55. Kozai, T. D. Y.; Langhals, N. B.; Patel, P. R.; Deng, X. P.; Zhang, H. N.; Smith, K. L.; Lahann, J.; Kotov, N. A.; Kipke, D. R., Ultrasmall Implantable Composite Microelectrodes with Bioactive Surfaces for Chronic Neural Interfaces. *Nature materials* 2012, 11, 1065-1073.

56. Miller, K.; Chinzei, K.; Orssengo, G.; Bednarz, P., Mechanical Properties of Brain Tissue in-Vivo: Experiment and Computer Simulation. *J Biomech* 2000, 33, 1369-76.

57. Gilletti, A.; Muthuswamy, J., Brain Micromotion around Implants in the Rodent Somatosensory Cortex. *Journal of neural engineering* 2006, 3, 189-95.

58. Lee, H.; Bellamkonda, R. V.; Sun, W.; Levenston, M. E., Biomechanical Analysis of Silicon Microelectrode-Induced Strain in the Brain. *Journal of neural engineering* 2005, 2, 81-9.

59. Subbaroyan, J.; Kipke, D. R., The Role of Flexible Polymer Interconnects in Chronic Tissue Response Induced by Intracortical Microelectrodes - a Modeling and an in Vivo Study. *2006 28th Annual International Conference of the IEEE Engineering in Medicine and Biology Society, Vols 1-15* 2006, 5782-5785.

60. Abidian, M. R.; Martin, D. C., Experimental and Theoretical Characterization of Implantable Neural Microelectrodes Modified with Conducting Polymer Nanotubes. *Biomaterials* 2008, 29, 1273-1283.

61. Orazem, M. E.; Tribollet, B., An Integrated Approach to Electrochemical Impedance Spectroscopy. *Electrochim Acta* 2008, 53, 7360-7366.

62. Cogan, S. F.; Ehrlich, J.; Plante, T. D.; Van Wagenen, R., Penetrating Microelectrode Arrays with Low-Impedance Sputtered Iridium Oxide Electrode Coatings. *Conference proceedings : ... Annual International Conference of the IEEE Engineering in Medicine and Biology Society. IEEE Engineering in Medicine and Biology Society. Conference* 2009, 2009, 7147-50.

63. Cogan, S. F.; Guzelian, A. A.; Agnew, W. F.; Yuen, T. G. H.; McCreery, D. B., Over-Pulsing Degrades Activated Iridium Oxide Films Used for Intracortical Neural Stimulation. *J Neurosci Meth* 2004, 137, 141-150.

64. Cogan, S. F.; Plante, T. D.; Ehrlich, J., Sputtered Iridium Oxide Films (Sirofs) for Low-Impedance Neural Stimulation and Recording Electrodes. *P Ann Int Ieee Embs* 2004, 26, 4153-4156.

65. Cogan, S. F.; Ehrlich, J.; Plante, T. D.; Smirnov, A.; Shire, D. B.; Gingerich, M.; Rizzo, J. F., Sputtered Iridium Oxide Films for Neural Stimulation Electrodes. *J Biomed Mater Res B* 2009, 89B, 353-361.

66. Cogan, S. F.; Troyk, P. R.; Ehrlich, J.; Plante, T. D., In Vitro Comparison of the Charge-Injection Limits of Activated Iridium Oxide (Airof) and Platinum-Iridium Microelectrodes. *Ieee T Bio-Med Eng* 2005, 52, 1612-1614.

67. Specht, H.; Kruger, F.; Wachter, H. J.; Keitel, O.; Leitold, C.; Frericks, M., Electrochemical Properties and Stability of Pvd Coatings for the Application in Cardiac and Neurological Stimulation. *Medical Device Materials III: Proceedings from the Materials & Processes for Medical Devices Conference 2005* 2006, 169-173.

68. Ludwig, K. A.; Uram, J. D.; Yang, J. Y.; Martin, D. C.; Kipke, D. R., Chronic Neural Recordings Using Silicon Microelectrode Arrays Electrochemically Deposited with a Poly(3,4-Ethylenedioxythiophene) (Pedot) Film. *Journal of neural engineering* 2006, 3, 59-70.

69. Venkatraman, S.; Hendricks, J.; King, Z. A.; Sereno, A. J.; Richardson-Burns, S.; Martin, D.; Carmena, J. M., In Vitro and in Vivo Evaluation of Pedot Microelectrodes for Neural Stimulation and Recording. *IEEE transactions on neural systems and rehabilitation engineering : a publication of the IEEE Engineering in Medicine and Biology Society* 2011, 19, 307-16.

70. Xiao, Y. H.; Cui, X. Y.; Martin, D. C., Electrochemical Polymerization and Properties of Pedot/S-Edot on Neural Microelectrode Arrays. *Journal of Electroanalytical Chemistry* 2004, 573, 43-48.

71. Yang, J.; Lipkin, K.; Martin, D. C., Electrochemical Fabrication of Conducting Polymer Poly(3,4-Ethylenedioxythiophene) (Pedot) Nanofibrils on Microfabricated Neural Prosthetic Devices. *Journal of biomaterials science. Polymer edition* 2007, 18, 1075-89.

72. Abidian, M. R.; Kim, D. H.; Martin, D. C., Conducting-Polymer Nanotubes for Controlled Drug Release. *Adv Mater* 2006, 18, 405-+.

73. Han, J.; Wang, L.; Guo, R., Facile Synthesis of Hierarchical Conducting Polymer Nanotubes Derived from Nanofibers and Their Application for Controlled Drug Release. *Macromol Rapid Comm* 2011, 32, 729-735.

74. Cui, D.; Tian, F.; Ozkan, C. S.; Wang, M.; Gao, H., Effect of Single Wall Carbon Nanotubes on Human Hek293 Cells. *Toxicol Lett* 2005, 155, 73-85.

75. Jan, E.; Kotov, N. A., Successful Differentiation of Mouse Neural Stem Cells on Layer-by-Layer Assembled Single-Walled Carbon Nanotube Composite. *Nano Lett.* 2007, 7, 1123-1128.

76. Lovat, V.; Pantarotto, D.; Lagostena, L.; Cacciari, B.; Grandolfo, M.; Righi, M.; Spalluto, G.; Prato, M.; Ballerini, L., Carbon Nanotube Substrates Boost Neuronal Electrical Signaling. *Nano Lett* 2005, 5, 1107-10.

77. Luo, X. L.; Weaver, C. L.; Zhou, D. D.; Greenberg, R.; Cui, X. Y. T., Highly Stable Carbon Nanotube Doped Poly(3,4-Ethylenedioxythiophene) for Chronic Neural Stimulation. *Biomaterials* 2011, 32, 5551-5557.

78. Wang, K.; Fishman, H. A.; Dai, H.; Harris, J. S., Neural Stimulation with a Carbon Nanotube Microelectrode Array. *Nano Lett.* 2006, 6, 2043-2048.

79. Keefer, E. W.; Botternan, B.; Romero, M. I.; Rossi, A. F.; Gross, G. W., Carbon Nanotube Coating Improves Neuronal Recordings. *Nat Nanotechnol* 2008, 3, 434-439.

80. Frank, S.; Poncharal, P.; Wang, Z. L.; Heer, W. A., Carbon Nanotube Quantum Resistors. *Science* 1998, 280, 1744-6.

81. Slavcheva, E.; Vitushinsky, R.; Mokwa, W.; Schnakenberg, U., Sputtered Iridium Oxide Films as Charge Injection Material for Functional Electrostimulation. *J Electrochem Soc* 2004, 151, E226-E237.

82. Seymour, J. P.; Elkasabi, Y. M.; Chen, H. Y.; Lahann, J.; Kipke, D. R., The Insulation Performance of Reactive Parylene Films in Implantable Electronic Devices. *Biomaterials* 2009, 30, 6158-67.

83. Kotzar, G.; Freas, M.; Abel, P.; Fleischman, A.; Roy, S.; Zorman, C.; Moran, J. M.; Melzak, J., Evaluation of Mems Materials of Construction for Implantable Medical Devices. *Biomaterials* 2002, 23, 2737-50.

84. Greenberg, R. J.; Talbot, N. H.; Neysmith, J.; Little, J. S.; Mech, B. V.; Humayun, M.; Guven, D.; Ripley, A. M. D. M. Flexible Circuit Electrode Array for Neural Stimulation. 2006-413689

2006259112, 20060428., 2006.

85. Hollenberg, B. A.; Richards, C. D.; Richards, R.; Bahr, D. F.; Rector, D. M., A Mems Fabricated Flexible Electrode Array for Recording Surface Field Potentials. *J Neurosci Methods* 2006, 153, 147-53.

86. Rousche, P. J.; Pellinen, D. S.; Pivin, D. P.; Williams, J. C.; Vetter, R. J.; Kipke, D. R., Flexible Polyimide-Based Intracortical Electrode Arrays with Bioactive Capability. *Ieee T Bio-Med Eng* 2001, 48, 361-371.

87. Stieglitz, T., Hansjorg, B., Schuettler, M. and Meyer, J.-U, Micromachined, Polyimide-Based Devices for Flexible Neural Interfaces. *Biomedical microdevices* 2000, 2, 283-294.

88. Shain, W.; Spataro, L.; Dilgen, J.; Haverstick, K.; Retterer, S.; Isaacson, M.; Saltzman, M.; Turner, J. N., Controlling Cellular Reactive Responses around Neural Prosthetic Devices Using Peripheral and Local Intervention Strategies. *IEEE Transactions on Neural Systems and Rehabilitation Engineering* 2003, 11, 186-188.

89. Zhong, Y.; Bellamkonda, R. V., Dexamethasone-Coated Neural Probes Elicit Attenuated Inflammatory Response and Neuronal Loss Compared to Uncoated Neural Probes. *Brain research* 2007, 1148, 15-27.

90. He, W.; McConnell, G. C.; Bellamkonda, R. V., Nanoscale Laminin Coating Modulates Cortical Scarring Response around Implanted Silicon Microelectrode Arrays. *J Neural Eng* 2006, 3, 316-326.

91. He, W.; McConnell, G. C.; Schneider, T. M.; Bellamkonda, R. V., A Novel Anti-Inflammatory Surface for Neural Electrodes. *Adv Mater* 2007, 19, 3529-+.

92. Zhong, Y.; Bellamkonda, R. V., Controlled Release of Anti-Inflammatory Agent Alpha-Msh from Neural Implants. *Journal of controlled release : official journal of the Controlled Release Society* 2005, 106, 309-18.

93. Chvatal, S. A.; Kim, Y. T.; Bratt-Leal, A. M.; Lee, H.; Bellamkonda, R. V., Spatial Distribution and Acute Anti-Inflammatory Effects of Methylprednisolone after Sustained Local Delivery to the Contused Spinal Cord. *Biomaterials* 2008, 29, 1967-75.

94. He, W.; McConnell, G. C.; Bellamkonda, R. V., Nanoscale Laminin Coating Modulates Cortical Scarring Response around Implanted Silicon Microelectrode Arrays. *Journal of neural engineering* 2006, 3, 316-26.

95. Winter, J. O.; Cogan, S. F.; Rizzo, J. F., 3rd, Neurotrophin-Eluting Hydrogel Coatings for Neural Stimulating Electrodes. *Journal of biomedical materials research. Part B, Applied biomaterials* 2007, 81, 551-63.

96. Cui, X.; Lee, V. A.; Raphael, Y.; Wiler, J. A.; Hetke, J. F.; Anderson, D. J.; Martin, D. C., Surface Modification of Neural Recording Electrodes with Conducting Polymer/Biomolecule Blends. *Journal of biomedical materials research* 2001, 56, 261-72.

97. Decher, G.; Hong, J. D.; Schmitt, J., Buildup of Ultrathin Multilayer Films by a Self-Assembly Process .3. Consecutively Alternating Adsorption of Anionic and Cationic Polyelectrolytes on Charged Surfaces. *Thin Solid Films* 1992, 210, 831-835.

98. Iler, R. K., Multilayers of Colloidal Particles. *J Colloid Interf Sci* 1966, 21, 569-&.

99. Tang, Z. Y.; Wang, Y.; Podsiadlo, P.; Kotov, N. A., Biomedical Applications of Layer-by-Layer Assembly: From Biomimetics to Tissue Engineering. *Adv Mater* 2006, 18, 3203-3224.

100. Pappas, T. C.; Wickramanyake, W. M. S.; Jan, E.; Motamedi, M.; Brodwick, M.; Kotov, N. A., Nanoscale Engineering of a Cellular Interface with Semiconductor Nanoparticle Films for Photoelectric Stimulation of Neurons. *Nano Lett* 2007, 7, 513-519.

101. Jan, E.; Hendricks, J. L.; Husaini, V.; Richardson-Burns, S. M.; Sereno, A.; Martin, D. C.; Kotov, N. A., Layered Carbon Nanotube-Polyelectrolyte Electrodes Outperform Traditional Neural Interface Materials. *Nano Lett* 2009, 9, 4012-8.

102. Shim, B. S.; Zhu, J.; Jan, E.; Critchley, K.; Ho, S.; Podsiadlo, P.; Sun, K.; Kotov, N. A., Multiparameter Structural Optimization of Single-Walled Carbon Nanotube Composites: Toward Record Strength, Stiffness, and Toughness. *Acs Nano* 2009, 3, 1711-1722.

103. Bai, Y. X.; Ho, S. S.; Kotov, N. A., Direct-Write Maskless Lithography of Lbl Nanocomposite Films and Its Prospects for Mems Technologies. *Nanoscale* 2012, 4, 4393-4398.

104. Pappas, T. C.; Wickramanyake, W. M. S.; Jan, E.; Motamedi, M.; Brodwick, M.; Kotov, N. A., Nanoscale Engineering of a Cellular Interface with Semiconductor Nanoparticle Films for Photoelectric Stimulation of Neurons. *Nano Lett.* 2007, 7, 513-519.

105. Gheith, M. K.; Pappas, T. C.; Liopo, A. V.; Sinani, V. A.; Shim, B. S.; Motamedi, M.; Wicksted, J. P.; Kotov, N. A., Stimulation of Neural Cells by Lateral Currents in Conductive Layer-by-Layer Films of Single-Walled Carbon Nanotubes. *Adv. Mater*. 2006, 18, 2975-2979.

106. Kam, N. W. S.; Jan, E.; Kotov, N. A., Electrical Stimulation of Neural Stem Cells Mediated by Humanized Carbon Nanotube Composite Made with Extracellular Matrix Protein. *Nano Lett.* 2009, 9, 273-278.

107. Jan, E.; Pereira, F. N.; Turner, D. L.; Kotov, N. A., In Situ Gene Transfection and Neuronal Programming on Electroconductive Nanocomposite to Reduce Inflammatory Response. *J Mater Chem* 2011, 21, 1109-1114.

Chapter 2

Tissue Compliant Neural Implants from Microfabricated Carbon Nanotube Multilayer Composite

2.1 Abstract

Current neural prosthetic devices (NPDs) induce chronic inflammation due to complex mechanical and biological reactions related, in part, to staggering discrepancies of mechanical properties with neural tissue. Relatively large size of the implants and traumas to blood-brain barrier contribute to inflammation reactions as well. Mitigation of these problems and the realization of long-term brain interface require a new generation of NPDs fabricated from flexible materials compliant with the brain tissue. However such materials will need to display hard-to-combine mechanical and electrical properties which are not available in the toolbox of classical neurotechnology. Moreover, these new materials will concomitantly demand

different methods of (a) device micromanufacturing and (b) surgical implantation in brains because currently used processes take advantage of high stiffness of the devices. Carbon nanotubes (CNTs) serve as a promising foundation for such materials because of their record mechanical and electrical properties but CNT-based tissue-compliant devices have not been realized yet. In this study, we formalize the mechanical requirements to tissue-compliant implants based on critical rupture strength of brain tissue and demonstrate that miniature CNT-based devices can satisfy these requirements. We fabricated them using MEMS-like technology and miniaturized them so that at least two dimensions of the electrodes would be comparable to brain tissue cells. The nanocomposite-based flexible neural electrodes were implanted into rat motor cortex using surgical procedure specifically designed for soft tissue-compliant implants. The post-surgery implant localization in motor cortex was successfully visualized with magnetic resonance and photoacoustic imaging. In vivo functionality was demonstrated by successful registration of the low frequency neural recording in live brain of anesthetized rats. Investigation of inflammation processes around these electrodes will be required to establish their prospects as long-term neural electrodes.

2.2 Introduction

Implantable neural prosthetic devices (NPDs) have attracted considerable attention in the field of fundamental and clinical neuroscience research. They can potentially

transform the treatments and diagnostics of many neurological disorders and traumas.[1-3] Furthermore, NPDs are the central technological component for advances towards a functional brain-computer interface.[4] Classical NPDs being used to record or stimulate neural cells, especially in the clinical setting, are typically noble metal microwires with diameters of 50 to 200 μm.[5, 6] Recently, improvements in neural electrodes research have been centered around silicon-based microfabricated devices[7-9] ENREF 7 that offers unprecedented control over the size, shape, and spacing of the neural electrodes. However, neither microwire nor silicon-based devices can reliably retain a NPD-tissue interface sustaining communication with neurons over long periods of time.[10] One of the distinctive reasons for the loss of device functionality is formation of the scar from glial cells around the brain implants due to chronic inflammation.[11, 12]

Initial electrode insertion inevitably damages the blood-brain barrier (BBB) by rupturing multiple blood vessels in the brain. Penetration of plasma proteins in brain tissue leads to activation of glial cells, initiation of immune response cascade[13] and onset of scarring. Minimization of the physical 'footprint' of NPDs to reduce the BBB damage is most significant at this stage.

With time, other physical characteristics of neural electrodes also contribute to inflammation that eventually becomes chronic. One could notice that there is a staggering mismatch between the mechanical properties of the electrodes and tissue.[14] The Young's modulus of silicon and metals – typical materials for most NPDs for brain -- span the range from 70 to 180 GPa. The stiffness values of typical implants

are about five orders of magnitude higher compare to the Young's modulus of the brain (1kPa). The mechanical behavior of NPDs in soft matrix depends on size/shape of implants; in the case when such behavior of NPD is non-compliant with the tissue, *i.e.* when the system does not behave as a single body and there is a discontinuity of deformations at the interfaces. Such strong discrepancy of stiffness of adjacent macroscopic objects cannot remain unnoticed by the cells especially over the long period of time because many cellular functions are reactive to mechanics of the cellular environment.[15] Importantly, the stiff inflexible nature of the implants generates mechanical stress around it due to the microscale motions between the stationary implant and the soft brain tissue in the course of everyday movements of the body. These mechanical stresses caused by the mismatch in mechanical properties are essential for consideration of glial scar formation because they are believed to (a) stimulate mechanoactivated signal transduction pathways of resident immune cells,[16] and (b) lead to chronic BBB disruption by continuous damage to surrounding blood vessels.[17] Soft and flexible neural electrodes are needed to reduce the mechanical mismatch and improve the mechanical compliance of NPDs in the brain tissue.

Besides the reduction of the initial damage and improvement of materials compliance between the material and the soft tissues, there is another reason to minimize the dimensions of NPDs. They need to be small with at least two physical dimensions comparable to that of cells (~10 μm) because crossing this threshold is expected to reduce the probability of macrophage adhesion,[18-20] while retaining the

ability to form tight junctions between neurons and electrodes should still be retained.[21] Indeed, carbon fiber NPDs with diameter of *ca* 8μm showed marked reduction of chronic inflammation,[20] while being able to record activity of single neurons in the motor cortex of rats. Carbon fiber, however, still has a Young's modulus as high as 250GPa to 500GPa and has suboptimal electrochemical parameters essential for neural implants (conductivity, impedance, charge storage capacity).

Additional aspect of NPDs related to the inflammation that needs to be addressed here is the implantation procedure. Typically it can be described as micromanipulator-controlled surgical insertion of the device in the tissue reaching a specific depth corresponding to the desirable cell layer in motor cortex or other part of the tissue. Notably the implant stiffness is quite helpful and enables its facile penetration into the soft brain tissue. Hard rod type of NPDs are being widely used, in part, for simplicity of the implantation procedure and the realization that this format of the device may not optimal for its subsequent functionality becomes apparent only after consideration of all the issues related to micromotions and stiffness mismatch described above. On the other hand, there is no alternative up to date to this surgical protocol because of the fundamental difficulties of penetrating of a soft object by an equally soft object.

Therefore, we can identify three interconnected NPD requirements for the reduction of the inflammatory reaction of the brain tissue and related improvement of their long-term functionality: (a) drastic improvement of electrode mechanical

compliance with the tissue; (b) reduction of its dimensions; and (c) development of new surgical procedure capable of implanting flexible compliant NPDs. These NPD requirements directly translate into material properties. Assuming that a device can be manufactured in some way and is non-toxic to neurons, the NPD inflammation problem can be restated in terms of materials properties as following: we need to have the material that simultaneously be (a) strong enough to enable miniaturization to dimensions <10μm; (b) flexible enough to be compliant with tissues at these dimensions; (c) conductive enough in the bulk to support sufficient amount of charge passing through it for neural recordings or stimulation; (d) forming cell-electrode interface with minimal charge transport losses, *i.e.* with minimal impedance, *Z*; (e) tough enough to withstand a variety of deformations during some kind of implantation procedure and over the period of its operations (several years) without deterioration of electrical and other properties. According to our calculations based on target resistance of 10 μm by 10 μm electrode (see Supplemental Information), the requirement for bulk conductivity is probably the easiest one to achieve and could be satisfied by many metals. However, the other requirements represent a challenge.

Many scientists realized the need for advanced materials to improve interfacial transport and minimize impedance between cells and NPDs. This led to tremendous amount of research effort resulting in the use of gold films,[22-24] iridium oxide (IrO_x),[25] conductive polymers,[9] carbon nanotubes (CNTs)[26] and other NPD materials. Nevertheless, these materials are utilized mostly as coating on electrodes made from other materials because the toughness and strength of free-standing thin

sheets of IrO_x and gold is not sufficient enough to with stand stresses typical for NPDs. Therefore, the most common approach for fabrication of the flexible electrodes is to combine polymer substrate with conductive coating.[22-24] However, such devices did not, so far, resolve the mechanical mismatch issue, which highlights the need for the new materials for neuroprosthetic devices. Their availability will help avoiding harsh compromises between the device functionality, its size, and the inflammatory side effect limiting the longevity.[27, 28]

A special analysis needs to be given to CNT-based NPDs because there have been an overwhelming number of studies demonstrating that CNTs have exceptional material properties for neural interfaces[29] in terms of electrochemical performance,[30] chemical stability,[31] and mechanical properties.[32] Surveying the state-of-the-art of NPDs from CNTs, we can see again how difficult it is to satisfy the materials requirements (a)-(e) discussed above and combine desirable mechanical and electrical properties. Typically, CNT layers were made on polymer substrates by using low-temperature growth conditions[33] as well as stamping techniques.[34, 35] These methods often give rise to weak adhesion between CNT and substrates. Consequently buckling behavior during device implantation lead to delamination and device failure.[36] Thus, electrodes with only with relatively large dimension of 200μm in width have been fabricated by these techniques.[34] Layer-by-layer assembled (LBL) of CNTs can improve adhesion and strength,[32] ENREF 37 flexibility, conductivity,[37, 38] and impedance[30] of the conductive films. Several *in vitro* studies reported successful neuron/neural stem cell culture and direct neural stimulation/recording on LBL-made

CNT substrates.[26, 39-44] *In vivo* studies with CNT-modified traditional electrodes showed that the CNT coatings enhanced the recording quality of NPDs[45] and improved the chemical stability of the recording materials.[31] Similarly to noble metals and IrO_x, all these studies describe the use of CNT ***coatings*** on traditional metal electrodes or on silicon substrates. A recent publication describes CNT-based fibers made by dielectrophoretic assembly.[46] This work can be an interesting example a free-standing CNT electrode, but, at the same time, these electrodes were implanted using standard hard-rod penetration technique and neural recordings were similar in quality to free-standing carbon fiber electrode.[20] The problems with the mismatch of mechanical properties, realization of the tissue-compliant devices, their miniaturization, development of a new surgical procedure for their implantation, and finding out the corresponding effects on long-term scarring, therefore, persists.

In this study, we aimed to demonstrate the fundamental possibility of flexible tissue-compliant devices with at least two dimensions comparable to those of cells, namely, thickness and width of the flexible strips. Since this goal led to necessary departure from the standard NPD protocols, we also searched for new methods to manufacture flexible substrate-less electrodes and their implantation in the brain tissue. We took advantage of mechanical and electrical properties of LBL-made CNT nanocomposites and manufactured flexible and compliant NPD devices. Their successful insertion in the motor cortex area could be visualized by two complementary imaging techniques, while their functionality was verified by registration of brain activity in this area in the form of low frequency neural recording.

2.3 Materials and Methods

High purity single wall carbon nanotubes (P2-SWNTs, >90% purity) were purchased from Carbon Solution, Inc. (Riverside, CA). Poly(vinyl alcohol) (PVA; MW 70k Fully hydrolyzed), poly(sodium 4-styrene-sulfonate) (PSS; MW 100k) were obtained from Sigma-Aldrich. All other chemicals were obtained from Sigma-Aldrich.

2.3.1 Layer-by-Layer Assembly of SWNT film

The LbL assembly was initially carried out on microscope glass slides cleaned in piranha solution (mixture of sulfuric acid and hydrogen peroxide DANGEROUS!) overnight and then thoroughly rinsed with deionized water prior to the use. SWNTs were first dispersed at 0.5 mg/mL in 2 mg/mL PSS (MW 100k) solution by ultrasonication. A 0.1 wt% PVA solution was prepared by dissolving the correct amount of PVA in near boiling water. For each deposition cycle, the electrode was immersed in the PVA solution for 2 min, following by rinsing with deionized water and drying with an air steam. Then the electrode was immersed in SWNT solution for 5 min, following by rinsing with deionized water and drying with an air jet. The cycle was repeated for 300 times by commercially available LBL deposition robot (NanoStrata Inc, Tallahassee, Florida).

2.3.2 Electrode Fabrication

800 nm parylene-C thin film was first deposited by chemical vapor deposition method (PDS 20350, SCS Equipment) on a clean glass slide. The first layer of parylene-C served as the bottom insulation layer for the electrodes. Then 1 m CNT:PSS/PVA nanocomposite was deposited on the parylene-C film using the layer-by-layer (LBL) assembly method. After the parylene-C and CNT composite deposition, positive photoresist (SPR220-3.0, Rohm Haas) was spin coated and exposed by the first mask on the CNT composite. After developing the photoresist, the entire substrate was treated by oxygen plasma (790 RIE, Plasma Therm) to pattern the base layer of the neural electrodes. After the oxygen plasma etching, a second layer of parylene-C was deposited onto the base layer. This served as the top insulation layer for the neural probe. Then positive photoresist was spin coated again and exposed by the second mask on top of the second layer of parylene-C. The entire substrate was etched slowly by oxygen plasma to avoid over-etch of the CNT composite. The second mask created the outline for the final electrode shape and opened the functional CNT site at the tip of the electrodes

2.3.2 Scanning Electron Microscopy (SEM)

SEM images were obtained using a FEI Nova Nanolab SEM at 10kV accelerating voltage. The samples were directly imaged with any additional coating.

2.3.3 Electrochemical Impedance Spectroscopy (EIS)

EIS was carried out on an Autolab PGSTAT 12; Frequency Response Analyzer software (EcoChemie, Utrecht, Netherlands) was used to record impedance spectra of the electrodes. A solution of 1x phosphate buffered saline (PBS, pH = 7) was used as an electrolyte in a three-electrode configuration. The working electrode was connected to the electrode site. The counter electrode was connected to a gold foil immersed in PBS, and an Ag/AgCl reference electrode was immersed in PBS. An AC sinusoidal signal of 25 mV in amplitude was used to record the impedance over a frequency range of 10−32000 Hz.

2.3.4 Cyclic Voltammetry (CV)

CV experiments were performed using an Autolab PGSTAT 12 instrument and General Purpose Electrochemical System software (EcoChemie, Utrecht, Netherlands) in a three-electrode configuration as described for EIS. For CV, a scan rate of 1 V/s was used and the potential on the working electrode was swept between −0.8 and 0.6 V. Three cycles were swept to ensure that the film had reached a stable state.

2.3.5 Craniotomy Preparation

Adult male Sprague-Dawley rats (Charles River Laboratories) 550-600 g were anesthetized with 2% isoflurane. The depth of anesthesia was observed by monitoring heart rate and blood oxygen saturation. The animal was placed into a stereotaxic frame and a 2 mm by 2 mm craniotomy was made over the motor cortex. Once the dura was incised and resected, the animal brain was ready for implantation.

2.3.6 *In-vivo* Electrophysiological Recording

Electrophysiological data were recorded using a TDT RX5 Pentusa Recording System (Tucker-Davis Technologies, Alachua, FL). These neuronal signals were acquired through a head-stage buffer amplifier to avoid signal loss in data transmission. Signals were sequentially filtered by an anti-aliasing filter in the preamplifier, digitized at a ~ 25-kHz sampling rate, and digitally band-pass filtered from 2 to 5000 Hz. Wideband signals were acquired to capture both spiking and local field potential (LFP) activity. Signals were continuously recorded in 10 minute intervals. Neural recording segments were analyzed offline using custom automated MATLAB (Mathworks Inc., MA) script. LFP power spectral density plots were created using a Hamming window for smoothing with a 32768-point fast Fourier transform (FFT).

2.3.7 Photoacoustic Microscopy

Photoacoustic Microscopy were carried out through a Nd:YAG laser (Spot-10-200-532, Elforlight Ltd, UK) working at 532 nm with a pulse duration of 2 ns and a repetition rate (PRR) of 0-50 KHz. The laser light was spatially filtered by an iris and then expanded to a parallel beam which was rastered over the tissue object by 2D Galvanometers. The intensity and the stability of the laser beam was monitored and calibrated by a photodiode (DET10A, Thorlabs, NJ). An achromatic lens with a focal length of 50 mm was used as the objective lens. Photoacoustic signals were detected by a calibrated needle hydrophone (HNC-1500, Onda, CA) with -10 dB bandwidth of 300 kHz-20 MHz. The distance between the hydrophone and the tissue was 5 mm, and the ultrasound coupling was through water. The detected photoacoustic signals, after a low noise amplifier (AH 2010, Onda, CA), was digitized by an A/D card (Razor CS14X2, GaGe, IL). The spatial resolution of this system was measured by imaging an USAF resolution template (T-20-P-TM, Applied Image Inc, NY). The lateral resolution was 5μm, determined by the optical focusing. The axial resolution of this system was 105 μm, which was limited by the central frequency and bandwidth of the hydrophone.

2.3.8 Magnetic Resonance Imaging

Magnetic Resonance Imaging was performed with a 3D gradient echo pulse sequence at 2.0 T (Varian Inc., Palo Alto, CA) using a home built RF coil. Data were

obtained with TR = 100 ms and TE = 10 ms, and with 100 microliter isotropic voxels. Following acquisition, the data were processed by scripts written in MATLAB (The Mathworks, Natick, MA).

2.3.8 Confocal Microscopy

Confoncal Microscopy was performed by a commercial Leica Inverted microscope. Nanocomposite electrode was stained by soaking in FITC-albumin solution (1mg/ml) for 1 hour. The brain tissue was stained by toluidine blue for an hour (5ml of 0.01mg/ml ethanol solution diluted in 45ml of 1% sodium chloride solution)

2.3 Results and Discussion

As a materials foundation of this project we decided to take LBL-assembled CNT composites that recommended themselves well in the form of coatings [26, 30] and in various tests for materials properties.[32, 38] Their toxicological profile,[47] strength, flexibility, conductivity, impedance, and toughness were demonstrate to be adequate to satisfy requirements (a)-(e) outlined above. Although we do not know enough about their long-term stability in tissues and biological effects on adjacent neuronal and other cells, these materials can be a starting point for this study. In this case, the first challenge on the way to small tissue-compliant LBL-made nanocomposite

electrodes is the development of microfabrication techniques adequate for miniature NPDs with dimensions of *ca* 10μm.

2.4.1 Microfabrication

We decided to address this challenge by integration the layered CNT nanocomposites with established microfabrication technologies that are similar to those used in MEMS devices from silicon. The composite neural electrodes were fabricated using a two-mask process with optical photolithography technique illustrated in Figure 2.1A. CNT nanocomposite was LBL-assembled from nanotubes wrapped with poly(sodium 4-styrene-sulfonate) (PSS) and poly(vinyl alcohol) (PVA) as partner polymer following the process described in our previous publications.[30, 32] As a substrate we used glass coated with parylene-C by chemical vapor deposition (CVD). Note that versatility of LBL assembly and its ability form strongly adhesive layers even on such an unlikely underlying material as hydrophobic parylene-C plays a significant role in the realization of this protocol. Equally important is the fact that photoresist can be uniformly spun on the LBL-made CNT composites. Both of these seemingly mundane attributes of the well-known process enable a wide spectrum of micromanufactured architectures and devices made from composite materials.

After developing the photoresist, the LBL-made CNT composite and the first parylene-C layer were etched by oxygen plasma. Compared to the manufacturing protocols for fabricating metal/polymer flexible electrodes used previously,[48] this

method eliminated the extraneous steps of lift-off and wet etch of metal that could introduce additional toxic components in the composite. The second layer of parylene-C was deposited after the plasma etching to serve as the top insulation layer for the neural probe. The entire substrate was etched slowly by oxygen plasma to avoid erosion into the CNT composite. This slow etching step served the purpose to expose the parylene covered CNT composite as the recording site. The electrodes were fabricated on glass substrate and were lifted-off with HF to produce free-standing devices after wire bonding to the circuit lead. HF is highly toxic to all cells but volatile. Within the limits of the current knowledge, it does not affect the biocompatibility of the nanocomposite devices.

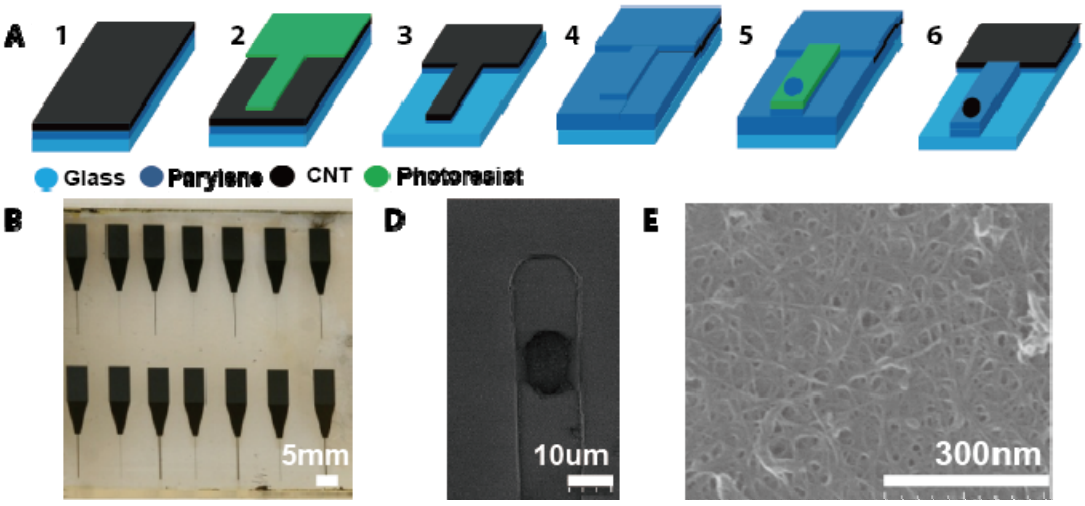

Figure 2.1 (A) Fabrication scheme of the nanocomposite electrodes combining LBL and MEMS-like microfabrication. (B) Optical image of composite electrodes on glass substrate.. (D) SEM image of a composite electrode with a width of 10 µm. The "window" in the parylene-C coating serves as the neural recording site and has high contrast with the insulating coating due to electrical conductivity of the LBL-made CNT composite. (E) The close-up SEM image of the CNT neural recording site on the 10 µm wide electrode.

The implantable part of the nanocomposite electrode had a thickness of 3µm along the shaft and 2µm at the recording site (Figure 2.2A and Figure 2.2B). These NPD dimensions are smaller than typical cell diameters and within the dimensional targets set for this project. Micron-scale thickness provided the electrodes with required flexibility. Deformations that might be considered to be extreme for NPD devices do not affect its integrity due to high strength and adhesion of CNT composite to parylene-C. The nanocomposite electrode can be flexed over 180 degrees without breaking (Figure 2.3A).

The width of the electrode is the second dimension that would be desirable to reduce to sizes comparable to that of a neuron. Here we varied the width of the electrodes in three sizes: 10 μm, 25 μm, and 50 μm. The smaller versions of the composite NPDs are within the desirable size range and dimensional targets for NPD width. They are equal or comparable to the smallest implantable electrodes reported so far.[20, 46,42] Our electrodes are also considerably smaller than other silicon based devices.[8, 9] The high strength of the LBL composites without high bending stiffness will facilitate their further miniaturization.

The recording sites were varied between three different sizes: *ca* 100 μm^2, *ca* 625 $\mu m^{2,}$ and *ca* 2500 μm^2 depending on the width of the implant. The examination of the micromanufactured NPDs by scanning electron microscopy (SEM, Figure 1D) showed that the 100 μm^2 recording site at the tip of the electrode was highly conductive while the rest of the composite electrode was insulated by parylene-C. A zoomed-in image of the recording site showed that the integrity of the CNT composite is preserved through the fabrication process (Figure 2.1E).

The total length of the shaft of the micromanufactured electrode was 5000 μm (Figure 2.1B) which is sufficient to reach deep structures within the rat and human brain. For comparison the depth of the motor cortex in rats is 5000 μm,[49] while the same for humans is 20000 μm.[49] Depending on the clinical purposes of neural recording, the smaller depths of implantation could be targeted and even preferred as well.

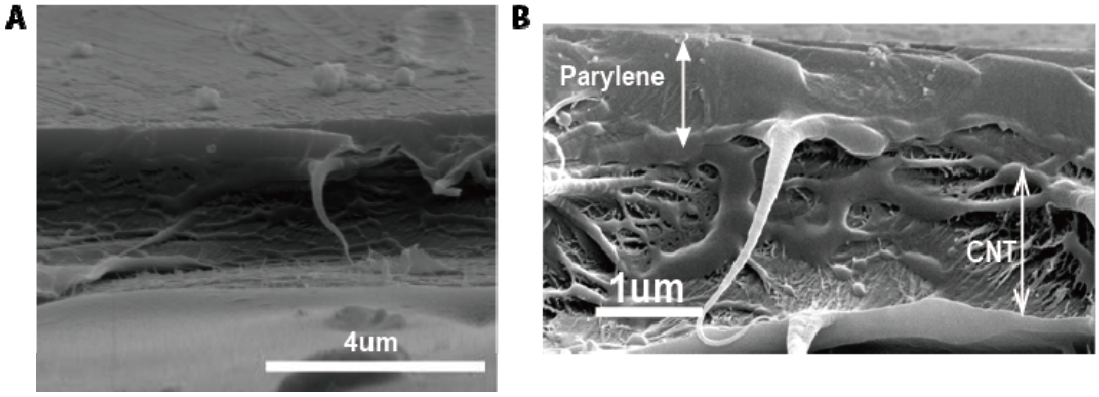

Figure 2.2 (A)) Cross-section SEM image of the fabricated electrodes (B) Cross-section SEM image of the recording site on the fabricated electrodes. Distortion of the parylene-C and composite layers of the device occurs due to sheer stress due to cutting. Note no delamination of CNT composite layer can be observed.

2.4.2 Mechanical properties

After successful fabrication of the electrodes, mechanical tests were performance to understand better the mechanical properties of the micromanufactured neural electrode (Figure 2.3B). The complete analysis will require detailed finite element modeling of the system consisting of hard beam with rectangular or cylindrical cross-section in a soft matrix for different deformations as well as for vibrations; which should be subject of a separate study. Here we suggest a simplified version of evaluation of mechanical compliance based on the mechanical damage of to the tissues upon deformations to the implant that is reflective of the chronic BBB trauma around implants. In this approximation, we describe mechanical compliance with brain tissue by comparing the pressure associated with buckling deformation of the implant and the critical rupture strength. If the pressure from the brain to buckle

the implant is higher than that the critical rupture strength of the brain tissue, this system will be considered to be non-compliant and *visa versa*.

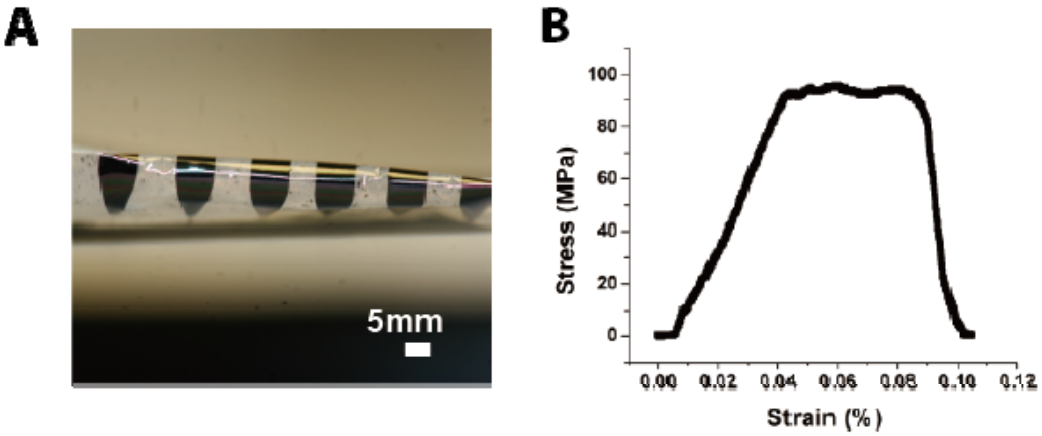

Figure 2.3 (A) Nanocomposite electrode on parylene-C sheet bent at 180 degrees to demonstrate flexibility (B) Tensile test of nanocomposite electrode, Young's modulus of 2.2GPa.

Buckling force for a simple beam is a function of geometry and Young's modulus. The specific expression for calculating buckling force of a rectangular beam is *Eq* (1).

$$F = \frac{\pi^2 EI}{(KL)^2} \qquad Eq\ (1).$$

where, E is the Young's Modulus, which is 2.2 GPa for the nanocomposite electrode (Figure 3B); I is the area moment of inertia, L is the unsupported length of the beam. K is the column effective length factor, which is 0.5 for two ends fixed beam. We can consider the nanocomposite electrode is a rectangular cross-sectional beam with

dimensions of 5000 μm in length, 3 μm in height, and 10 μm in width. For this geometry, the area moment of inertia is:

$$I = \frac{h^3 w}{12} \qquad Eq\ (2).$$

where, h is the height and w is the width. We can calculate the force required for the electrode to buckle and convert this force to a pressure term by considering the footprint of the electrodes. This pressure is about 2.37kPa for the nanocomposite electrode. It is smaller than the critical rupture strength of the brain tissue, which is typical about 3 kPa.[50] This indicated that the composite electrode will likely deform before inducing the brain tissue rupture.

2.4.3 Electrical Properties

We evaluated their electrochemical performance in terms of impedance (Z) and charge storage capacity (CSC) measured in a three-electrode electrochemical set-up and calculated with a custom MATLAB (Mathworks Inc., MA) script. The exact Z and CSC needed for NPDs depend on neural tissues and the type of the projected treatment/interface.[27] Nevertheless, the minimization of Z and maximization of CSC are the typical requirements for implantable electrodes as they reflect the key electrochemical parameters for their reduction of noise in NPDs, reduction of electrical damage to the tissue, and improving their long-term performance. Impedance was measured by a frequency response analyzer from 10 Hz to 32 kHz for

three different sizes of electrodes (Figure 2.4B). As expected, we observed a negative correlation between electrode size and impedance since larger electrodes have higher electrical conductance and larger surface area for the functional site. The impedance decreased as the voltage frequency increased which was also expected from the resistor/capacitor model for impedance[51] because Z is inversely related to frequency. Capacitive response dominates the impedance values at high frequencies. Importantly, we found that the impedance of the 10 μm wide electrode with 100 μm^2 site is *ca* 1 MOhm at 1 kHz, which is the physiological relevant spiking frequency of neurons. Z=1-2 MOhm is considered to be sufficiently low to allow for successful recordings of neural activity.[27]

Cyclic voltammetry (CV) curves obtained at a scan rate of 1 V/s from -0.6 V to 0.8 (Figure 2.4B) were used to calculate CSC. For quantitative comparison among electrodes of different sizes, we plotted the impedance magnitude of the electrodes at 1 kHz and the total amount of charge injected by integrating the area enclosed in the CV curve, which is a key parameter for neural stimulation (Figure 2.4B). The correlation between electrode size and electrochemical properties indicated the precision over the control of the electrode's functional site. We obtained CSC value of 1.55(±0.34) mC/cm^2 for 100μm^2 recording site and 2.57(±0.76) mC/cm^2 for 2500 μm^2 recording sites (Figure 2.4C).

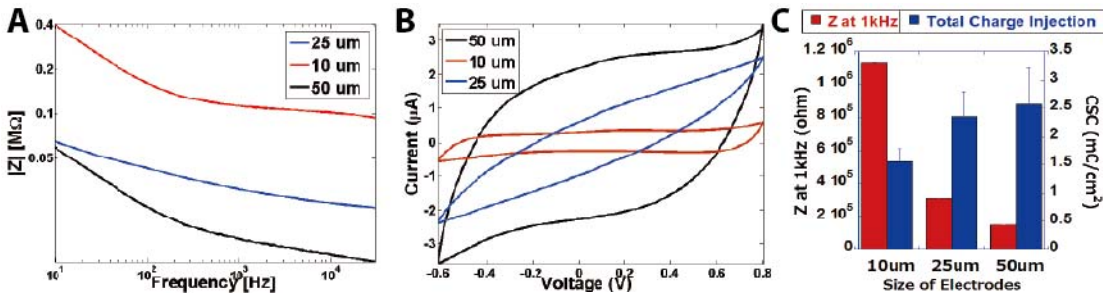

Figure 2.4(A) Typical impedance (Z) of the electrodes with different sizes of the functional sites. (B) Typical cyclic voltammetry of the electrodes with different sizes of the functional sites, sweep from 0.8 V to -0.6 V at 1V/s scan rate. (C) Cumulative electrochemical properties of the nanocomposite electrodes. Eight electrodes were tested for each size.

2.4.4 Surgical Procedure

As expected, the softness and flexibility of the nanocomposite electrodes became a major challenge during the electrode insertion into the brain. Several methods were considered to circumvent the problem of insertion of a soft rod into soft matrix, such as using water-soluble polymers to temporarily stiffen the probes[52] and chemically modified probe-releasing shuttles.[53] The use of stiffening materials was not favored by us because they (a) inherently restricts the size of implant to those that can perform as stiff rods, which limits the possibilities of microminiaturization; (b) remnants of the polymers can cause inflammation; and (c) if products of biodegradation of such polymers remain at the NPD-tissue interface, they will increase interfacial impedance *Z*.

To have a more universal technique to implant soft electrodes we tested the use of an electrode-releasing shuttle taking advantage of capillary interactions between the composite strip and a simple gold wire (60 μm in diameter, A-M Systems). The gold wire was used as received and was not modified or micromanufactured in any way except antiseptic treatment. A completed description of the procedure of electrode's insertion is given in Supplemental Information Figure S2. In brief, the flexible micromanufactured electrode and the metal wire were initially stored in dry ice for 1h+. Then the electrode and the needle were removed from the dry ice and kept at room temperature until water condensed on both objects. The composite electrode was placed on top of the wire adhering to it *via* condensed water. The entire assembly was stored in a refrigerator at -20°C until the implantation. After the craniotomy on the animal was performed, the electrode-on-the-needle assembly was removed from the refrigerator, transferred in a dry ice to the surgical table, and quickly inserted into the brain tissue by a micromanipulator. When the interfacial ice layer between the shuttle and electrode melted, the shuttle was removed while the flexible electrode remained inside the brain. This method allowed us to insert the produced flexible electrodes without any additional chemicals. We believe it can also be equally applicable to other tissue-compliant NPDs because the capillary forces are generic and temporary attachment of the flexible strips to gold needle can also be accomplished for other materials. The initial footprint of the shuttle can be further miniaturized by selecting/manufacturing smaller and thinner needles that can be potentially as thin as nanowires.

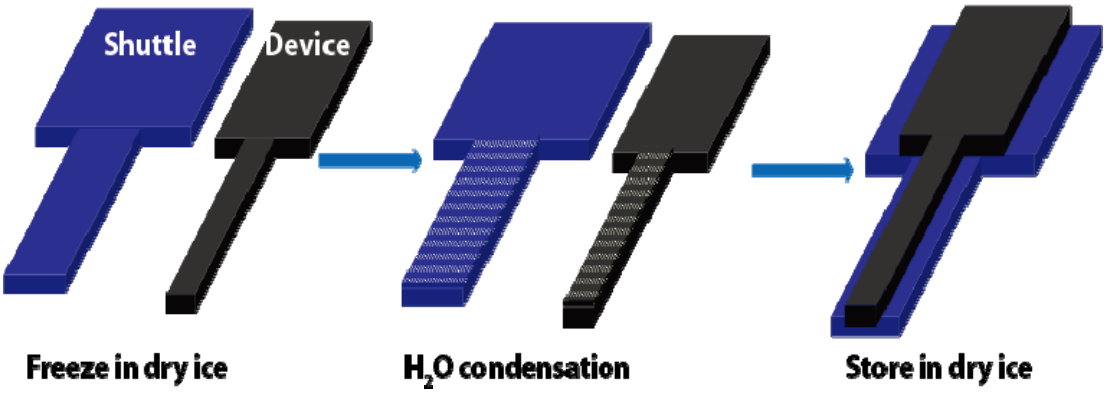

Figure 2.5 Schematic of the electrode/shuttle system

2.4.5 Post-Surgery Imaging:

To assess the integrity of the electrode after the implantation and its resilience to shear forces during the surgery we removed the electrode from the brain and investigated the cross-section of the implanted electrode by SEM (Figure 2.6G). As one can see the structure of the device was well-preserved and no obvious delamination of neither the top or the bottom layer of the electrode occurred.

Several aspects of implantation method need further evaluation for its routine usage, such as the effect of the initial low temperature condition to the brain, sterile condition of the ambient condensed water, and initial acute damage from the shuttle. Here we made a preliminary investigation of the tissue damage induced by the procedure using *ex vivo* by confocal microcopy. The electrode was green stained with FITC-albumin solution prior to implantation (Figure 2.6F); the brain tissue cells were stained with toluidine blue having red luminescence after electrode implantation. We

observed concentration of brain cells close to the electrode (bright red emission). The size of this particular area is similar to the shuttle footprint (50μm). It is possibly because the shuttle insertion damaged extracellular matrix and packed brain cells close together. Alternatively, the same imaging effect could be associate the cellular damage that is reflected by the higher permeability of the dye. The effect of this damage on the long-term functionality of the CNT electrodes and its relationship to chronic inflammation will require further study.

In addition to trauma assessment, non-invasive and label-free imaging techniques are important to guide/monitor the electrode through different stages of the implantation.[54] In this study, the state of the electrodes after implantation was examined by two imaging modalities *ex vivo*: photoacoustic microscopy (PAM)[55, 56] and magnetic resonance imaging (MRI).

Prior to electrode insertion and after craniotomy, one needs to closely assess the insertion site to identify the specific region of interest and also avoid blood vessels to minimize bleeding and BBB trauma. PAM combines optical and acoustic imaging techniques to produce images with excellent optical contrast and great imaging depth. This technique is based on the difference of optical absorption in tissues and was realized by rastering laser beam over the brain tissue (Figure 2.6A). It offers higher imaging depth than optical microscopy, and provides the same functional information. It would be an excellent tool for monitoring vasculature within the region of the interest. In our specific set up, photoacoustic signals were

detected by a calibrated needle hydrophone and the ultrasound coupling was through water. With this imaging system, we can achieve lateral resolution of 5 μm and axial resolution of 100 μm. Figure 3B represents a surface PAM image of the nanocomposite electrode inserted into the brain tissue. Due to its strong optical absorption, the nanocomposite electrodes displayed high contrast in the image, which is the portion of the electrode outside of the brain in Figure 2.6B. CNT electrodes were curved from the sided due to its flexibility, and we purposefully curved the particular part of the electrode to observe where the electrode was inserted. Moreover, we could also visualize the vasculature near the brain surface due to strong absorption of hemoglobin. Three dimensional mapping of the blood vessels is very important for electrode insertion. PAM makes possible high resolution mapping of blood vessels in the brain tissue which can be utilized to minimize their rupture during the insertion procedure, thus reducing insertion trauma, and preserving neurons. Combining electrodes with high PAM contrast image of blood vessels could be a valuable tool for clinical neural surgery.

Assessing implanted flexible neural electrodes inside of the brain during and after the surgery is also crucial,[54] especially after the electrodes were closely sealed inside of the skull. MRI is a well-established technique that can provide a non-invasive and high depth 3D image of the nanocomposite electrodes inside the brain.[57] It could monitor precisely the position of the electrode with the skull intact. We acquired MRI images after implanting the compliant electrode from nanotubes (Figure 2.6C-E). The high contrast of the nanocomposite electrode is attributed to

both the loss of water proton and disturbance of the magnetic field created by the nanocomposite electrodes. Figure 2.6C is the cross-sectional view of the electrodes in the brain. We observed the implant procedure successfully delivered the electrode into the brain without any kinks or curvature. Figure 2.6E is the zoomed out image of the cross-sectional view. We can identify the position of the electrode and the depth of the electrode in the brain to be 500 microns, which is the forelimb control area of the primary motor cortex in in rats.

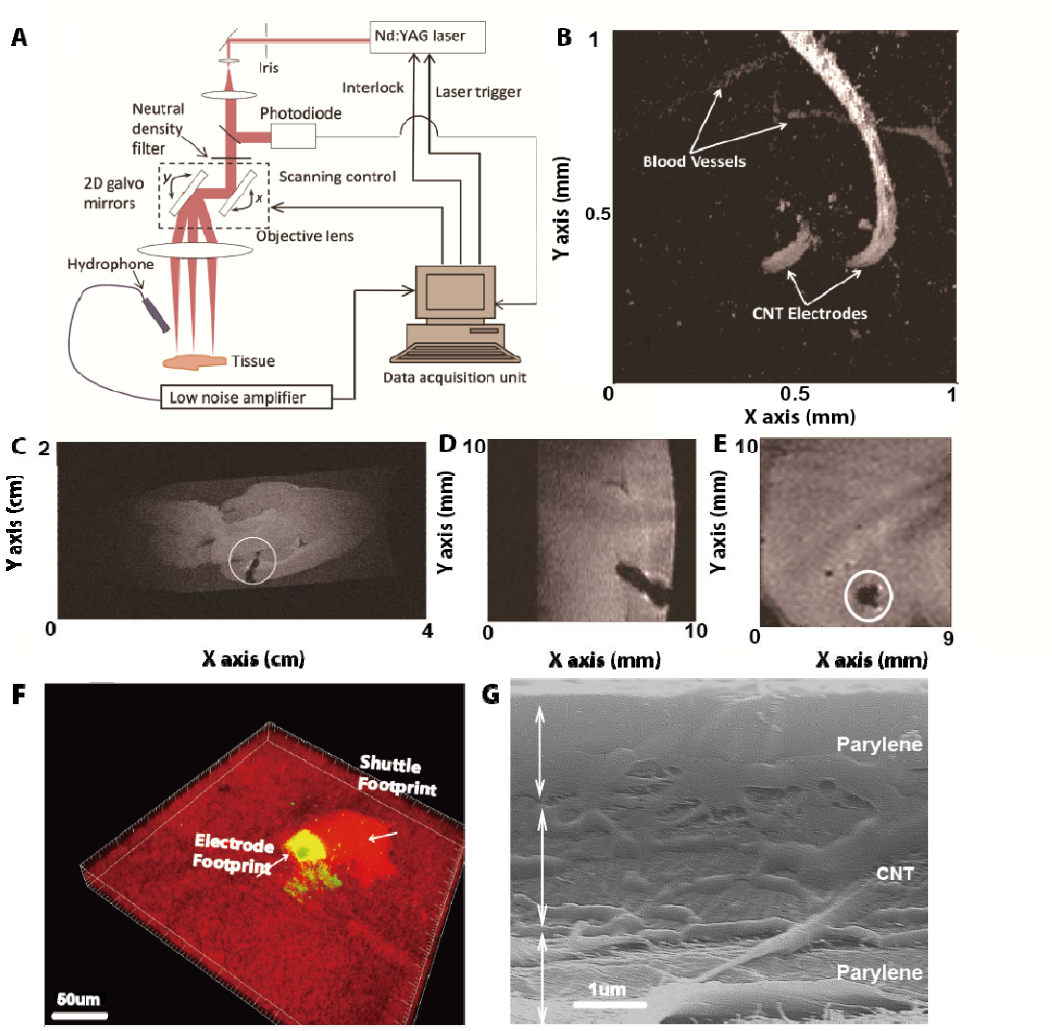

Figure 2.6 (A) Schematic of the photoacoustic microscopy (PAM) setup. (B) PAM image of two electrodes inserted into the brain. (C) MRI image of the implant in the y-z plane (Sagittal plane) (D) Zoom in MRI image of the y-z plane (Sagittal plane). (E) MRI image of the x-y plane (transverse plane). (F) Confocal microscopy of brain tissue and inserted electrode. Electrode was stained with FITC (green color) and cells were stained with toluidine blue (red color). (G) Cross-section SEM image of the electrode after brain insertion. There are three distinct layers as labeled in the graph.

2.4.6 Recording of Brain Activity

After verifying the electrochemical performance of the as-fabricated neural electrodes and carefully assessing the state of the neural electrodes, we conducted *in vivo* physiological recording experiments with rats. The typical procedure of the animal preparation and neural recording was published previously[9] and described in the methods section. The neural electrode with 100 um^2 recoding site was inserted into the brain tissue as described in the previous paragraph. Total of four electrodes were inserted into four different animals. Acute neural recording were conducted immediately after electrode insertion. Figure 2.7C is the typical low frequency neural signal recorded over time. The color spectrum of the plot represents the intensity of the local field potential. We observed high signal intensity (dark red color) in the low frequency range (0 to 20 Hz) over the entire recording session. We concluded that the electrode can record low frequency signal consistently over time. To further identify the peak of the low frequency neural recording, we accumulated the intensity data over time to generate a power spectrum. The power spectrum showed a peak around 5 Hz. We did not observe any intensity peak at 60 Hz, which is common for instrumental background noise. The power spectrum clearly demonstrated that the neural electrode could specifically identify the low frequency neural signal from instrumental noise (Figure 2.6C). Furthermore, we conducted a blank recording experiment in buffer saline solution. We observed much lower signal power compare to the recoding in the animal brain (Figure 2.7D and Figure 2.7E). We did not observe single neural spike in our recording session, it is possibly due to the effect of isoflurane.

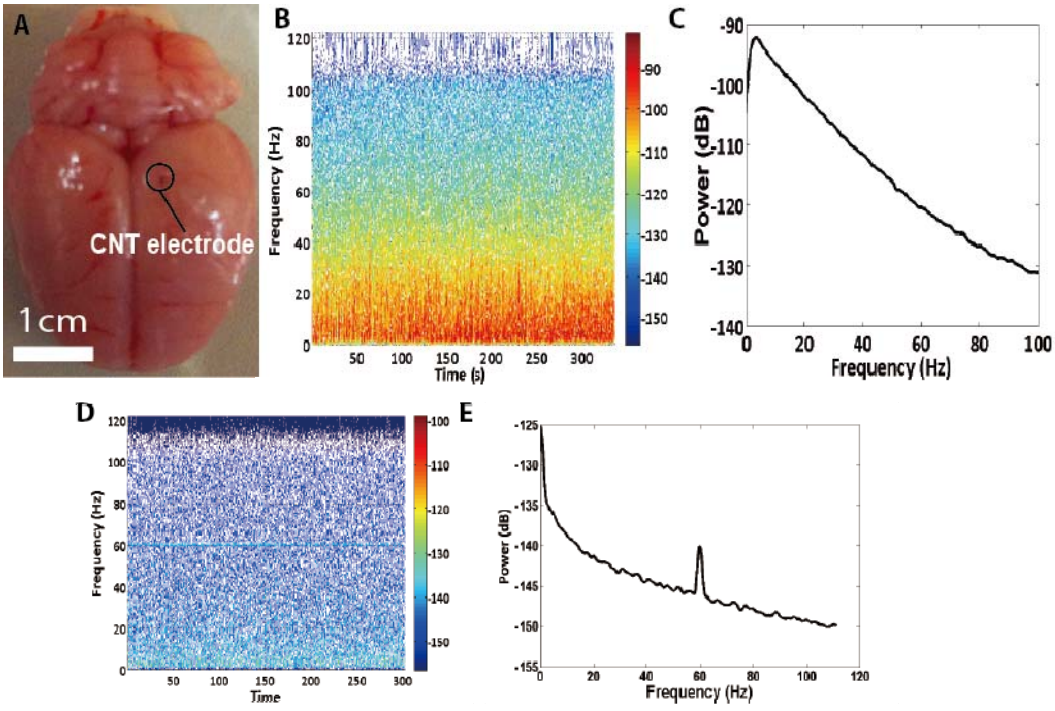

Figure 2.7 (A) Harvested animal brain after recording experiment. (B) Low frequency signal recorded from the brain with the 10 μm wide nanocomposite electrode (100μm^2 recording site) (C) Power spectrum of the low frequency signal recording, signal peak at 5 Hz. . Blank recording experiment in phosphate buffered saline (PBS) (D) Local field potential recorded from PBS. (E) Power Spectrum of the recorded local field potential.

2.4 Conclusions

This study demonstrated that LBL assembly is capable of producing tissue-compliant CNT nanocomposites with electrochemical performance particularly suitable for neuroprosthetic devices. These composites can be microfabricated with required precision using standard photolithography technology into flexible neural

electrodes. The footprint of the electrodes can be miniaturized to 10 μm in width with thicknesses as small as 3μm, which is smaller than any stiff[18] or flexible[50] functional NPDs reported to date. Importantly, the process of implantation of such compliant devices was developed which could be applied to other devices with similar mechanical properties made from nanocomposites or other suitable materials satisfying conditions discussed above. We want to point out that better understanding of the mechanics of the flexible brain implants in soft brain tissue, and therefore, requirements to the materials used in neuroprosthetic devices is needed.

The low frequency neural signal was recorded in the animal model to demonstrate the functionality of the neural electrodes. Further exploration of high frequency recordings of neuronal signals and microfabrication of arrays of tissue compliant electrodes is necessary. The ability to record high frequency signals and single neuronal activity require changes in electrode design. Similarly to our previous study,[18] the evaluation of the chronic tissue response should also be carried out to demonstrate the long-term functionality and inflammation response of this new class of nanocomposite electrodes. We also utilized both emerging and well established imaging modalities to examine these flexible neural electrodes in the brain. In aggregate the results reported in this paper takes us a step further to the use of nanocomposite-based neural prosthetics in clinical setting.

2.6 References

1. Kennedy, P. R.; Bakay, R. A., Restoration of Neural Output from a Paralyzed Patient by a Direct Brain Connection. *Neuroreport* 1998, 9, 1707-11.

2. Donoghue, J. P., Connecting Cortex to Machines: Recent Advances in Brain Interfaces. *Nat Neurosci* 2002, 5 Suppl, 1085-8.

3. Callaghan, J. C., Early Experiences in the Study and Development of an Artificial Electrical Pacemaker for Standstill of the Heart: View from 1949. *Pacing Clin Electrophysiol* 1980, 3, 618-9.

4. Hochberg, L. R.; Serruya, M. D.; Friehs, G. M.; Mukand, J. A.; Saleh, M.; Caplan, A. H.; Branner, A.; Chen, D.; Penn, R. D.; Donoghue, J. P., Neuronal Ensemble Control of Prosthetic Devices by a Human with Tetraplegia. *Nature* 2006, 442, 164-71.

5. Strumwasser, F., Long-Term Recording' from Single Neurons in Brain of Unrestrained Mammals. *Science* 1958, 127, 469-70.

6. Ellis, T. L.; Stevens, A., Deep Brain Stimulation for Medically Refractory Epilepsy. *Neurosurgical focus* 2008, 25, E11.

7. Rousche, P. J.; Normann, R. A., Chronic Recording Capability of the Utah Intracortical Electrode Array in Cat Sensory Cortex. *Journal of neuroscience methods* 1998, 82, 1-15.

8. Campbell, P. K.; Jones, K. E.; Huber, R. J.; Horch, K. W.; Normann, R. A., A Silicon-Based, Three-Dimensional Neural Interface: Manufacturing Processes for an

Intracortical Electrode Array. *IEEE transactions on bio-medical engineering* 1991, 38, 758-68.

9. Ludwig, K. A.; Uram, J. D.; Yang, J.; Martin, D. C.; Kipke, D. R., Chronic Neural Recordings Using Silicon Microelectrode Arrays Electrochemically Deposited with a Poly(3,4-Ethylenedioxythiophene) (Pedot) Film. *J Neural Eng* 2006, 3, 59-70.

10. Ward, M. P.; Rajdev, P.; Ellison, C.; Irazoqui, P. P., Toward a Comparison of Microelectrodes for Acute and Chronic Recordings. *Brain research* 2009, 1282, 183-200.

11. Biran, R.; Martin, D. C.; Tresco, P. A., Neuronal Cell Loss Accompanies the Brain Tissue Response to Chronically Implanted Silicon Microelectrode Arrays. *Exp Neurol* 2005, 195, 115-26.

12. Edell, D. J.; Toi, V. V.; McNeil, V. M.; Clark, L. D., Factors Influencing the Biocompatibility of Insertable Silicon Microshafts in Cerebral Cortex. *IEEE transactions on bio-medical engineering* 1992, 39, 635-43.

13. Fawcett, J. W.; Asher, R. A., The Glial Scar and Central Nervous System Repair. *Brain research bulletin* 1999, 49, 377-91.

14. Subbaroyan, J.; Martin, D. C.; Kipke, D. R., A Finite-Element Model of the Mechanical Effects of Implantable Microelectrodes in the Cerebral Cortex. *J Neural Eng* 2005, 2, 103-13.

15. Discher, D. E.; Janmey, P.; Wang, Y.-l., Tissue Cells Feel and Respond to the Stiffness of Their Substrate. *Science* 2005, 310, 1139-1143.

16. Keohan, F.; Wei, X. F.; Wongsarnpigoon, A.; Lazaro, E.; Darga, J. E.; Grill, W. M., Fabrication and Evaluation of Conductive Elastomer Electrodes for Neural Stimulation. *J Biomater Sci Polym Ed* 2007, 18, 1057-73.

17. Seymour, J. P.; Kipke, D. R., Neural Probe Design for Reduced Tissue Encapsulation in Cns. *Biomaterials* 2007, 28, 3594-607.

18. Kim, Y. T.; Hitchcock, R. W.; Bridge, M. J.; Tresco, P. A., Chronic Response of Adult Rat Brain Tissue to Implants Anchored to the Skull. *Biomaterials* 2004, 25, 2229-2237.

19. Sanders, J. E.; Stiles, C. E.; Hayes, C. L., Tissue Response to Single-Polymer Fibers of Varying Diameters: Evaluation of Fibrous Encapsulation and Macrophage Density. *J Biomed Mater Res* 2000, 52, 231-7.

20. Kozai, T. D.; Langhals, N. B.; Patel, P. R.; Deng, X.; Zhang, H.; Smith, K. L.; Lahann, J.; Kotov, N. A.; Kipke, D. R., Ultrasmall Implantable Composite Microelectrodes with Bioactive Surfaces for Chronic Neural Interfaces. *Nature materials* 2012, 11, 1065-73.

21. Hai, A.; Shappir, J.; Spira, M. E., In-Cell Recordings by Extracellular Microelectrodes. *Nat Methods* 2010, 7, 200-2.

22. Rousche, P. J.; Pellinen, D. S.; Pivin, D. P., Jr.; Williams, J. C.; Vetter, R. J.; Kipke, D. R., Flexible Polyimide-Based Intracortical Electrode Arrays with Bioactive Capability. *IEEE transactions on bio-medical engineering* 2001, 48, 361-71.

23. Seo, J.-M.; Kim, S. J.; Chung, H.; Kim, E. T.; Yu, H. G.; Yu, Y. S., Biocompatibility of Polyimide Microelectrode Array for Retinal Stimulation. *Materials Science and Engineering: C* 2004, C24, 185-189.

24. Boppart, S. A.; Wheeler, B. C.; Wallace, C. S., A Flexible Perforated Microelectrode Array for Extended Neural Recordings. *IEEE transactions on bio-medical engineering* 1992, 39, 37-42.

25. Cogan, S. F.; Ehrlich, J.; Plante, T. D.; Van Wagenen, R., Penetrating Microelectrode Arrays with Low-Impedance Sputtered Iridium Oxide Electrode Coatings. *Conference proceedings : ... Annual International Conference of the IEEE Engineering in Medicine and Biology Society. IEEE Engineering in Medicine and Biology Society. Conference* 2009, 2009, 7147-50.

26. Gheith, M. K.; Pappas, T. C.; Liopo, A. V.; Sinani, V. A.; Shim, B. S.; Motamedi, M.; Wicksted, J. P.; Kotov, N. A., Stimulation of Neural Cells by Lateral Currents in Conductive Layer-by-Layer Films of Single-Walled Carbon Nanotubes. *Adv Mater* 2006, 18, 2975-2979.

27. Cogan, S. F., Neural Stimulation and Recording Electrodes. *Annu Rev Biomed Eng* 2008, 10, 275-309.

28. Kotov, N. A.; Winter, J. O.; Clements, I. P.; Jan, E.; Timko, B. P.; Campidelli, S.; Pathak, S.; Mazzatenta, A.; Lieber, C. M.; Prato, M.; Bellamkonda, R. V.; Silva, G. A.; Kam, N. W. S.; Patolsky, F.; Ballerini, L., Nanomaterials for Neural Interfaces. *Adv Mater* 2009, 21, 3970-4004.

29. Malarkey, E. B.; Parpura, V., Carbon Nanotubes in Neuroscience. *Act Neur S* 2010, 106, 337-341.

30. Jan, E.; Hendricks, J. L.; Husaini, V.; Richardson-Burns, S. M.; Sereno, A.; Martin, D. C.; Kotov, N. A., Layered Carbon Nanotube-Polyelectrolyte Electrodes Outperform Traditional Neural Interface Materials. *Nano letters* 2009, 9, 4012-8.

31. Luo, X.; Weaver, C. L.; Zhou, D. D.; Greenberg, R.; Cui, X. T., Highly Stable Carbon Nanotube Doped Poly(3,4-Ethylenedioxythiophene) for Chronic Neural Stimulation. *Biomaterials* 2011, 32, 5551-7.

32. Shim, B. S.; Zhu, J.; Jan, E.; Critchley, K.; Ho, S.; Podsiadlo, P.; Sun, K.; Kotov, N. A., Multiparameter Structural Optimization of Single-Walled Carbon Nanotube Composites: Toward Record Strength, Stiffness, and Toughness. *ACS Nano* 2009, 3, 1711-1722.

33. Shao, M. W.; Wang, D. B.; Yu, G. H.; Hu, B.; Yu, W. C.; Qian, Y. T., The Synthesis of Carbon Nanotubes at Low Temperature Via Carbon Suboxide Disproportionation. *Carbon* 2004, 42, 183-185.

34. Lin, C. M.; Lee, Y. T.; Yeh, S. R.; Fang, W. L., Flexible Carbon Nanotubes Electrode for Neural Recording. *Biosens Bioelectron* 2009, 24, 2791-2797.

35. Zhou, Y. X.; Hu, L. B.; Gruner, G., A Method of Printing Carbon Nanotube Thin Films. *Appl Phys Lett* 2006, 88.

36. Abadi, P. P. S. S.; Hutchens, S. B.; Greer, J. R.; Cola, B. A.; Graham, S., Buckling-Driven Delamination of Carbon Nanotube Forests. *Appl Phys Lett* 2013, 102, 223103.

37. Shim, B. S.; Zhu, J. A.; Jan, E.; Critchley, K.; Kotov, N. A., Transparent Conductors from Layer-by-Layer Assembled Swnt Films: Importance of Mechanical Properties and a New Figure of Merit. *ACS Nano* 2010, 4, 3725-3734.

38. Zhu, J.; Shim, B. S.; Di Prima, M.; Kotov, N. A., Transparent Conductors from Carbon Nanotubes Lbl-Assembled with Polymer Dopant with Pi-Pi Electron Transfer. *J Am Chem Soc* 2011, 133, 7450-7460.

39. Kam, N. W. S.; Jan, E.; Kotov, N. A., Electrical Stimulation of Neural Stem Cells Mediated by Humanized Carbon Nanotube Composite Made with Extracellular Matrix Protein. *Nano letters* 2009, 9, 273-278.

40. Jan, E.; Kotov, N. A., Successful Differentiation of Mouse Neural Stem Cells on Layer-by-Layer Assembled Single-Walled Carbon Nanotube Composite. *Nano letters* 2007, 7, 1123-1128.

41. Lovat, V.; Pantarotto, D.; Lagostena, L.; Cacciari, B.; Grandolfo, M.; Righi, M.; Spalluto, G.; Prato, M.; Ballerini, L., Carbon Nanotube Substrates Boost Neuronal Electrical Signaling. *Nano letters* 2005, 5, 1107-10.

42. Malarkey, E. B.; Fisher, K. A.; Bekyarova, E.; Liu, W.; Haddon, R. C.; Parpura, V., Conductive Single-Walled Carbon Nanotube Substrates Modulate Neuronal Growth. *Nano letters* 2009, 9, 264-268.

43. Cellot, G.; Cilia, E.; Cipollone, S.; Rancic, V.; Sucapane, A.; Giordani, S.; Gambazzi, L.; Markram, H.; Grandolfo, M.; Scaini, D.; Gelain, F.; Casalis, L.; Prato, M.; Giugliano, M.; Ballerini, L., Carbon Nanotubes Might Improve Neuronal Performance by Favouring Electrical Shortcuts. *Nat Nanotechnol* 2009, 4, 126-133.

44. Wang, X.; Xie, X.; Ku, G.; Wang, L. V.; Stoica, G., Noninvasive Imaging of Hemoglobin Concentration and Oxygenation in the Rat Brain Using High-Resolution Photoacoustic Tomography. *Journal of biomedical optics* 2006, 11, 024015.

45. Keefer, E. W.; Botterman, B. R.; Romero, M. I.; Rossi, A. F.; Gross, G. W., Carbon Nanotube Coating Improves Neuronal Recordings. *Nat Nanotechnol* 2008, 3, 434-9.

46. Yoon, I.; Hamaguchi, K.; Borzenets, I. V.; Finkelstein, G.; Mooney, R.; Donald, B. R., Intracellular Neural Recording with Pure Carbon Nanotube Probes. *PLoS ONE* 2013, 8, e65715.

47. Jan, E.; Byrne, S. J.; Cuddihy, M.; Davies, A. M.; Volkov, Y.; Gun'ko, Y. K.; Kotov, N. A., High-Content Screening as a Universal Tool for Fingerprinting of Cytotoxicity of Nanoparticles. *ACS Nano* 2008, 2, 928-938.

48. Stieglitz, T., Hansjorg, B., Schuettler, M. and Meyer, J.-U, Micromachined, Polyimide-Based Devices for Flexible Neural Interfaces. *Biomedical Microdevices* 2000, 2, 283-294.

49. Kandel, E. R.; Schwartz, J. H.; Jessell, T. M., *Principles of Neural Science*. 4th ed.; McGraw-Hill, Health Professions Division: New York, 2000; p xli, 1414 p.

50. Franceschini, G. The Mechanics of Human Brain Tissue University of Trento, 2006.

51. Merrill, D. R.; Bikson, M.; Jefferys, J. G., Electrical Stimulation of Excitable Tissue: Design of Efficacious and Safe Protocols. *Journal of neuroscience methods* 2005, 141, 171-98.

52. Fan, W.; Maesoon, I.; Euisik, Y. In *A Flexible Fish-Bone-Shaped Neural Probe Strengthened by Biodegradable Silk Coating for Enhanced Biocompatibility*, Solid-State Sensors, Actuators and Microsystems Conference (TRANSDUCERS), 2011 16th International, 5-9 June 2011; 2011; pp 966-969.

53. Kozai, T. D.; Kipke, D. R., Insertion Shuttle with Carboxyl Terminated Self-Assembled Monolayer Coatings for Implanting Flexible Polymer Neural Probes in the Brain. *Journal of neuroscience methods* 2009, 184, 199-205.

54. Kozai, T. D.; Vazquez, A. L.; Weaver, C. L.; Kim, S. G.; Cui, X. T., In Vivo Two-Photon Microscopy Reveals Immediate Microglial Reaction to Implantation of Microelectrode through Extension of Processes. *J Neural Eng* 2012, 9, 066001.

55. Hu, S.; Maslov, K.; Wang, L. V., Second-Generation Optical-Resolution Photoacoustic Microscopy with Improved Sensitivity and Speed. *Opt Lett* 2011, 36, 1134-6.

56. Xie, Z.; Jiao, S.; Zhang, H. F.; Puliafito, C. A., Laser-Scanning Optical-Resolution Photoacoustic Microscopy. *Opt Lett* 2009, 34, 1771-3.

57. Aine, C. J., A Conceptual Overview and Critique of Functional Neuroimaging Techniques in Humans: I. Mri/Fmri and Pet. *Crit Rev Neurobiol* 1995, 9, 229-309.

Chapter 3

Gold Nanoparticles for Neural Prosthetic Devices

3.1 Abstract

Treatments of neurological diseases and the realization of brain-computer interfaces require ultrasmall electrodes which are “invisible” to resident immune cells. Functional electrodes smaller than 50μm are impossible to produce with traditional materials due to high interfacial impedance at the characteristic frequency of neural activity and insufficient charge storage capacity. The problem can be resolved by using gold nanoparticle nanocomposites. Careful comparison indicates that layer-by-layer assembled films from Au NPs provide more than three-fold improvement in interfacial impedance and one order of magnitude increase in charge storage capacity. Prototypes of microelectrodes could be made using traditional photolithography. Integration of unique nanocomposite materials with microfabrication techniques

opens the door for practical realization of the ultrasmall implantable electrodes. Further improvement of electrical properties is expected when using special shapes of gold nanoparticles.

3.2 Introduction

Neural prosthetic devices (NPDs), like artificial pacemakers[1] and cochlear implants[2] are becoming increasingly relevant for the diagnosis and treatments of many neurological conditions and traumas. Commonly, these devices utilize electrodes to interact with neural tissues and achieve targeted stimulation or recording. For example, chronic deep brain stimulation (DBS) can alleviate symptoms of Parkinson's[3] and even Alzheimer's disease.[4] NPDs have also allowed patients of ayomyotrophic lateral sclerosis to regain motor functions.[5] Recently, brain-computer interfaces have received increased attention due to the possibility of using multi-site recording NPD platforms for restoration of mobility and prosthetic devices for limbs.[6, 7] Despite initial clinical successes, there are still many challenges in creating long-lasting, high-performance neural prosthetic devices.

To improve the long-term stability and performance of current NPDs, it is necessary to minimize the inflammatory response induced by NPDs. Typically, after implantation, a layer of scar tissue forms around the NPD due to accumulation of resident immune cells.[8, 9] This layer will create a barrier between the device and the target neural tissue, which causes the device to lose its functionality overtime.[10]

Studies have suggested that inflammatory response is substantially reduced as the implant becomes smaller.[11, 12] The ideal dimensions of implantable neural electrodes should not exceed 10 μm in either width or thickness.[13] Moreover, it was demonstrated that subcellular-sized electrodes allow the formation of tight junction between neurons and electrodes, thus creating effective electrical coupling at the neuron/electrode interface.[14] Mechanical properties of the electrodes are also closely related to inflammation. Electrodes made of rigid materials, such as noble metals and semiconductors, have large mismatch in mechanical properties with neural tissues.[15, 16] This mismatch becomes particularly significant when considering the inevitable microscale motion of electrodes relative to the brain tissues.[17] This motion triggers additional immune response through mechanical signal transduction.[12] Smaller flexible electrodes have better compliance with soft tissues and are expected to help reduce the additional activation of immune pathways and scar formation.

While the concept of ultrasmall flexible electrodes is well understood, the pathway to its practical realization is not. The ultrasmall electrodes bring up challenging material issues. The electrical properties of all current classical and advanced materials exemplified by platinum, doped silicon, polypyrrole, poly(3,4-ethylenedioxythiophene)(PEDOT), and iridium oxide (IrOx), greatly limit the functionalities of electrodes smaller than 50-100 μm. The charge storage capacity (CSC) and interfacial impedance (Z) of these materials are not sufficient to reliably record signals from electrodes below this size.

To resolve these issues, it is necessary to develop new materials with improved Z and CSC than current materials.[18] Lower electrical impedance improves signal-to-noise ratio and the long-term recording quality of NPDs[19, 20] and reduces harmful overpotential. High CSC materials can deliver a higher charge per area of the electrodes to the surrounding tissue for neural stimulation. The general strategy for improving Z and CSC is to increase the electrochemical surface area of the electrodes for a given geometric surface area.[21, 22] Most advanced materials used for neural electrodes, including platinum black,[23] conductive polymer,[24] and iridium oxide[25] have high-roughness surfaces to increase the ratio of electrochemical surface area and geometric surface area, consequently improving the Z and CSC. Evidently, conductive nanomaterials would be ideal for engineering the surfaces of the neural electrodes.

Currently, most research on nanomaterials for neural interface is mainly focused on CNT-based material.[20, 26-36] It has been demonstrated that CNT coating improves *in vivo* neural recording both in rats and primates.[20] Despit*e* excellent mechanical properties of CNT, the electrochemical performance of CNT composites is still not as high as needed for the ultrasmall NPDs with dimensions $\leq$10μm. Biocompatibility and related inflammation processes initiated by electrodes from CNT or other materials with respect to long-term implantation (on the scale of years) remains a concern[37] that needs to be addressed in the future. These challenges drive us to explore other nanomaterials and further optimize the electrochemical properties of neural interface materials.[38, 39] Additionally, nanoporous gold and gold

nanopowder were also investigated for neural interface applications.[22, 40] Both studies demonstrated the possibility of creating high roughness gold surfaces. However, these techniques require extensive instrumentation (ultra high vacuum deposition and mold fabrication) and high processing temperatures.

Solution processed gold nanoparticles (Au NPs) have been studied extensively for their biological applications.[41] They have minimal toxicity,[42] are highly conductive,[43] and are very simple to fabricate.[44] Au NP/polymer composites have great potential for NPD applications in term of electrochemical performance and biocompatibility, but *Au NPs have never been used for neural interface applications*. A lot of attention paid to carbon nanotubes (CNT) probably overshadowed Au NPs as material suitable for neural interface. CNTs were considered *a priori* to be a better choice due to their fibrous morphology, high electron mobility, and high surface area. [26] Here we demonstrate that this assumption was probably incorrect and materials with better electrochemical performance can be made from Au NPs. Measurements of electrochemical properties on NPD prototypes indicate that in respect to Z and CSC, Au NP films substantially outperform SWNT composites. Since the microfabrication process developed here for Au NP composites is compatible with current microelectrode technology, this study opens the way to a new generation of implantable electrodes.

3.3 Material and Methods

High purity single wall carbon nanotubes (P2-SWNTs) were purchased from Carbon Solution, Inc. (Riverside, CA), respectively. Poly(vinyl alcohol) (PVA; MW 70k), poly(sodium 4-styrene-sulfonate) (PSS; MW 100k), and Poly(diallyldimethylammonium chloride) (PDDA)were obtained from Sigma-Aldrich. All other chemicals were obtained from Sigma-Aldrich

3.3.1 Synthesis of Gold Nanoparticles

The synthesis of Au NPs followed the standard citrate reduction method. Briefly, 90 mg of HAuCl4 were dissolved in 500 ml of water. The solution was heated on a hot plate until boiling. Then 25ml of 0.1% sodium citrate aqueous solution was added to the gold salt solution. The mixture was stirred and reboiled on a hot plate. After 20 minutes, the solution became a red color, which indicated the formation of Au NPs. The Au NPs were concentrated 10X by centrifuging at 9000 rpm for 50 minute and removing 90% of the supernatant

3.3.2 Layer-by-Layer Assembly of Au NP film and SWNT film

LbL assembly was initially carried out on microscope glass slides cleaned in piranha solution overnight and then thoroughly rinsed with deionized water prior to the use. For LBL assembly, a glass slide was immersed in 0.1 wt % solution of PDDA for 5 min, rinsed with DI water for 1 min, dried, and then immersed in

concentrated Au NP solution for 10 min, rinsed for 1 min, and dried again. The procedure was then repeated with PDDA and Au NP solution.

SWNTs were first dispersed at 0.5 mg/mL in 2mg/ml PSS (MW 100k) solution by ultrasonication. 0.1 wt % PVA solution was prepared by dissolving correct amount of PVA in near boiling water. For each deposition cycle, the electrode was immersed in the PVA solution for 2 min, following by rinsing with deionized water and drying with an air jet. Then the electrode was immersed in SWNT solution for 5 min , following by rinsing with deionized water and drying with an air jet.

3.3.3 Fabrication of LBL Coated Electrode

Electrode fabrication involved several standard microfabrication procedures. Briefly, positive photoresist (SPR-220 3.0, Rohm and Haas) was first deposited and developed on a glass slide. Then 500nm of metallic gold were deposited by electron beam (Enerjet Evaporator, Denton) at a base pressure of 2*10^-6 torr onto the photoresist coated glass slides. After evaporation, gold were lifted off from the glass in acetone to form the electrode layer. The same positive photoresist were deposited again and developed to form lift-off layer for the LBL film. Afterward, LBL assembly process was applied to the electrode. Once the LBL film achieved the target thickness, the glass slide was transferred in acetone for LBL film lift-off. Lastly, the final layer of positive photoresist was deposited and developed as an insulation layer.

3.3.4 Electrochemical Impedance Spectroscopy (EIS)

EIS was carried out on an Autolab PGSTAT 12; Frequency Response Analyzer software (EcoChemie, Utrecht, Netherlands) was used to record impedance spectra of the electrodes. A solution of 1 M phosphate buffered saline (PBS, pH = 7) was used as an electrolyte in a three-electrode configuration. The working electrode was connected to the electrode site. The counter electrode was connected to a gold foil immersed in PBS, and an Ag/AgCl reference electrode was immersed in PBS. An AC sinusoidal signal of 25 mV in amplitude was used to record the impedance over a frequency range of 10−32000 Hz.

3.3.4 Cyclic Voltammetry (CV) and Voltage Transients

CV and Voltage Transients experiments were performed using an Autolab PGSTAT 12 instrument and General Purpose Electrochemical System software (EcoChemie, Utrecht, Netherlands) in a three-electrode configuration as described for EIS. For CV, a scan rate of 1 V/s was used and the potential on the working electrode was swept between −0.8 and 0.6 V. Three cycles were swept to ensure that the film had reached a stable state. For the voltage transient experiment, a cathodic current pulse (5μA, 2ms) were sourced and voltage change were recording during the experiment.

3.3.5 NG108-15 Cell Culture and Biocompatibility Test

NG108-15 cell line was obtained from American Type Culture Collection (ATCC: HB 12317). The cells were culture with DMEM high glucose media (Gibco: 11965-092) + Hypoxanthine - Aminopterin – Thymidine supplement (ATCC: 69-X) +10% fetal bovine serum at 37°C with 5% CO_2. Once the cells reached 90% confluence, they were detached from the culture flask and 1*10^6 cells were seeded onto a 1cm by 1 cm glass slide coated with Au NP/PDDA film. The cells were culture in the same condition for three days on the glass slide before the biocompatibility test. The biocompatibility of the Au NP/PDDA films was tested by a LIVE/DEAD Biohazard Cell Viability Kit (Invitrogen: L-7013) according to the exact protocol provided the vendor. Then the live and dead cells were counted and cell viability was calculated by dividing the number of live cells by the total number of the cell on the substrate.

3.3.6 Scanning Electron Microscopy (SEM)

LbL samples were deposit on a silicon wafer. SEM images were obtained using a FEI Nova Nanolab SEM at 10kV accelerating voltage.

2.3.7 Atomic Force Microscopy (AFM)

LbL samples were deposit on a silicon wafer. AFM images were obtained using Digital Instrument Nanoscope (R) at a scan rate of 0.5 Hz and tip speed of 30 μm/s.

3.3.8 Transmition Electron Microscopy (TEM)

20 μl of as prepared nanoparticle solution were dropped on a standard TEM grids (Cuppor mesh with carbon membrane) and dried in room temperature. TEM images were obtained using a JEOL 3010 TEM with acceleration voltage of 300kV.

2.4 Results and Discussion

Previous comparative evaluation of IrOx and PEDOT with CNT composite concluded that CNT composite outperform IrOx and PEDOT with respect to both electrical and mechanical properties upon cyclic excitation.[26] The major effort here is to answer the question of whether materials even better than CNT composite could be created. Au NPs attracted our attention because the conductivity of macroscale composite materials made from Au NPs is higher than any other CNT composites thus far.[45, 46] The charge transport in a single carbon nanotube can be exceptionally fast, but this does not mean that it is possible to translate it to macroscale materials. Unfortunately, the insulating gaps between the nanotubes and the Schottky barrier at the interfaces between the semiconductor and metallic nanotubes greatly frustrate the electron transport in CNT materials in macro- and microscale. [47] Further

improvements in CNT synthesis could potentially resolve some of these issues. At the same time, these prompted us to explore alternatives presented by other nanomaterials exemplified by Au NPs. Besides high conductivity of macroscale composites, Au NPs provide exceptionally high surface area, which can potentially reduce Z. The challenge in this case will be to balance the surface area with the interconnectivity of NPs.

Latest results indicated that carbon nanostructures could undergo biodegradability upon long-term exposure to biological media,[48] which could present a problem for NPD applications. According to existing data,[49] Au NPs at a certain level do not interfere with tissue function even after many years of residence time, which is a substantial advantage for NPD implants.

For valid comparison between CNTs and Au NPs, the same technique of film preparation is needed. The universality of the layer-by-layer (LBL) assembly offers this possibility. Compare to some other methods of thin film deposition, such as electrophoresis, chemical vapor, and solvent evaporation,[50] LBL requires milder operating conditions, simpler instrumentations, and most importantly, provides a higher degree of structural control. It also allows one to combine organic and inorganic materials, which is necessary for biomedical applications. Last, but not the least, LBL makes it possible to accurately control the thickness of the coatings by controlling the number of deposition cycles, *n*. This is particularly important for the adequate comparison between Au NP and CNT film. By and large, LBL can be

depicted as a versatile method to engineer multifunctional coatings down to the nanometer scale[51] and to fine tune the entire spectrum of materials properties: mechanical, electrical, optical, and biological to achieve the balanced combination specific for the particular application.[52-54]

Therefore, LBL assembly was applied for the preparation of Au NP and SWNT composite thin films on electrodes. SWNT LBL films were assembled from SWNT aqueous dispersions stabilized by poly(styrene sulfonate) (PSS) using poly(vinyl alcohol) as a partner LBL polymer following the protocol described in our previous study and the method section.[46, 55] Au NP LBL films were made using concentrated citrate-stabilized NPs in water. In this case, we used standard polymer, poly(diallydimethylammonium chloride) (PDDA) as an LBL-partner, which was used in many previous LBL applications.[56] We specifically selected for this project the polymers that are electrochemically "silent" in the window of potential relevant for neural stimulation. Besides making it easier to understand the electrochemical performance of the coatings (see below), having electrochemically inactive polymers as partners for NPs and CNTs is important in order to avoid their redox decomposition, which is certainly undesirable.

From atomic force microscopy (AFM) images and ellipsometry data (Figure 3.1), one can establish that Au NPs and CNT LBL films can be successfully deposited in the sequential manner despite a complex film growth curve (Figure 3.1D). The NP LBL film displays a rough surface with close packed Au NPs. The surface

morphology of the Au NP films can be described as globular while the CNT films are fibrous with random orientation of the nanotubes within X-Y plane. Both nanoscale morphologies are important for increasing electrochemical surface area and improving the NPD performance. Scanning electron microscopy (SEM) images of Au NP and SWNT films also exhibit similar geometrical features (Figure 3.2).

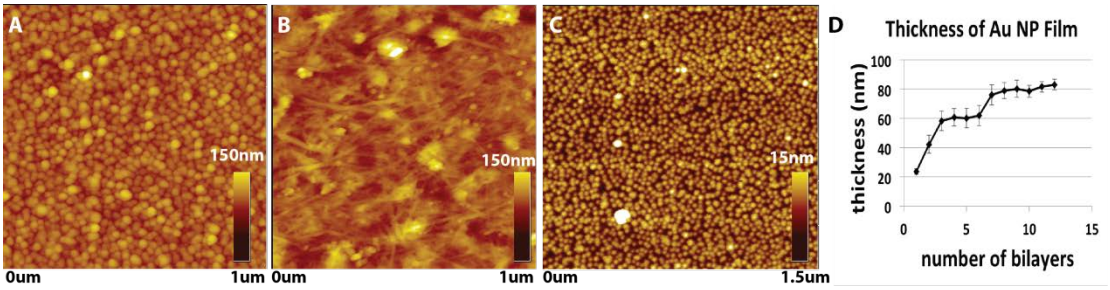

Figure 3.1 (A) AFM image of 15 bilayers of Au NP LBL film. (B) AFM image of 25 bilayers of CNT LBL film. (C) First bilayer of Au NP LBL film. (D) Ellipsometric thickness of Au NP LBL films for different number of bilayers.

The total number of LBL deposition cycles was adjusted for both nanomaterials to obtain the same coating thickness. Cross-sectional SEM images for CNT and Au NP films obtained after 25 and 15 deposition cycles respectively show a thickness of 100±8 nm. The same image also indicates high content and interconnectivity of Au NP in the films.

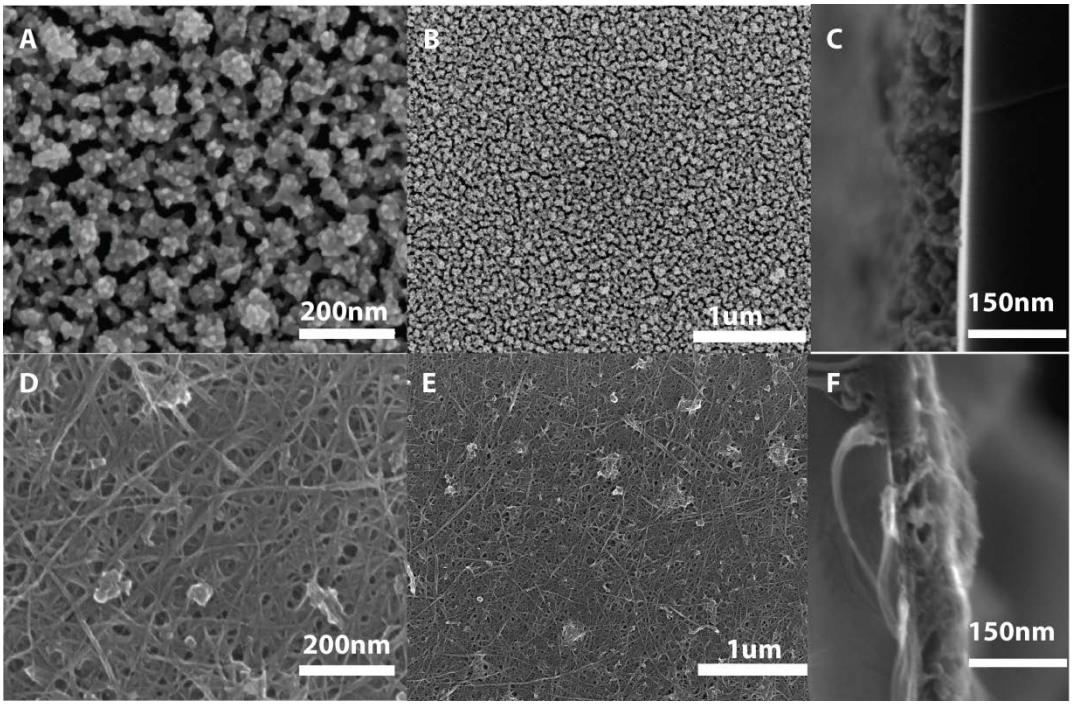

Figure 3.2 SEM images of Au NP film and CNT film. (A, B) SEM images of Au NP film at different magnifications. (C) Cross-section image of Au NP film. (D, E) SEM images of CNT film at different magnifications. (F) Cross-section image of CNT film.

We first compared the performance of the CNT coating in our study with the previous study. The same wire electrode were fabricated and tested under the identical conditions to those previous ones. The impedance of our CNT coating is about 170Ω compare to previously reported 277Ω at the physically relevant frequency. And the CSCs of the two coatings are also very similar, approximately 10mC/cm^2.

To further ensure accurate electrochemical measurements, we designed a lithographic scheme to integrate LBL nanocomposite films into the microelectrode fabrication process (Figure 3.3A). The electrode design guarantees that all films tested have the same surface area and their geometry is perfectly reproducible from batch to batch. The chosen microfabrication process (Figure 3.3A) allows minimal exposure of the nanocomposite films to other process chemicals. EDAX spectroscopy indicates that the nanocomposite films are unaltered after the microfabrication process and that there are no residual chemicals on the surfaces of the films (Figure 3.4). Besides its convenience and accuracy, the design of these microelectrodes can be adapted to virtually any type of implants including those with dimensions of 10 μm and less.

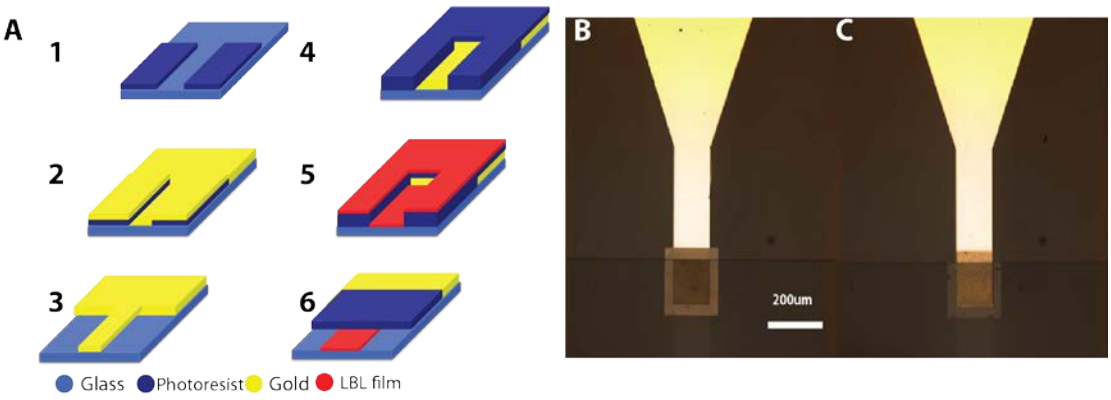

Figure 3.3 (A) Fabrication process of the microelectrodes with LBL films of Au NPs and CNTs (1) deposition and development of the positive photoresist; (2) E-beam deposition of the metal gold; (3) lift-off of the metal gold layer; (4) deposition and development of the positive photoresist (5) depo-sition of the LBL film (6) lift-off of LBL film and deposition/development of insulating photo-resist layer. (B) Optical

image of Au NP LBL film coated electrode. (C) Optical image of CNT LBL film coated electrode.

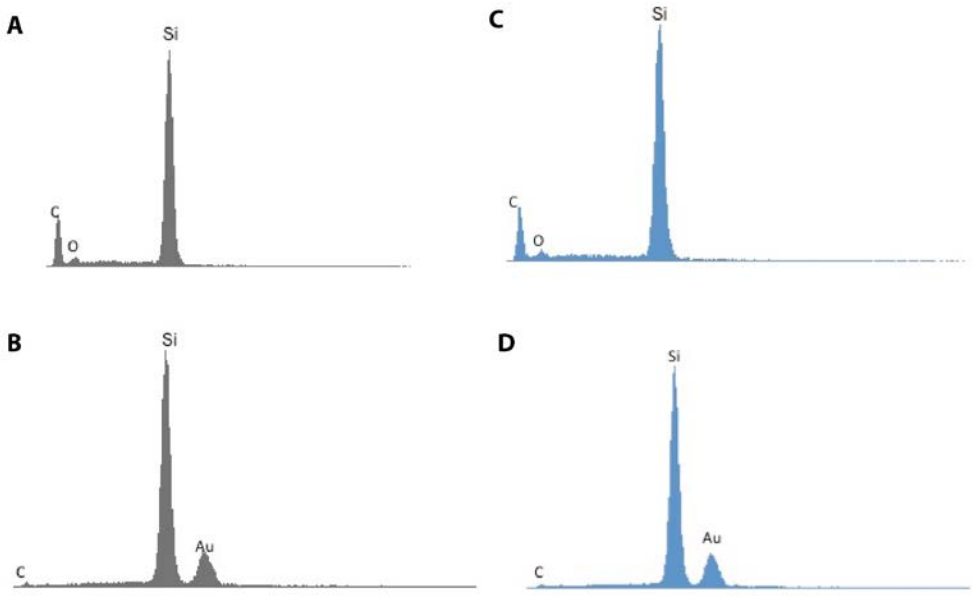

Figure 3.4 EDAX spectra of CNT (A, C) and Au NPs (B, D) LBL films before (A, B) and after (C, D) microfabrication on silicon substrates.

Impedance (*Z*) and charge storage capacity (CSC) were investigated in a three-electrode electrochemical set-up, which is most suitable for the measurement of these properties. Impedance was measured by a frequency response analyzer from 10 Hz to 31 kHz. Au NP film has lower Z than SWNT film for the entire spectrum of frequencies relevant for NPDs. The characteristic impedance phase angles (Φ) for Au NP film across the entire frequency domain are smaller than SWNT film, which implies the higher conductivity of Au NP film (Figure 3.4 A, B). This is further

confirmed by the conductivity measurements in an ambient environment with a standard four-point probe. The conductivity of Au NP film is $8.6*10^6$ S/m; this is more than a magnitude higher than conductivity of CNT film equal, $1.1*10^5$ S/m.[57] The area enclosed in the CV curve, *S*, of Au NP film is much larger than SWNT film for the same scan rate, *v*, indicating a substantially higher CSC.

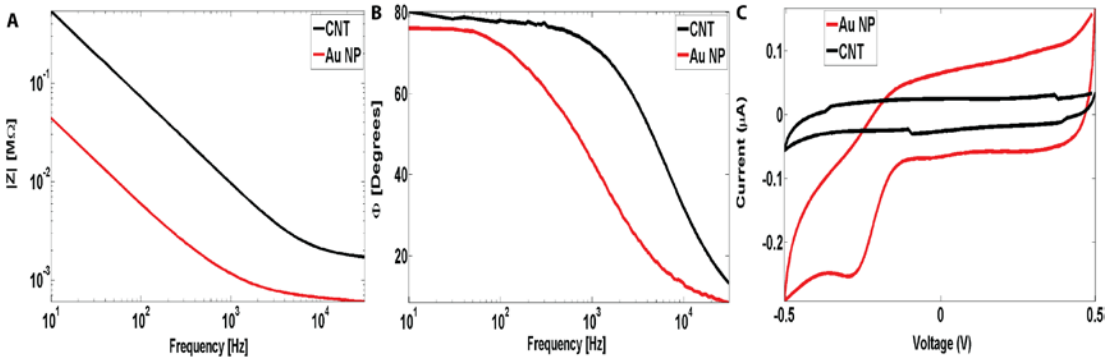

Figure 3.4 Typical electrochemical behavior of Au NP film (red) and CNT films (black): (A) Frequency dependence of impedance, Z. (B) Frequency dependence of the impedance phase angle, Φ; (C) Typical cyclic voltammetry from 0.5 V to -0.5 V.

Detailed comparison of Au NP and CNT film are made by using impedance values measured for 1 kHz and cathodic CSC. In Figures 3.5A, the average measurements of 32 samples indicate that Au NP film outperform SWNT film with respect to both *Z* and cathodic *CSC*. P-values for Z and CSC were less than 0.01 for a two-tail Student t-test, indicating that the differences between CNT and Au NP film are statically significant. The *Z* value of Au NP film is almost four times lower than

SWNT film while the cathodic *CSC* of the Au NP film is close to one magnitude higher than the SWNT film.

Total CSC is also quite informative, although it is somewhat more difficult to compare. Previously, the total CSC of electrodes made from multiwalled carbon nanotubes, PEDOT, and IrO have been reported. The total CSC of these materials for 100 nm thick coatings and a scan rate of 0.1 V/s from -0.9V to 0.5 V ranged from 6 to 9 mC/cm^2.[27] In our study, the total CSC of the 100nm thick Au NP films at a scan rate of 1 V/s from -0.6V to 0.8V was 2.56 mC/cm^2 (Figure 3.5A). The actual voltage window is determined by the specific redox properties of the material and can be rarely matched exactly. The effect of the scan rate can be incorporated as a scaling factor because CSC is inversely proportional to the scan rate. Note that the width of the voltage window was, nevertheless, identical in each case and equal to 1.4V. Recalculating the literature data to a 1 V/s scan rate scale shows that the total CSC for Au NP film is at least three times higher than analogous data in the previous report.[27] The 1kHz impedance of Au NP film is about 3kOhm for a surface area of 3000 μm^2 and coating thickness of 100nm. Previous studies using different sizes of electrodes have reported 1kHz impedance of 30kOhm for nanoporous Au22 and 10kOhm for Au nanopower40. The physical characteristics of the materials coatings are different for each study. It is difficult to compare electrochemical data of these coatings in detail. Nevertheless, we see significant improvement of the impedance with nanoscale engineering of the electrode surfaces in all three studies

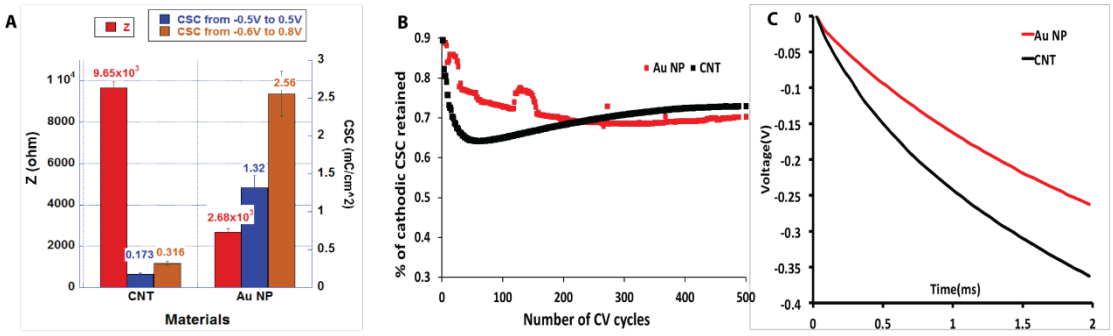

Figure 3.5 Summary of electrical chemical properties and stability of Au NP and CNT films: (A) Cumulative electrochemical properties of Au NP and CNT films. The data were calculated for sample size of 32 samples. (B) Evaluation of stability of Au NP and CNT films over 500 CV cycles at 1 V/s scan rate for repeating electrochemical excitation. (C) Voltage transient experiment with cathodic current pulses (5μA, 2ms)

Besides determining CSC, CV experiments also offer additional information at the electrode/electrolyte interface. We noticed a reduction peak in the CV curve of Au NP film. In order to identify this reduction peak, we conducted a control CV experiment with argon gas purged PBS solution instead of regular PBS solution. The reduction peak disappeared after the argon purge of the PBS solution. This indicates that the peak is from the reduction of oxygen, which is observed on many metal electrodes, including gold electrodes. [40]

Furthermore, we also conducted voltage transient experiments to evaluate the performance of Au NP film and CNT film. This technique is commonly used to determine the charge injection limit of an electrode for a given voltage limit.[21]

Cathodic current pulse (-5μA, 2ms) was applied to the electrodes while the voltage was recorded. For the same amount of charge, Au NP film has a lower voltage excursion compared to CNT film (Figure 3.5C). This indicates that Au NP film has a high charge injection limit compared to CNT film for a given voltage limit. This result correlates well with the impedance data because lower impedance generally reduces overpotential and lowers the voltage excursion.

The circuit analogs of impedance data can be used to gain detailed insight about the materials properties and interfacial properties of an NPD. The circuit analog used here (Figure 3.6) assumed the measured impedance was a product of electrical resistance of the film (R_s), charge transport losses at the film-electrolyte interface (R_f), and interfacial capacitance of the film (C_d). Walburg impedance (W) was previously included in many analog circuits as well. However, W is only relevant for systems with strong mass transport limitations. For the operating environment of NPDs, one can consider that the transport limitations to be minimal due to the large amount of ions present and the small amount of charge transferred. By fitting the impedance data using this circuit analog (Figure 3.6), the experimental impedance Z is lower for Au NP film (Figures 3.4A) due to the lower R_s, and R_f. The high *CSC* values for Au NP films can be correlated with high value of C_d. This indicates that the high surface area created by NPs and the high interconnectivity among NPs in the composite materials play essential roles in determining the macroscale electrochemical functionalities. It might be important to note that *CSC* of solid noble films is typically low. Platinum/Iridium alloy which is the best choice for metallic neural

electrode, only has a theoretical maximum *CSC* of 0.3 mC/cm^2, [21] and the *CSC* of pure metallic Au is even lower. The marginal *CSC* of noble metals prevents the possibility of fabricating high performance stimulating microelectrodes from the classical evaporation+microfabrication techniques.

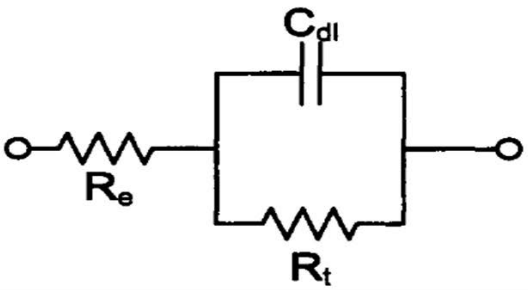

$$Z = R_e + \frac{R_t}{1 + j\omega R_t C_{dl}}$$

	R_e(kOhm)	C_{dl} (nF)	R_t(kOhm)
Au NP	1.1±0.5	130±15	540±76
CNT	1.9±0.2	18±2.1	810±78

Figure 3.6 Circuit analog of the impedance data

To further evaluate the feasibility of Au NP LBL film for neural interface applications, we conducted electrochemical stability tests for both Au NP and SWNT

LBL films. In part, it was also important for comparative purposes because SWNT films are known for their remarkable environmental resilience. Therefore, both films were subjected to a 500 CV scanning cycle at a fast scan rate of 1 V/s. As illustrated in Figure 4E, the *CSC* of both films decreases initially, then stabilizes around 400 cycles. This demonstrates that Au LBL films offer similar stability compared to the SWNT films, which is quite remarkable considering the exceptional mechanical properties of individual CNTs and the fact that they have virtually perfect planar orientation in LBL films (Figure 3.1), which provides the best translation of their mechanical properties to the composites.

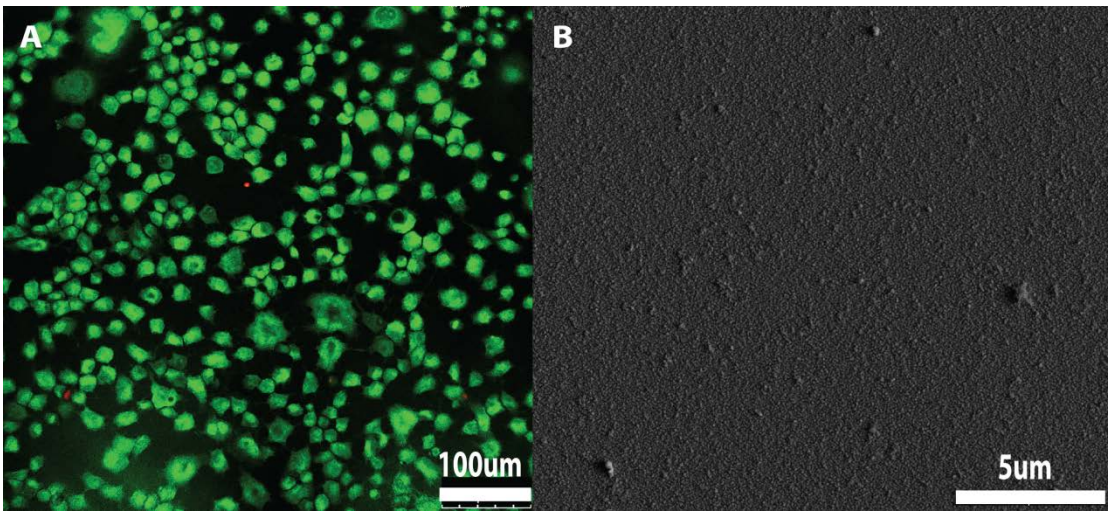

Figure 3.7 (A) Sample confocal fluorescent image of LIVE/DEAD assay (Green:Live Red:Dead). (B) SEM image of Au NP/PDDA LBL film after insertion of rat brain.

Besides excellent electrochemical properties, neuron adhesion/surface biocompatibility is also very important for high quality *in vivo* recording. A close

interface between electrode/neuron improves the quality of the recording.[14, 20] The biocompatibility of the Au NP/PDDA coating was tested with *in-vitro* culture of NG108-15 cells, a type of mouse neuroblastoma/glioma hybrid cells, which are typically used in many biocompatibility/toxicity protocols[58]. Cells were seeded and cultured on glass slides coated with Au NP/PDDA film. Optical images showed NG108 cells could adhere well on the coating and differentiate into neuron-like morphology. (See Supplemental Information) Live/Dead assay were also performed and indicated that 99.9% of cells were live on the surface of the Au NP/PDDA coating (Figure 3.7A). Additionally, the mechanical integrity of Au NP film was also examined by an *ex-vivo* insertion test. The electrodes coated with Au NP/PDDA were inserted into a fresh harvested rat brain and kept at 4°C for 3 days. Then the electrodes were removed from the brain, rinsed with PBS, and imaged with SEM. The Au NP/PDDA coating surface retains the same nanoscale roughness as observed before the insertion (Figure 3.5B).

2.4 Conclusion

Quite unexpectedly, Au NP films were found to have remarkable charge transfer capacity, substantially lower impedance and comparable electrochemical stability under fast voltage scans than CNT films made using the same technology, which were previously considered to be the most promising new materials for the next generation of implantable neuroprosthetic devices (NPDs). Besides the

electrochemical performance, we also see additional advantages of the described Au NP films with respect to other (nano)materials: (1) the long-standing clinical record of gold in both nano- and macroscale forms will facilitate their acceptance; (2) LBL assembly offers tremendous possibilities for further optimization and adaptation to additional NPD functions, which for instance can include *in-situ* gene delivery.[59] Further improvement of materials performance is also possible using LBL films from novel Au NPs, such as nanoshells and nanostars.

A general microfabrication process for Au NP LBL composites suitable for preparation of ultrasmall implantable electrodes that can be virtually "invisible" to the immune system was designed and realized. Integration of LBL film deposition technology and traditional lithography opens many possibilities for utilization of nanostructured LBL composites from CNTs, NPs, etc and their unique properties in many applications.

Further optimization at the system level combining the material properties of Au NP composites and microfabrication techniques must also be pursued. Fabrication of electrodes, which are mechanically compliant with the soft neural tissues and *in vivo* evaluation of this type of microelectrodes, should be the next logical step in this field. A flexible and high performance electrode made out of Au NP film could minimize the tissue stress and provide long-term stability for future neural prosthetic devices.

2.5 References

1. Callaghan, J. C.; Bigelow, W. G., An Electrical Artificial Pacemaker for Standstill of the Heart. *Ann Surg* 1951, 134, 8-17.

2. Fallon, J. B.; Irvine, D. R.; Shepherd, R. K., Cochlear Implants and Brain Plasticity. *Hear Res* 2008, 238, 110-7.

3. Pena, C.; Bowsher, K.; Samuels-Reid, J., Fda-Approved Neurologic Devices Intended for Use in Infants, Children, and Adolescents. *Neurology* 2004, 63, 1163-1167.

4. Hamani, C.; McAndrews, M. P.; Cohn, M.; Oh, M.; Zumsteg, D.; Shapiro, C. M.; Wennberg, R. A.; Lozano, A. M., Memory Enhancement Induced by Hypothalamic/Fornix Deep Brain Stimulation. *Ann Neurol* 2008, 63, 119-23.

5. Nijboer, F.; Sellers, E. W.; Mellinger, J.; Jordan, M. A.; Matuz, T.; Furdea, A.; Halder, S.; Mochty, U.; Krusienski, D. J.; Vaughan, T. M.; Wolpaw, J. R.; Birbaumer, N.; Kubler, A., A P300-Based Brain-Computer Interface for People with Amyotrophic Lateral Sclerosis. *Clinical neurophysiology : official journal of the International Federation of Clinical Neurophysiology* 2008, 119, 1909-16.

6. Velliste, M.; Perel, S.; Spalding, M. C.; Whitford, A. S.; Schwartz, A. B., Cortical Control of a Prosthetic Arm for Self-Feeding. *Nature* 2008, 453, 1098-101.

7. Moritz, C. T.; Perlmutter, S. I.; Fetz, E. E., Direct Control of Paralysed Muscles by Cortical Neurons. *Nature* 2008, 456, 639-42.

8. Biran, R.; Martin, D. C.; Tresco, P. A., Neuronal Cell Loss Accompanies the Brain Tissue Response to Chronically Implanted Silicon Microelectrode Arrays. *Exp Neurol* 2005, 195, 115-26.

9. Edell, D. J.; Toi, V. V.; McNeil, V. M.; Clark, L. D., Factors Influencing the Biocompatibility of Insertable Silicon Microshafts in Cerebral Cortex. *IEEE Trans Biomed Eng* 1992, 39, 635-43.

10. Davies, S. J.; Fitch, M. T.; Memberg, S. P.; Hall, A. K.; Raisman, G.; Silver, J., Regeneration of Adult Axons in White Matter Tracts of the Central Nervous System. *Nature* 1997, 390, 680-3.

11. Kim, Y. T.; Hitchcock, R. W.; Bridge, M. J.; Tresco, P. A., Chronic Response of Adult Rat Brain Tissue to Implants Anchored to the Skull. *Biomaterials* 2004, 25, 2229-37.

12. Keohan, F.; Wei, X. F.; Wongsarnpigoon, A.; Lazaro, E.; Darga, J. E.; Grill, W. M., Fabrication and Evaluation of Conductive Elastomer Electrodes for Neural Stimulation. *J Biomater Sci Polym Ed* 2007, 18, 1057-73.

13. Sanders, J. E.; Stiles, C. E.; Hayes, C. L., Tissue Response to Single-Polymer Fibers of Varying Diameters: Evaluation of Fibrous Encapsulation and Macrophage Density. *J Biomed Mater Res* 2000, 52, 231-7.

14. Hai, A.; Shappir, J.; Spira, M. E., In-Cell Recordings by Extracellular Microelectrodes. *Nat Methods* 2010, 7, 200-2.

15. Subbaroyan, J.; Martin, D. C.; Kipke, D. R., A Finite-Element Model of the Mechanical Effects of Implantable Microelectrodes in the Cerebral Cortex. *J Neural Eng* 2005, 2, 103-13.

16. Seymour, J. P.; Kipke, D. R., Neural Probe Design for Reduced Tissue Encapsulation in Cns. *Biomaterials* 2007, 28, 3594-607.

17. Gilletti, A.; Muthuswamy, J., Brain Micromotion around Implants in the Rodent Somatosensory Cortex. *J Neural Eng* 2006, 3, 189-95.

18. Merrill, D. R.; Bikson, M.; Jefferys, J. G., Electrical Stimulation of Excitable Tissue: Design of Efficacious and Safe Protocols. *J Neurosci Methods* 2005, 141, 171-98.

19. Harnack, D.; Winter, C.; Meissner, W.; Reum, T.; Kupsch, A.; Morgenstern, R., The Effects of Electrode Material, Charge Density and Stimulation Duration on the Safety of High-Frequency Stimulation of the Subthalamic Nucleus in Rats. *J Neurosci Methods* 2004, 138, 207-16.

20. Keefer, E. W.; Botterman, B. R.; Romero, M. I.; Rossi, A. F.; Gross, G. W., Carbon Nanotube Coating Improves Neuronal Recordings. *Nat Nanotechnol* 2008, 3, 434-9.

21. Cogan, S. F., Neural Stimulation and Recording Electrodes. *Annu Rev Biomed Eng* 2008, 10, 275-309.

22. Seker, E.; Berdichevsky, Y.; Begley, M. R.; Reed, M. L.; Staley, K. J.; Yarmush, M. L., The Fabrication of Low-Impedance Nanoporous Gold Multiple-

Electrode Arrays for Neural Electrophysiology Studies. *Nanotechnology* 2010, 21, 125504.

23. Marrese, C. A., Preparation of Strongly Adherent Platinum Black Coatings. *Anal Chem* 1987, 59, 217-218.

24. Richardson-Burns, S. M.; Hendricks, J. L.; Foster, B.; Povlich, L. K.; Kim, D. H.; Martin, D. C., Polymerization of the Conducting Polymer Poly(3,4-Ethylenedioxythiophene) (Pedot) around Living Neural Cells. *Biomaterials* 2007, 28, 1539-52.

25. Blau, A.; Ziegler, C.; Heyer, M.; Endres, F.; Schwitzgebel, G.; Matthies, T.; Stieglitz, T.; Meyer, J. U.; Gopel, W., Characterization and Optimization of Microelectrode Arrays for in Vivo Nerve Signal Recording and Stimulation. *Biosens Bioelectron* 1997, 12, 883-92.

26. Jan, E.; Hendricks, J. L.; Husaini, V.; Richardson-Burns, S. M.; Sereno, A.; Martin, D. C.; Kotov, N. A., Layered Carbon Nanotube-Polyelectrolyte Electrodes Outperform Traditional Neural Interface Materials. *Nano Letters* 2009, 9, 4012-4018.

27. Jan, E.; Kotov, N. A., Successful Differentiation of Mouse Neural Stem Cells on Layer-by-Layer Assembled Single-Walled Carbon Nanotube Composite. *Nano Letters* 2007, 7, 1123-1128.

28. Kam, N. W. S.; Jan, E.; Kotov, N. A., Electrical Stimulation of Neural Stem Cells Mediated by Humanized Carbon Nanotube Composite Made with Extracellular Matrix Protein. *Nano Letters* 2009, 9, 273-278.

29. Gheith, M. K.; Sinani, V. A.; Wicksted, J. P.; Matts, R. L.; Kotov, N. A., Single-Walled Carbon Nanotube Polyelectrolyte Multilayers and Freestanding Films as a Biocompatible Platformfor Neuroprosthetic Implants. *Advanced Materials* 2005, 17, 2663-+.

30. Luo, X.; Weaver, C. L.; Zhou, D. D.; Greenberg, R.; Cui, X. T., Highly Stable Carbon Nanotube Doped Poly(3,4-Ethylenedioxythiophene) for Chronic Neural Stimulation. *Biomaterials* 2011, 32, 5551-7.

31. Lovat, V.; Pantarotto, D.; Lagostena, L.; Cacciari, B.; Grandolfo, M.; Righi, M.; Spalluto, G.; Prato, M.; Ballerini, L., Carbon Nanotube Substrates Boost Neuronal Electrical Signaling. *Nano Letters* 2005, 5, 1107-1110.

32. Malarkey, E. B.; Fisher, K. A.; Bekyarova, E.; Liu, W.; Haddon, R. C.; Parpura, V., Conductive Single-Walled Carbon Nanotube Substrates Modulate Neuronal Growth. *Nano Letters* 2009, 9, 264-268.

33. Cellot, G.; Cilia, E.; Cipollone, S.; Rancic, V.; Sucapane, A.; Giordani, S.; Gambazzi, L.; Markram, H.; Grandolfo, M.; Scaini, D.; Gelain, F.; Casalis, L.; Prato, M.; Giugliano, M.; Ballerini, L., Carbon Nanotubes Might Improve Neuronal Performance by Favouring Electrical Shortcuts. *Nat Nanotechnol* 2009, 4, 126-133.

34. Malarkey, E. B.; Parpura, V., Carbon Nanotubes in Neuroscience. *Act Neur S* 2010, 106, 337-341.

35. Luo, X. L.; Weaver, C. L.; Zhou, D. D.; Greenberg, R.; Cui, X. Y. T., Highly Stable Carbon Nanotube Doped Poly(3,4-Ethylenedioxythiophene) for Chronic Neural Stimulation. *Biomaterials* 2011, 32, 5551-5557.

36. Wang, K.; Fishman, H. A.; Dai, H. J.; Harris, J. S., Neural Stimulation with a Carbon Nanotube Microelectrode Array. *Nano Letters* 2006, 6, 2043-2048.

37. Firme, C. P., 3rd; Bandaru, P. R., Toxicity Issues in the Application of Carbon Nanotubes to Biological Systems. *Nanomedicine* 2010, 6, 245-56.

38. Cohen-Karni, T.; Qing, Q.; Li, Q.; Fang, Y.; Lieber, C. M., Graphene and Nanowire Transistors for Cellular Interfaces and Electrical Recording. *Nano Letters* 2010, 10, 1098-1102.

39. Qing, Q.; Pal, S. K.; Tian, B. Z.; Duan, X. J.; Timko, B. P.; Cohen-Karni, T.; Murthy, V. N.; Lieber, C. M., Nanowire Transistor Arrays for Mapping Neural Circuits in Acute Brain Slices. *P Natl Acad Sci USA* 2010, 107, 1882-1887.

40. Hu, Z.; Zhou, D. M.; Greenberg, R.; Thundat, T., Nanopowder Molding Method for Creating Implantable High-Aspect-Ratio Electrodes on Thin Flexible Substrates. *Biomaterials* 2006, 27, 2009-17.

41. Sperling, R. A.; Rivera Gil, P.; Zhang, F.; Zanella, M.; Parak, W. J., Biological Applications of Gold Nanoparticles. *Chem Soc Rev* 2008, 37, 1896-908.

42. Zhang, X. D.; Wu, H. Y.; Wu, D.; Wang, Y. Y.; Chang, J. H.; Zhai, Z. B.; Meng, A. M.; Liu, P. X.; Zhang, L. A.; Fan, F. Y., Toxicologic Effects of Gold Nanoparticles in Vivo by Different Administration Routes. *Int J Nanomedicine* 2010, 5, 771-81.

43. Critchley, K.; Khanal, B. P.; Gorzny, M. L.; Vigderman, L.; Evans, S. D.; Zubarev, E. R.; Kotov, N. A., Near-Bulk Conductivity of Gold Nanowires as

Nanoscale Interconnects and the Role of Atomically Smooth Interface. *Advanced Materials* 2010, 22, 2338-42.

44. Turkevich, J.; Stevenson, P. C.; Hillier, J., A Study of the Nucleation and Growth Processes in the Synthesis of Colloidal Gold. *Discuss Faraday Soc* 1951, 55-&.

45. Liu, Y. J.; Wang, Y. X.; Claus, R. O., Layer-by-Layer Ionic Self-Assembly of Au Colloids into Multilayer Thin-Films with Bulk Metal Conductivity. *Chemical Physics Letters* 1998, 298, 315-319.

46. Shim, B. S.; Zhu, J.; Jan, E.; Critchley, K.; Ho, S. S.; Podsiadlo, P.; Sun, K.; Kotov, N. A., Multiparameter Structural Optimization of Single-Walled Carbon Nanotube Composites: Toward Record Strength, Stiffness, and Toughness. *Acs Nano* 2009, 3, 1711-1722.

47. Odintsov, A. A., Schottky Barriers in Carbon Nanotube Heterojunctions. *Phys Rev Lett* 2000, 85, 150-153.

48. Kagan, V. E.; Konduru, N. V.; Feng, W. H.; Allen, B. L.; Conroy, J.; Volkov, Y.; Vlasova, I. I.; Belikova, N. A.; Yanamala, N.; Kapralov, A.; Tyurina, Y. Y.; Shi, J. W.; Kisin, E. R.; Murray, A. R.; Franks, J.; Stolz, D.; Gou, P. P.; Klein-Seetharaman, J.; Fadeel, B.; Star, A.; Shvedova, A. A., Carbon Nanotubes Degraded by Neutrophil Myeloperoxidase Induce Less Pulmonary Inflammation. *Nat Nanotechnol* 2010, 5, 354-359.

49. Thakor, A. S.; Jokerst, J.; Zavaleta, C.; Massoud, T. F.; Gambhir, S. S., Gold Nanoparticles: A Revival in Precious Metal Administration to Patients. *Nano Letters* 2011, 11, 4029-4036.

50. Kotov, N. A.; Winter, J. O.; Clements, I. P.; Jan, E.; Timko, B. P.; Campidelli, S.; Pathak, S.; Mazzatenta, A.; Lieber, C. M.; Prato, M.; Bellamkonda, R. V.; Silva, G. A.; Kam, N. W. S.; Patolsky, F.; Ballerini, L., Nanomaterials for Neural Interfaces. *Advanced Materials* 2009, 21, 3970-4004.

51. Srivastava, S.; Kotov, N. A., Composite Layer-by-Layer (Lbl) Assembly with Inorganic Nanoparticles and Nanowires. *Acc Chem Res* 2008, 41, 1831-41.

52. Shim, B. S.; Zhu, J.; Jan, E.; Critchley, K.; Ho, S.; Podsiadlo, P.; Sun, K.; Kotov, N. A., Multiparameter Structural Optimization of Single-Walled Carbon Nanotube Composites: Toward Record Strength, Stiffness, and Toughness. *Acs Nano* 2009, 3, 1711-22.

53. Zhu, J.; Shim, B. S.; Di Prima, M.; Kotov, N. A., Transparent Conductors from Carbon Nanotubes Lbl-Assembled with Polymer Dopant with Pi-Pi Electron Transfer. *J Am Chem Soc* 2011, 133, 7450-60.

54. Shim, B. S.; Zhu, J.; Jan, E.; Critchley, K.; Kotov, N. A., Transparent Conductors from Layer-by-Layer Assembled Swnt Films: Importance of Mechanical Properties and a New Figure of Merit. *Acs Nano* 2010, 4, 3725-34.

55. Shim, B. S.; Tang, Z. Y.; Morabito, M. P.; Agarwal, A.; Hong, H. P.; Kotov, N. A., Integration of Conductivity Transparency, and Mechanical Strength into

Highly Homogeneous Layer-by-Layer Composites of Single-Walled Carbon Nanotubes for Optoelectronics. *Chemistry of Materials* 2007, 19, 5467-5474.

56. Sinani, V. A.; Koktysh, D. S.; Yun, B. G.; Matts, R. L.; Pappas, T. C.; Motamedi, M.; Thomas, S. N.; Kotov, N. A., Collagen Coating Promotes Biocompatibility of Semiconductor Nanoparticles in Stratified Lbl Films. *Nano Letters* 2003, 3, 1177-1182.

57. Zhu, J.; Shim, B. S.; Di Prima, M.; Kotov, N. A., Transparent Conductors from Carbon Nanotubes Lbl-Assembled with Polymer Dopant with Pi-Pi Electron Transfer. *J Am Chem Soc* 2011, 133, 7450-7460.

58. Adler, M.; Shafer, H.; Hamilton, T.; Petrali, J. P., Cytotoxic Actions of the Heavy Metal Chelator Tpen on Ng108-15 Neuroblastoma-Glioma Cells. *Neurotoxicology* 1999, 20, 571-82.

59. Jan, E.; Pereira, F. N.; Turner, D. L.; Kotov, N. A., In Situ Gene Transfection and Neuronal Programming on Electroconductive Nanocomposite to Reduce Inflammatory Response. *Journal of Materials Chemistry* 2011, 21, 1109-1114.

Chapter 4

Aramid Nanofiber and Epoxy Composite as Multifunctional Insulation Material for Implantable Electronics

4.1 Abstract

Insulation materials are vital for the functionality and biocompatibility of the implantable electronics. Delamination of insulation materials leads to device failure. Ideally, insulation material should be chemically inert, biocompatible, and has great adhesion etc. However, many materials currently developed has limited performance in term of these desirable properties. We successfully create a nanocomposite material by combining aramid nanofiber, epoxy resin, and polyethylene glycol. The final nanocomposite demonstrates superior adhesion, biocompatibility, and antifouling property, compared to parylene C. This study opens doors to a new nanocomposite approach to design insulation materials for implantable electronics.

4.2 Introduction

Implantable microelectronic devices are crucial for advancing diagnostics and therapy of many medical conditions.[1] Cochlear implant,[2, 3] deep brain stimulation electrodes,[4] implantable neural recording devices[5, 6] exemplify some of the major achievements in this area. Recent studies on implantable electronics reveal that mechanically flexible devices might have many advantages in term of biocompatibility.[7] Therefore, much research has been devoted to create electronic circuits on flexible polymer substrates. [8-12] Advances in microfabrication technology allow us to create high density electrical components for development of the ultrasmall and multifunctional implantable electronic devices on flexible substrate.

High density and ultrasmall electrode arrays have the advantage of targeting specific tissue regions, covering larger spatial area, and acquiring high signal to noise ratio data.[13] Insulation material is the key component to achieve these desirable functionalities of the high density electrode arrays. First of all, in the multi-electrode array configuration, it is necessary to have each electrode function independently. Insulation materials are commonly applied to separation each electrodes and prevent "cross talk" from neighboring electrodes.[14] As such, the adhesion properties of the insulation materials are very important. Additionally, the electrical components of these implantable systems require isolation from the biological fluids. Otherwise, the contact of the biological fluid with electrical component would create short circuit or erode the electrical component.[15] Insulation materials serve as a barrier to protect the

electronic circuits. The insulation materials are utilized to define the specific functional sites of the electrical components that interact with surrounding tissue. The amount of the electrically active surface area in contact with the surround tissue is also crucial to the functionality of the devices. In this case, delamination of insulation materials inevitably induces other device failure modes.[16] Thus, it is important to develop reliable adhesion materials for insulation.

Insulation materials for implantable electronics also have close interaction with the surrounding tissue. Therefore, the surface properties and bioactivity of the insulation materials are key factors for tissue response and the functionality of implantable devices, in addition to the adhesion properties. For instance, anti-fouling surfaces with polyethylene glycol on biomedical devices are known for reducing the interaction between the device and biological fluid.[17] This reduction of protein absorption on the devices surface improves device acceptance by biological tissues. Drug releasing coatings on bare metal and artificial hips have been well developed and commercialized in the clinical setting to improve the long term functionality and biocompatibility of the devices.[18-20] Studies on brain implants also demonstrated that anti-inflammation coating and adhesion protein coating also improve the biocompatibility of the devices. [21, 22] Therefore, it is advantageous to have ability to modulate the surface properties of the insulation coating.

To summarize, there are several material requirements for an ideal flexible insulation material: a) electrical insulation to prevent electron transfer and short

circuiting, b) strong metal adhesion to protect the metal component under physiological condition c) strong interfacial adhesion between layers to avoid delamination, d) excellent biocompatibility for chronic applications e) excellent barrier for ion, water, and oxygen, and f) compatible with microfabrication process. Parylene C has been widely adopted as an insulation material for implantable electronics. It is deposited through the chemical vapor deposition method (CVD). The final product is uniform and pinhole free, which is ideal for the microfabrication process. Additionally, parylene C is chemically inert and has high electrical resistivity.[23] Advances in parylene synthesis also developed parylene with additional functional group. This allows further functionalization of the parylene surface, which is very attractive for biomedical applications.[16, 24] Nevertheless, due to the hydrophobic nature of parylene C, it has known complications with adhesion on metal and interfacial adhesion, which causes chronic device failure.[25-27] Several different approaches have been developed to improve the adhesion of the parylene C. High temperature and pressure treatment has been approved as an effective method to improve the adhesion of parylene C.[28] However, this method requires high temperature and pressure conditions, which could have adverse effect on the other components of the devices. Alternatively, researchers also developed parylene with additional function groups for further crosslinking and improving interfacial adhesion.[16] Nevertheless, parylene with additional functional groups is not readily available commercially yet. Many polymeric materials are also considered as an insulating layer, including Telfon,[29] epoxy resin,[30] and polyimide.[31] However, there

are very limit studies related to systematic evaluation of the adhesion performance of these materials.

Recent developments in aramid nanofiber dispersion offer a new framework to design composite materials with tailored functionalities.[32, 33] By dissolution of aramid bulk fibers in solvents, aramid nanofibers in dimethyl sulfoxide (DMSO) can be controlled from 3 nm to 30nm in diameter.[32] The uniform dispersion of the nanofibers in solution and the branched structures of the nanofibers allow us to create uniform and highly porous film via spin coating. Moreover, the uniform and porous film from ANF can serve a platform for other material components to filtrate into the film. The utilization of the spin coating technique also offers precise and versatile control over the thickness and composition of the final composite.

Here, we propose a nanocomposite approach to create multifunctional insulation materials for implantable electronics. We developed nanocomposite based on aramid nanofiber and epoxy resin. Systemic evaluation of adhesion properties between this nanocomposite and parylene C demonstrates that this nanocomposite exhibits a superior adhesion properties than parylene C. We also demonstrates the surface properties of the nanocomposite can be easily modulated by additional functional polymers.

4.3 Materials and Methods

Right-twisted bulk Kevlar 69 was purchased from Thread Exchange. System 2000 Epoxy Resin was purchased from Fibre Glast Developments Corporation. All other chemicals were obtained from Sigma-Aldrich

4.3.1 ANF Nanofiber Dispersion

1g of purchased aramid thread was dissolved in 100ml of DMSO with 4 g of KOH to prepare a 10mg/ml ANF nanofiber dispersion. The solution was stirred in a sealed container at room temperature for a week to ensure the complete dissolution of the nanofiber.

4.3.2 ANF/Epoxy Nanocomposite

The nanocomposite film was created through a spin-coating assisted deposition process. 1ml of as-prepared ANF nanofiber dispersion was spin-coated on a 1.5-inch by-1.5 inch silicon oxide wafer at 1000 rpm. After spin coating, the film was rinsed with water to remove the excess DMSO in the film, then spin-coated at 1000 rpm. After rinsing with water, 1 ml of 3% epoxy resin in acetone was spin-coated on top of the ANF nanofiber film and dried in the oven at 100 degrees Celsius for 1 min. In order to achieve a pinhole-free film, the epoxy resin solution was spin-coated again after the first layer of the epoxy resin solution. The process was repeated

until the desired film thickness was achieved. Typically, six repeated cycles results in a 3 um thick film.

4.3.3 PEG Functionalized ANF/Epoxy Nanocomposite

To functionalize the surface, 2mg/ml PEG solution in water is spin-coated on the top of the as-prepared ANF/epoxy nanocomposit, then cured in the oven at 60 degree Celsius for 2 hours.

4.3.4 Interdigitated Electrode Fabrication

The procedure to fabricate interdigitated electrodes is described previously. Briefly, after assembling the bottom layer of the ANF/epoxy film, positive photoresist (SPR220-3.0, Rohm Haass) is spin-coated and developed to create the outline of the metal electrodes. Then Cr/Au/Cr (20nm/400nm/20nm) is deposited by an E-beam evaporator (Enerjet Evaporator, Lesker) and lifted off in acetone. Then the top layer of the ANF/epoxy film is deposited on top of the liftoff metal structures. Positive photoresist (SPR-220-7.0, Rohm Haas) is spin-coated and developed again for the overall layout of the electrodes. Then the ANF/epoxy film is etched in oxygen plasma with 10% SF_6 gas. Lastly, platinum microwire is attached on the bond pads of the electrodes by conductive silver epoxy. For parylene C testing, 3 um parylene film is

deposited instead of ANF/epoxy film. Parylene is etched in pure oxygen plasma, instead of oxygen plasma with 10% SF6 gas.

4.3 4 Metal Adhesion Test

ANF/epoxy nanocomposite first deposits on E-beam evaporated metals Cr/Au/Cr (20nm/400nm/20nm). Then the ANF/epoxy film is etched in oxygen plasma with 10% SF6 gas to selectively open a square shape to expose the metals underneath. Parylene C film is etched in pure oxygen plasma. To ensure experimental accuracy, both etched ANF/epoxy nanocomposite and parylene C film are etched in Cr etchant for 30 seconds simultaneously, then rinsed in water for 5 minutes.

4.3.5 Electrochemical Impedance Spectroscopy (EIS)

The impedance is carried out on an Autolab PGSTAT 12; Frequency Response Analyzer software (EcoChemie, Utrecht, Netherlands) is used to record impedance spectra of the electrodes. There are two electrodes in the interdigitated electrode design. For interfacial impedance, the working electrode is connected to one of the electrodes. The counter/reference is connected to another electrode. An AC sinusoidal signal of 25 mV in amplitude was used to record the impedance over a frequency range of 10−32000 Hz. For transient impedance, the working electrode is connected to one of the electrodes. The counter electrode is connected to a gold foil

immersed in PBS, and an Ag/AgCl reference electrode is immersed in phosphate saline buffer (PBS).

4.3.6 Long Term Soaking Test

For measuring long term performance, both ANF/epoxy and parylene C coated interdigitated electrodes are soaked in 1x phosphate saline buffer (PBS) at 37 degree Celsius. The impedance of the interdigitated electrodes is measured prior to soaking test in the PBS. Then the impedance is measured again after soaking in PBS for 45 days.

4.3.7 Protein Resistance Test

1ml of 1mg/ml FITC conjugated albumin in water solution is casted on the PEG functionalized ANF/epoxy nanocomposite and the plain ANF/epoxy nanocomposite for 2 hours. Then both substrates are rinse in water for 10 minutes. After rinsing, both substrates are imaged under an optical microscope with a FITC filter.

4.3.8 Scanning Electron Microscopy (SEM)

LbL samples were deposit on a silicon wafer. SEM images were obtained using a FEI Nova Nanolab SEM at 10kV accelerating voltage.

4.4 Result and Discussion

To validate our nanocomposite approach to create superior insulation materials, we rationally design a nanocomposite based on ANF and epoxy resin. The design principle is based on filtration of epoxy resin solution into the porous nanofiber structure of the ANF reported previously. The process is illustrated in Figure 1A. Briefly, ANF dispersion in DMSO is spin coated on a substrate, and then the DMSO in the spin coated thin film is exchanged out of the thin film in a water bath. The excess water is removed by quick spin coating after solvent exchange. Then epoxy solution is spin coated on top of the spun ANF thin film. The process is repeated in a cycle to create films with desired thickness.

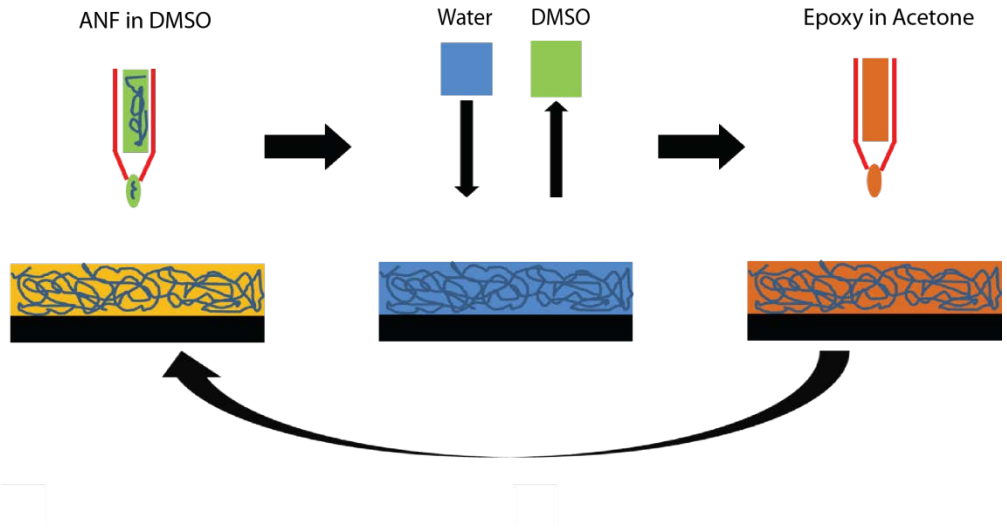

Figure 4.1 Illustration of the spin coating process

From the cross section SEM image of the six bilayer ANF epoxy film, we can estimate the thickness of the average ANF/epoxy layer is about 500nm (Figure 1B). The surface morphology of the ANF epoxy film is observed under the SEM. We observe a uniform surface with nanoscale fibrous structures (Figure 1C). The primary function of the insulation materials is to serve as a barrier between the electrical components and the physiological fluid. Therefore, it is crucial for the epoxy resin to completely filtrate into the ANF network. From the cross section SEM image, we observe the cross section is uniform and complete filled with epoxy (Figure 1B). Further experiments also are conducted to understand this layered spin coating process. We discover that it is important to spin coat the epoxy solution while the water is still present in the porous ANF network. The water serves as a support for the porous ANF network and prevents the network collapse. This will allow the diffusion of the epoxy solution into the ANF network. To illustrate this point, the epoxy

solution is spin coated on the ANF thin film after removing water. We can clearly observe the epoxy solution is on top of the ANF thin film, not within the ANF thin film (Figure 1E). Also, we further examined the cross section of the six layer ANF thin film without any epoxy solution (Figure1D). We observed the thickness of the film is significantly smaller than the ANF/epoxy film. This further indicates the collapse of the ANF network after drying without epoxy resin filler.

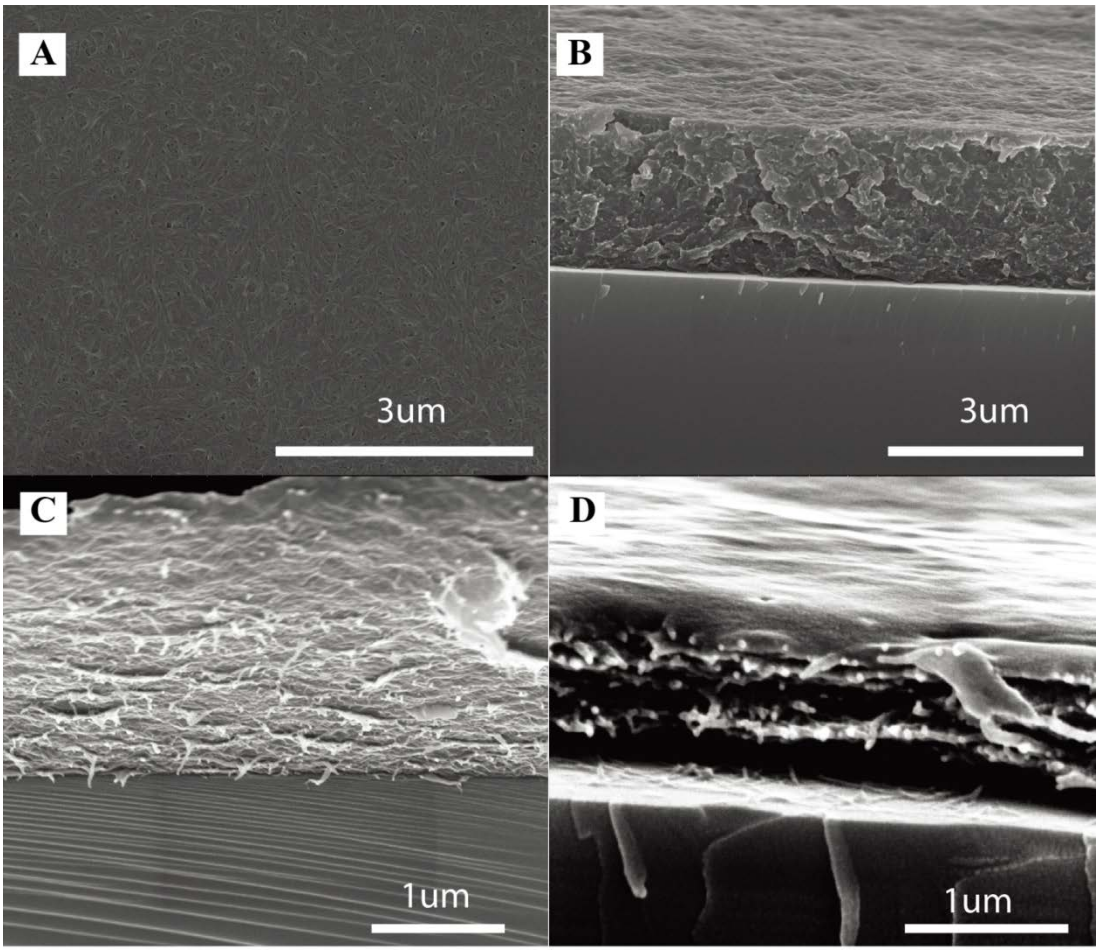

Figure 4.2 (A) SEM image of ANF/epoxy composite, six layers (B) SEM image of the cross section of ANF/epoxy composite (C) SEM image of the cross section of layered ANF film (E) SEM image of the cross section of the dried ANF film with epoxy

Adhesion performance of the materials for microfabrication devices can be separated in two categories: metal adhesion and interfacial adhesion. Both types of

adhesion performance are crucial for device functionality. Metal adhesion refers to the adhesion strength between the insulation layer and the metal layer. The insulation layer typically defines the critical portion of the metal layer that is exposed to the tissue. If the adhesion strength between the insulation layer and metal layer is weak, it will inevitably lead to delamination and expose unintended metal layer to the surrounding tissue. Therefore, the foremost objective of this study is to compare the metal adhesion between the ANF/epoxy nanocomposite and parylene C.

Both the ANF/epoxy nanocomposite and parylene are deposited on silicon substrates coated with triple metal layers Cr/Au/Cr (20nm/400nm/20nm). Au has a known issue of poor adhesion with other material, such as silicon. Therefore, Cr is commonly used in the microfabrication process to improve adhesion. Moreover, the use of the Cr layer here will offer us to the ability to quickly observe the insulation layer adhesion strength. After the deposition of the insulation films, photolithography technique is used to define an area on the films, then both films are etched in plasma to expose the Cr layers underneath. After the plasma process, both films are soaked in phosphate saline buffer (PBS) solution for 12 hours at room temperature. Both films are etched in Cr etchant for 30 second, and then observed under optical microscope. If the adhesion between the film and metal is strong, the Cr etchant would only have limited access to the Cr surface, especially the area underneath the film. However, if delamination occurs, the Cr etchant would have much more access to the Cr surface underneath the film and we would observe a fastest etching rate. The Au underneath the Cr provides good contrast for observation under optical

microscope. The optical microscopy images after etching are shown in Figure 2. In comparing the etch rate of Cr for both film, we can clearly observe a faster etch rate for the parylene C coating substrate than the ANF/epoxy composite. This indicates a stronger metal adhesion for the ANF/epoxy composite over parylene C

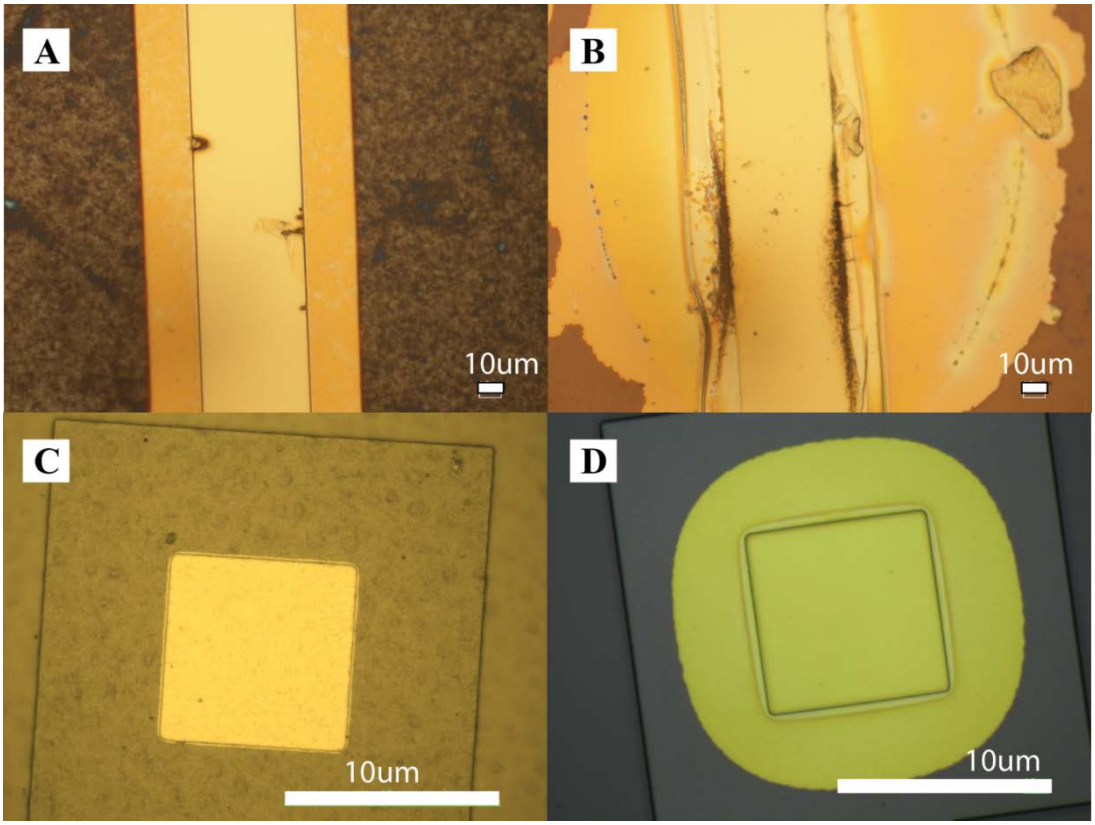

Figure 4.3 Metal adhesion test (A) Wet Cr etch of ANF/epoxy composite, rectangular strip opening (B) Wet Cr etch of parylene, rectangular strip opening (C) Wet Cr etch of ANF/epoxy composite, square opening (D) Wet Cr etch of parylene, square opening

The metal adhesion test provided preliminary result on the superior adhesion performance of the ANF/epoxy composite. Nevertheless, the adhesion performance of the ANF composite requires more rigorous test model to further validate its purpose in practical applications. Therefore, we design an interdigitated electrode (IDE) approach to further test the long term adhesion performance.

The IDE structure is illustrated in Figure 3. Simply, the IDE design involves two electrodes in a closed spatial arrangement sandwiched between two layers of the insulation materials. This type of layered configurations is common in bioelectronic devices. In this configuration, there are two interfacial boundary layers, shown in Figure 3A . One is the polymer-polymer interface. If this interface has poor adhesion, it will increase the cross-talk between the electrodes, and cause dramatic decrease in the lateral impedance, $Z_{lat.}$ Another interface is the metal-polymer interface, which was previously illustrated. The delamination of the metal-polymer interface also can cause the decline of the $Z_{lat.}$ Therefore, the Z_{lat} is a highly sensitive measurement of the interfacial adhesion, especially from microstructures.

In order to compare the Z_{lat} of parylene and ANF/epoxy composite, we must fabricate the IDE on both films. We purposely design an ultrasmall and high aspect ratio IDE electrodes (1.5um width and 700 um long) to test the photolithography limit of the both films (Figure 3B). Parylene is known for its compatibility with photolithography process, thus it is widely accepted as insulation materials for implantable electronics. Therefore it is important for us to compare the ability to

create microscale structures on parylene and ANF/epoxy composite. The overall structure of the IDE on parylene is shown in Figure 3B, demonstrates a successfully fabricated IDE structures. The details of the IDE fabrication are included in the Methods section. Then we further examine the fine electrode structures by optical microscopy. Comparing Figure 3C and 3D, we can conclude that the same microscale structures can be fabricated on ANF/epoxy composite as on parylene, although we observe more roughness of the ANF/epoxy comparing to parylene under optical microscope.

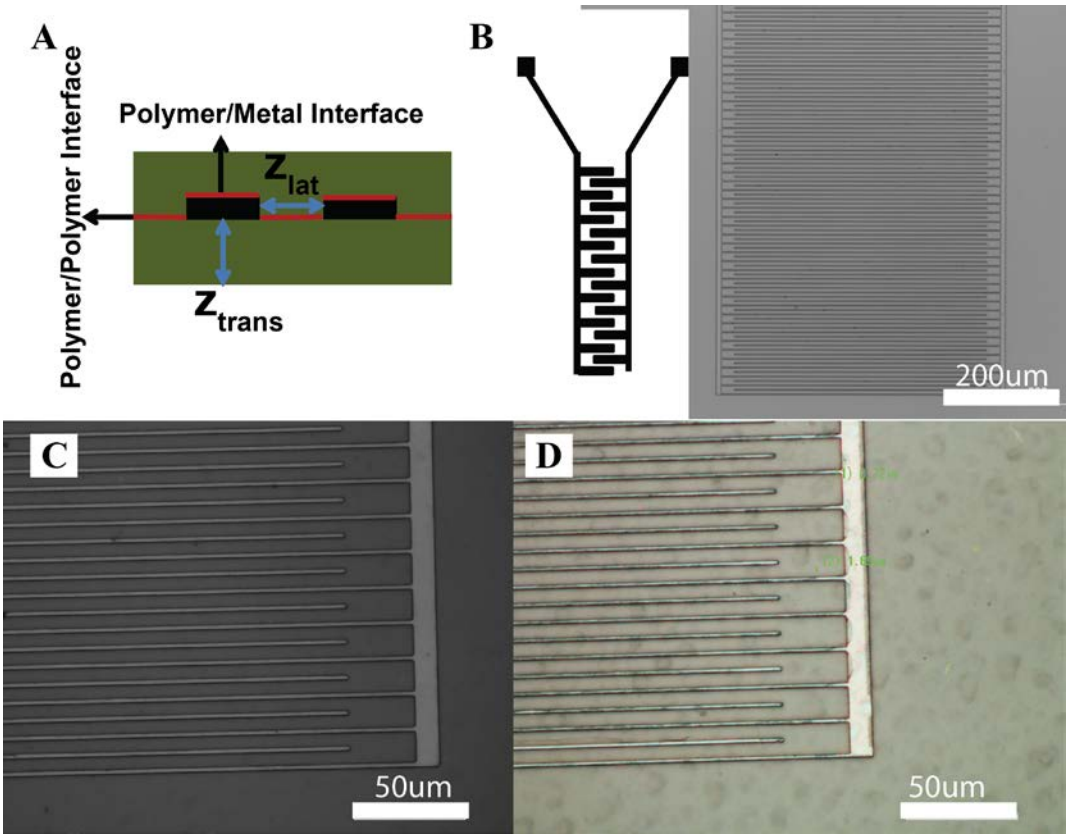

Figure 4.4 (A) Illustration of the interfaces in IDE (B) Fabricated IDE structure (C) Zoom in IDE structure on parylene film (D) Zoom in IDE structure on ANF/epoxy composite

After we establish the successful protocol to fabricate the IDE on both substrates, we conduct long term soak test to compare the adhesion performance of parylene and ANF/epoxy composite. The long term soak test is conducted in phosphate saline buffer (PBS) at 37 C. 16 IDE electrodes for from each type of the films were soaked in the PBS for 45 days in a temperature controlled water bath.

Prior to the soaking test, the impedance of the electrodes in dry state is also measured. The measurement protocol is also described in the Materials and Methods section. In Figure 4A, it shows the Z_{lat} measurements of parylene and ANF/epoxy after 45 days of soak testing. For comparison purpose, we also plot the dry state Z_{lat} measurement. Because there is no difference in dry Z_{lat} measurement for parylene and ANF/epoxy composite, only one dry Z_{lat} measurement is plotted on the graph. The dry impedance measurement follows typical pure capacitor behavior in a circuit analogy. As we observe in Figure 4A, the dry impedance in low frequency is extremely high, in the Gohm range. This indicates that the electrodes are well insulated from each other by the thin films. The magnitude of the capacitance is positively proportional to the frequency. And the magnitude of the impedance is inversely proportional to the capacitance. Therefore, the impedance of the system decreases as the frequency increase. Moreover, the dry impedance measurement is linearly correlated with the frequency on a logarithmic scale plot. This also indicates a capacitor behavior since capacitors follow a power law relationship with frequency. All three impedance measurements follow the same trend over frequency. However, the Z_{lat} measurement in the lower frequency after soak test decreases one or two magnitudes compare to the dry impedance test. This is expected because the long term soak test will induce compromises in the interface. Furthermore, we observed that the impedance over frequency does not follow a linear trend on the logarithmic scale after the soak test in either case. As we mentioned previously, the system does not behavior as a pure capacitor anymore and additional circuit components need to be added to describe the

system. This further indicates the compromise in the interface. Nevertheless, comparing the Z_{lat} measurements of the parylene and ANF/epoxy composite, we observe that the Z_{lat} of the parylene is significantly lower than ANF/epoxy composite across the frequency spectrum. This is a strong indication that ANF/epoxy composite has a better adhesion performance than parylene. In addition to $Z_{lat,}$ Z_{trans} are also measured to ensure the overall integrity of the IDE. In Figure 4B, we can observe that both IDEs have the same Z_{trans} , which domenstrates that the difference in Z_{lat} is from the interface of the IDEs , not the overall IDE structures.

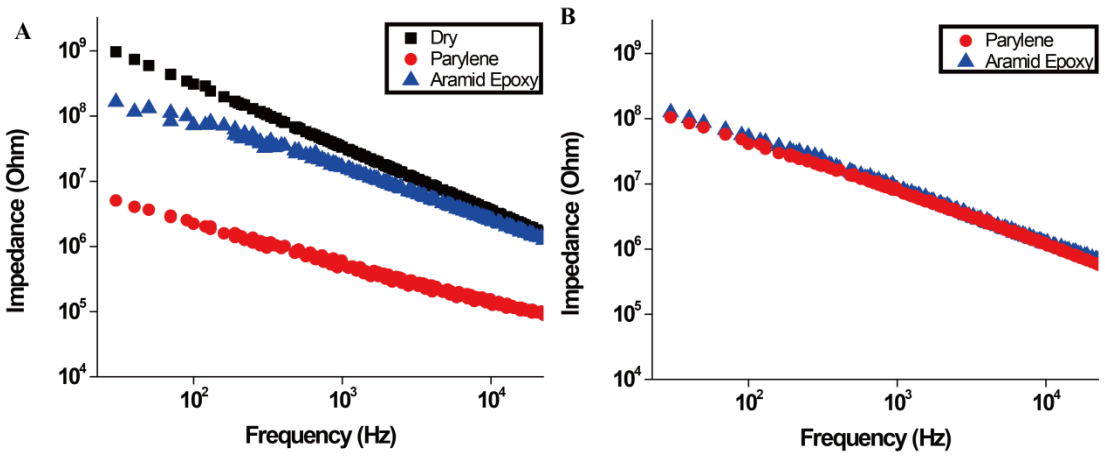

Figure 4.5 (A) Lateral impedance of different IDEs (B) Transverse impedance of different IDEs

After establishing the superior adhesion properties of the ANF/epoxy composite, we should address concerns of the potential toxicity issue and biocompatible issue relate to this nanocomposite. Therefore, we cultured NG108

hydrid neuroblastoma cells on both ANF/epoxy composite (Figure 6A) and parylene (Figure 6B) to understand cell viability and adhesion. In Figure 6A, we observe that the NG108 cells can attach and differentiate on the ANF/epoxy composite very well. However, on the parylene surface, we observe very limited cell attachment, with the majority of the cells suspended in the culture medium. The few cells attached on the parylene surface also appear to be unhealthy. This demonstrates that the ANF/epoxy composite is indeed biocompatible to the general cell population.

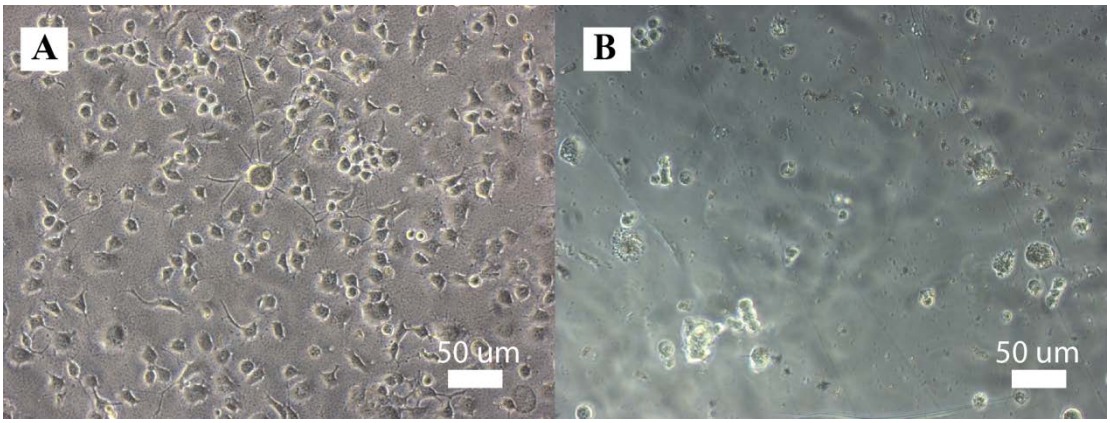

Figure 4.6 (A) NG108 cell culture on ANF/epoxy composite (B) NG108 cell culture on parylene

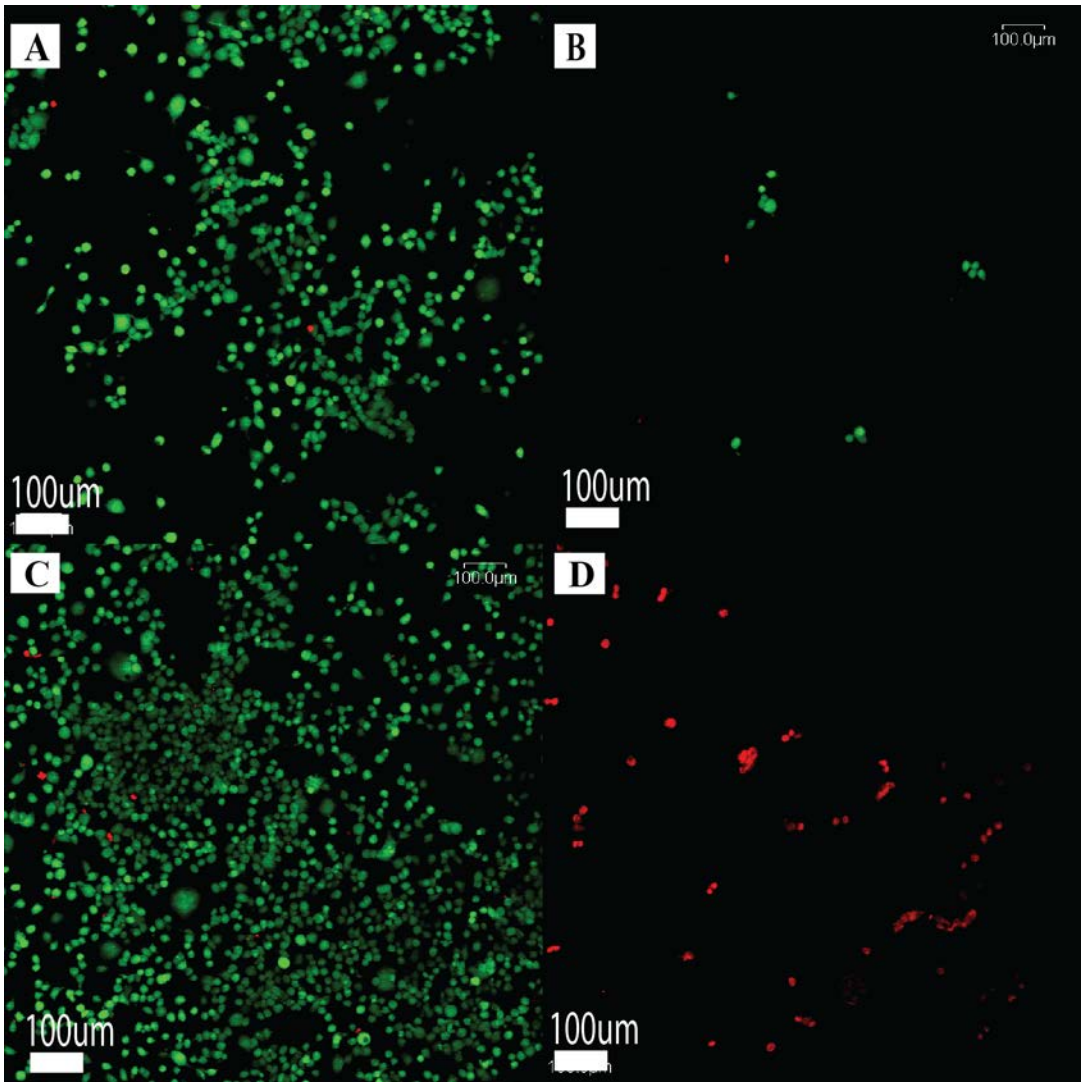

Figure 4.7 Live/Dead Assay of NG108 cells on various substrates. (Green:Live Red: Dead) (A) NG108 cell culture on tissue culture coverslip glass (B) NG108 cell culture on parylene (C) NG108 cell culture on ANF/epoxy (D) NG108 cell culture on ANF/epoxy treated with 70% ethanol solution.

Live/Dead assay are also performed to understand viability of the cells on the substrates. NG108 cells are cultured three different substrates: regular cover slip glass

(Figure 4.7 A), parylene coated on glass (Figure 4.7 B), ANF/epoxy coated on glass (Figure 4.7 C, D). Compare Figure 4 A and C, we observe high density live cells with a small fraction of dead cell (less than 1%) on ANF/epoxy substrate and regular glass substrate. On the parylene substrate, we observe low cell density and higher percentage of dead cells. The limited cell attachment on parylene, prohibits cell proliferation and leads to cell dead. The cells in Figure 4.7D are treated with ethanol to serve as a negative control for the assay. In Figure 4.7D, we observe no live cells after ethanol treatment.

In addition to establish the superior adhesion properties and biocompatibility of ANF/epoxy composite, we further explore the possibility of creating multifunctional insulation material through ANF network. As we mentioned previously, anti-fouling property is very attractive for materials in implantable applications. Here, we intend to demonstrate that the possibility of functionalized ANF/epoxy composite with PEG by simple filtration process into the ANF network. To functionalized PEG onto ANF/epoxy composite, we simply spin-coat an additional layer of PEG solution in water after the final layer of epoxy solution during composite fabrication. Afterwards, the entire composite is dried in the oven at 60 degree Celsius to remove excess water. Then we conduct protein absorption test by fluorescent human albumin protein on both PEG functionalized and non-functionalized ANF/epoxy composite. Prior to the absorption test, both composite is rinsed in PBS to remove excess PEG, then the albumin solution is casted on both composite and stored at room temperature for 12 hours. After 12 hours, both

composites are rinsed in PBS again to remove the excess protein, then observed under an optical microscopy with FITC filter (Figure 5C and Figure 5D). Figure 5D is the fluorescent filtered optical image. The substrate on the left is the non-functionalized ANF/epoxy composite and on the right is the PEG-functionalized substrate. We observe very strong fluorescent intensity on the non-functionalized substrate, which indicates protein absorption. On the contrary, we observed minimal fluorescent intensity on the composite with PEG. This indicates that we can successfully functionalize additional polymer to the ANF network to create multifunctional composite.

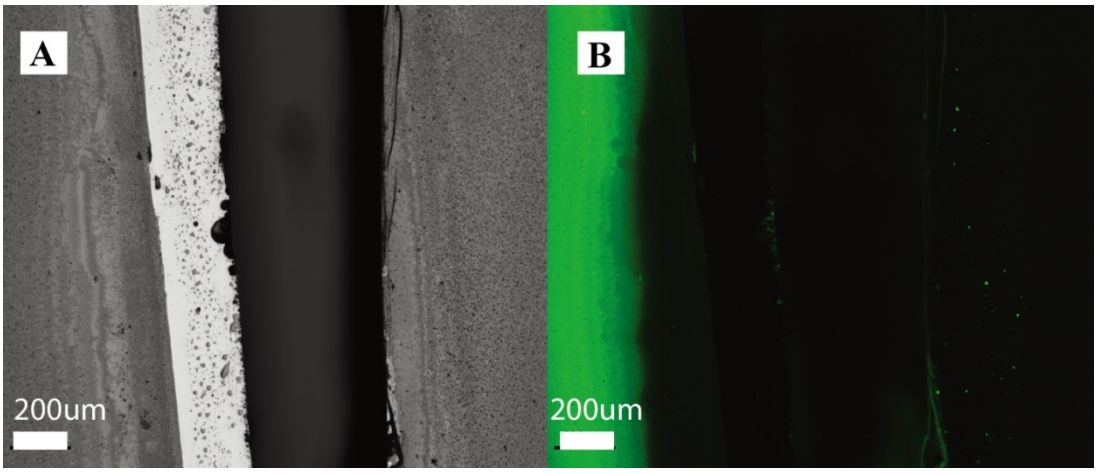

Figure 4.7 (A) Optical image of ANF/Epoxy composite and ANF/epoxy/PEG composite (B) fluorescent image of ANF/epoxy composite and ANF/epoxy/PEG composite after albumin absorption

4.5 Conclusion

We demonstrate the possibility of utilizing ANF as a frame network to create multifunctional insulation materials. We conduct multiple adhesion tests to systematically evaluate the adhesion performance of ANF/epoxy composite. The results from metal etching test and long term soak test indicate that ANF/epoxy composite indeed has a superior adhesion performance than parylene. Neural cell culture experiments are also performed to validate the biocompatibility of the ANF/epoxy composite. Lastly, the robustness of the ANF network allows us to create gradient composite with epoxy and PEG. Protein absorption test indicates that PEG can be successfully functionalized on top of the epoxy resin within the ANF network. This demonstrates that this approach of utilized ANF network can open up opportunities for multifunctional material design. Although our study revealed this new composite approach to design superior insulation materials, further studies on using this ANF/epoxy for functional implantable electronics are required to establish the feasibility of this composite approach for *in vivo* applications.

4.6 References

1. Berger, T. W.; Baudry, M.; Brinton, R. D.; Liaw, J. S.; Marmarelis, V. Z.; Park, A. Y.; Sheu, B. J.; Tanguay, A. R., Brain-Implantable Biomimetic Electronics as the Next Era in Neural Prosthetics. *P Ieee* 2001, 89, 993-1012.

2. House, W. F., Cochlear Implants. *Ann Oto Rhinol Laryn* 1976, 85, 3-93.

3. House, W. F., Cochlear Implants - Its Time to Rethink. *Am J Otol* 1994, 15, 573-587.

4. Perlmutter, J. S.; Mink, J. W., Deep Brain Stimulation. *Annu Rev Neurosci* 2006, 29, 229-257.

5. Wise, K. D., Silicon Microsystems for Neuroscience and Neural Prostheses. *Engineering in Medicine and Biology Magazine, IEEE* 2005, 24, 22-29.

6. Maynard, E. M.; Nordhausen, C. T.; Normann, R. A., The Utah Intracortical Electrode Array: A Recording Structure for Potential Brain-Computer Interfaces. *Electroencephalography and clinical neurophysiology* 1997, 102, 228-39.

7. Polikov, V. S.; Tresco, P. A.; Reichert, W. M., Response of Brain Tissue to Chronically Implanted Neural Electrodes. *J Neurosci Meth* 2005, 148, 1-18.

8. Hollenberg, B. A.; Richards, C. D.; Richards, R.; Bahr, D. F.; Rector, D. M., A Mems Fabricated Flexible Electrode Array for Recording Surface Field Potentials. *J Neurosci Methods* 2006, 153, 147-53.

9. Fan, W.; Maesoon, I.; Euisik, Y. In *A Flexible Fish-Bone-Shaped Neural Probe Strengthened by Biodegradable Silk Coating for Enhanced Biocompatibility*, Solid-State Sensors, Actuators and Microsystems Conference (TRANSDUCERS), 2011 16th International, 5-9 June 2011; 2011; pp 966-969.

10. Krulevitch, P.; Polla, D. L.; Maghribi, M. N.; Hamilton, J. Flexible Electrode Array for Artificial Vision. 2001-992248

2003097166, 20011116., 2003.

11. Stieglitz, T.; Gross, M., Flexible Biomems with Electrode Arrangements on Front and Back Side as Key Component in Neural Prostheses and Biohybrid Systems. *Sens. Actuators, B* 2002, B83, 8-14.

12. Takeuchi, S.; Suzuki, T.; Mabuchi, K.; Fujita, H., 3d Flexible Multichannel Neural Probe Array. *Journal of Micromechanics and Microengineering* 2004, 14, 104-107.

13. Wise, K. D.; Angell, J. B.; Starr, A., An Integrated-Circuit Approach to Extracellular Microelectrodes. *Biomedical Engineering, IEEE Transactions on* 1970, BME-17, 238-247.

14. Wilke, R. G. H.; Moghadam, G. K.; Lovell, N. H.; Suaning, G. J.; Dokos, S., Electric Crosstalk Impairs Spatial Resolution of Multi-Electrode Arrays in Retinal Implants. *J Neural Eng* 2011, 8.

15. Bowman, L.; Meindl, J. D., The Packaging of Implantable Integrated Sensors. *Ieee T Bio-Med Eng* 1986, 33, 248-255.

16. Seymour, J. P.; Elkasabi, Y. M.; Chen, H. Y.; Lahann, J.; Kipke, D. R., The Insulation Performance of Reactive Parylene Films in Implantable Electronic Devices. *Biomaterials* 2009, 30, 6158-67.

17. Onuki, Y.; Bhardwaj, U.; Papadimitrakopoulos, F.; Burgess, D. J., A Review of the Biocompatibility of Implantable Devices: Current Challenges to Overcome Foreign Body Response. *Journal of diabetes science and technology* 2008, 2, 1003-15.

18. Suzuki, T.; Kopia, G.; Hayashi, S.; Bailey, L. R.; Llanos, G.; Wilensky, R.; Klugherz, B. D.; Papandreou, G.; Narayan, P.; Leon, M. B.; Yeung, A. C.; Tio, F.;

Tsao, P. S.; Falotico, R.; Carter, A. J., Stent-Based Delivery of Sirolimus Reduces Neointimal Formation in a Porcine Coronary Model. *Circulation* 2001, 104, 1188-93.

19. Scheller, B.; Hehrlein, C.; Bocksch, W.; Rutsch, W.; Haghi, D.; Dietz, U.; Bohm, M.; Speck, U., Treatment of Coronary in-Stent Restenosis with a Paclitaxel-Coated Balloon Catheter. *The New England journal of medicine* 2006, 355, 2113-24.

20. Zilberman, M.; Elsner, J. J., Antibiotic-Eluting Medical Devices for Various Applications. *J Control Release* 2008, 130, 202-215.

21. He, W.; McConnell, G. C.; Bellamkonda, R. V., Nanoscale Laminin Coating Modulates Cortical Scarring Response around Implanted Silicon Microelectrode Arrays. *Journal of neural engineering* 2006, 3, 316-26.

22. He, W.; McConnell, G. C.; Schneider, T. M.; Bellamkonda, R. V., A Novel Anti-Inflammatory Surface for Neural Electrodes. *Adv. Mater.* 2007, 19, 3529-3533.

23. Meng, E.; Tai, Y. C., Parylene Etching Techniques for Microfluidics and Biomems. *Proc Ieee Micr Elect* 2005, 568-571.

24. Lahann, J., Vapor-Based Polymer Coatings for Potential Biomedical Applications. *Polym Int* 2006, 55, 1361-1370.

25. Yasuda, H.; Yu, Q. S.; Chen, M., Interfacial Factors in Corrosion Protection: An Eis Study of Model Systems. *Prog Org Coat* 2001, 41, 273-279.

26. Yamagishi, F. G., Investigation of Plasma-Polymerized Films as Primers for Parylene-C Coatings on Neural Prosthesis Materials. *Thin Solid Films* 1991, 202, 39-50.

27. Sharma, A. K.; Yasuda, H., Effect of Glow-Discharge Treatment of Substrates on Parylene-Substrate Adhesion. *J Vac Sci Technol* 1982, 21, 994-998.

28. Metzen, R.; Stieglitz, T., The Effects of Annealing on Mechanical, Chemical, and Physical Properties and Structural Stability of Parylene C. *Biomed Microdevices* 2013, 15, 727-735.

29. Nicolelis, M. A.; Dimitrov, D.; Carmena, J. M.; Crist, R.; Lehew, G.; Kralik, J. D.; Wise, S. P., Chronic, Multisite, Multielectrode Recordings in Macaque Monkeys. *Proceedings of the National Academy of Sciences of the United States of America* 2003, 100, 11041-6.

30. Xindong, L.; McCreery, D. B.; Carter, R. R.; Bullara, L. A.; Yuen, T. G. H.; Agnew, W. F., Stability of the Interface between Neural Tissue and Chronically Implanted Intracortical Microelectrodes. *Rehabilitation Engineering, IEEE Transactions on* 1999, 7, 315-326.

31. Stieglitz, T., Hansjorg, B., Schuettler, M. and Meyer, J.-U, Micromachined, Polyimide-Based Devices for Flexible Neural Interfaces. *Biomedical Microdevices* 2000, 2, 283-294.

32. Yang, M.; Cao, K. Q.; Sui, L.; Qi, Y.; Zhu, J.; Waas, A.; Arruda, E. M.; Kieffer, J.; Thouless, M. D.; Kotov, N. A., Dispersions of Aramid Nanofibers: A New Nanoscale Building Block. *Acs Nano* 2011, 5, 6945-6954.

33. Cao, K. Q.; Siepermann, C. P.; Yang, M.; Waas, A. M.; Kotov, N. A.; Thouless, M. D.; Arruda, E. M., Reactive Aramid Nanostructures as High-

Performance Polymeric Building Blocks for Advanced Composites. *Adv Funct Mater* 2013, 23, 2072-2080.

Chapter 5

Flexible High Performance Nanocomposite Microelectrodes for Neural Interface

5.1 Abstract

Mechanical flexibility of electrode materials is important to mitigate the chronic inflammation response of implantable neural electrodes. Gold nanocomposites featuring low Young's modulus, high electrical conductivity, and excellent electrochemical performance could be a promising high performance material for neural electrodes. Nevertheless, traditional flexible insulators suffer from inferior adhesive properties, which ultimately lead to devices failure. Aramid nanofiber composites have demonstrated excellent adhesion on metal, and could improve the chronic functionality of implantable devices. This study demonstrates the direct integration of two high performance nanocomposite materials to fabricate microelectrodes, as well as validates the *in vivo* functionality of the integrated nanocomposite electrode

5.2 Introduction

Implantable electrodes have been the essential technological component for many neural interface systems.[1-6] Recent developments in brain computer interface offer us the possibility to extract neural signals from the brain and control external devices.[7-9] This could have tremendous impact on patients suffering from neural diseases and traumas. Particularly, recording electrodes are commonly used to detect neural signals and transport this signal to external electrical components.[5] The performance and reliability of implantable recording electrodes are crucial for maintaining an efficient and sustainable brain computer interface.[10]

Metal microwire electrodes and silicon microelectrodes have achieved enormous success in early clinical applications. Metal microwire arrays were first developed for animal experiments due to the simplicity of array assembly and high electrical conductivity of the metals.[11-14] After the development of metal microwire arrays, the next technological innovation in microelectrodes came from the silicon based microfabrication process,[15-18] when more precise and sophisticated electrode arrays were required. Indeed, we have much control over shape, size, position, density, and materials of electrodes today. Advanced functionalities, such as wireless transmission[19, 20] and on-chip signal processing[21] are also available. Nevertheless, neither type of the electrode sustains its functionality for more than a year (for over a year? For a few months? How long do they normally last?).[10] This issue of chronic device failure has significantly hindered the future development of the brain computer interface and its applications in clinical setting.

There are many failure modes for implantable recording electrodes. This discussion focuses on two major device failure modes: mechanical mismatch at the tissue/electrode interface and delamination of insulating materials. Mechanical mismatch between the electrode and brain tissue has been recognized as a key issue for chronic device functionality.[10, 22] Brain tissue is very soft and under dynamic motion constantly.[23-25] Typical metal or silicon electrodes are stiff materials and have large mechanical mismatch with brain tissue. This mechanical mismatch will consistently interrupt the brain-blood barrier and initiate immune response.[22, 24] Chronic immune response will inevitably lead to the formation of scar tissue and create barriers between electrodes and targeted neurons.[26] Moreover, in order to obtain neural signals from a single neuron, the electrode has to be in close spatial arrangement with the targeted neuron, a distance of approximately 100 um.[27] Rigid electrodes are more likely to damage nearby neurons during dynamic movement of the brain. This also contributes to signal loss and recording inconsistency of chronic neural electrodes. Flexible electrodes have been developed to mitigate this mechanical mismatch.[28-33] These electrodes typically are fabricated by using polymers as a backbone and metal thin film as an electrical conductor. These types of electrodes are much more flexible than silicon or metal wires. In addition , the combined mechanical properties of polymer and metal are still much higher than brain tissue. Nanocomposite materials could be an alternative approach to fabricating electrodes. By incorporating conductive nanomaterials into a polymer matrix, it is possible to create flexible nanocomposites with high electrical conductivity. Recent

studies have demonstrated that tailored nanocomposites can have high electrical conductivity,[34] high electrochemical performance,[35] and the feasibility of fabricating neural electrodes.[36] Particularly, gold nanoparticle (Au NP) nanocomposites have exhibited both high electrical conductivity and outstanding interfacial electrochemical properties.[37] These properties indicate that gold nanocomposites could be an excellent choice for neural electrode material. However, gold nanocomposites have not yet been fabricated into *in vivo* neural electrodes.

In addition to mechanical mismatch, delamination of the insulating material can also contribute to device failure, especially for flexible devices.[38] Insulating materials are crucial for device functionality because they define the electrical active area of the neural electrodes. If the delamination occurs at the electrical/insulating material interface, the active area of the electrode will be altered. This greatly affects the signal reception of the electrodes and leads to device failure. Moreover, engineering flexible neural electrodes, requires not only the electrically conductive materials to be flexible, but also the insulating materials. It is very important to develop flexible materials with great adhesion. Parylene is a common material for flexible electronics; however, it has challenges with metal adhesion due to its hydrophobic nature.[39-41] Nanocomposites based on aramid nanofibers (ANF) and epoxy have shown great adhesion and biocompatibility in recent studies. Thus, it is advantageous to incorporate ANF/epoxy nanocomposites into functional neural electrodes.

In this study, we integrate both Au NP nanocomposites and ANF nanocomposites to create all nanocomposite electrodes. We first establishe the

protocol to fabricate nanocomposite electrodes, then we demonstrate its functionality *in vivo*.

5.3 Materials and Method

Right-twisted bulk Kevlar 69 was purchased from Thread Exchange. System 2000 Epoxy Resin was purchased from Fibre Glast Developments Corporation. All other chemicals were obtained from Sigma-Aldrich

5.3.1 ANF Nanofiber Dispersion

1g of purchased aramid thread was dissolved in 100ml of DMSO with 4 g of KOH to prepare a 10mg/ml ANF nanofiber dispersion. The solution was stirred in a sealed container at room temperature for a week to ensure the complete dissolution of the nanofiber.

5.3.2 ANF/Epoxy Nanocomposite

The nanocomposite film was created through a spin-coating assisted deposition process. 1ml of as-prepared ANF nanofiber dispersion was spin-coated on a 1.5-inch by-1.5 inch silicon oxide wafer at 1000 rpm. After spin coating, the film was rinsed with water to remove the excess DMSO in the film, then spin-coated at 1000 rpm. After rinsing with water, 1 ml of 3% epoxy resin in acetone was spin-

coated on top of the ANF nanofiber film and dried in the oven at 100 degrees Celsius for 1 min. In order to achieve a pinhole-free film, the epoxy resin solution was spin-coated again after the first layer of the epoxy resin solution. The process was repeated until the desired film thickness was achieved. Typically, six repeated cycles results in a 3 um thick film.

5.3.3 Synthesis of Gold Nanoparticles

The synthesis of Au NPs followed the standard citrate reduction method. Briefly, 90 mg of HAuCl4 were dissolved in 500 ml of water. The solution was heated on a hot plate until boiling. Then 25ml of 0.1% sodium citrate aqueous solution was added to the gold salt solution. The mixture was stirred and reboiled on a hot plate. After 20 minutes, the solution became a red color, which indicated the formation of Au NPs. The Au NPs were concentrated 10X by centrifuging at 9000 rpm for 50 minute and removing 90% of the supernatant

5.3.4 Layer-by-Layer Assembly of Au NP film

LBL assembly was initially carried out on microscope glass slides cleaned in piranha solution overnight and then thoroughly rinsed with deionized water prior to use. For LBL assembly, a glass slide was immersed in 0.1 wt % solution of PDDA for 5 min, rinsed with DI water for 1 min, dried, and then immersed in concentrated Au

NP solution for 10 min, rinsed for 1 min, and dried again. The procedure was then repeated with PDDA and Au NP solution.

5.3.5 Electrode Fabrication

2μm ANF/epoxy nanocomposite was first deposited via spin-coating on a silicon wafer with 2 μm thermal oxide. The first layer of ANF/epoxy nanocomposite served as the bottom insulating layer for the electrodes. Then 100 nm Au NP nanocomposite was deposited on the ANF/epoxy layer by using the layer-by-layer (LBL) assembly method. After the Au NP composite deposition, positive photoresist (SPR220-3.0, Rohm Haas) was spin coated and exposed by the first mask on the gold composite. After developing the photoresist, the entire substrate was etched in gold etchant (Gold Etchant TFA, Transene Company, Inc.) for 20 seconds to pattern the base layer of the neural electrodes. After wet etching, a layer of chromium was deposited onto the base layer to protect the Au NP composite. Next, a second layer of ANF/epoxy composite was deposited. This served as the top insulating layer for the neural probe. Then, positive photoresist was spin-coated again and exposed by the second mask on top of the second layer of parylene-C. The entire substrate was etched in oxygen with 10% sulfur hexafluoride. The second mask created the outline for the final electrode shape and opened the functional Au NP sites at the tip of the electrodes. Lastly, copper wires were attached onto the electrodes by silver epoxy paste. The entire device was then released from the silicon wafer by hydrogen fluoride.

5.3.6 Scanning Electron Microscopy (SEM)

SEM images were obtained using a FEI Nova Nanolab SEM at a 10kV accelerating voltage. The samples were sputter coated with gold prior to SEM imaging.

5.3.7 Electrochemical Impedance Spectroscopy (EIS)

EIS was carried out on an Autolab PGSTAT 12. Frequency Response Analyzer software (EcoChemie, Utrecht, Netherlands) was used to record impedance spectra of the electrodes. A solution of 1 M phosphate buffered saline (PBS, pH = 7) was used as an electrolyte in a three-electrode configuration. The working electrode was connected to the electrode site. The counter electrode was connected to a gold foil immersed in PBS, and an Ag/AgCl reference electrode was immersed in PBS. An AC sinusoidal signal of 25 mV in amplitude was used to record the impedance over a frequency range of 10−32000 Hz.

5.3.8 Craniotomy Preparation

Adult male Sprague-Dawley rats (Charles River Laboratories) 550-600 g were anesthetized with 2% isoflurane and 1mg/ml ketamine. The depth of anesthesia was observed by monitoring heart rate and blood oxygen saturation. The animal was placed into a stereotaxic frame and a 2 mm-by-2 mm craniotomy was made over the visual cortex. Once the dura was incised and resected, the animal brain was ready for implantation.

5.3.9 *In-vivo* Electrophysiological Recording

Electrophysiological data was recorded using a TDT RX5 Pentusa Recording System (Tucker-Davis Technologies, Alachua, FL). These neuronal signals were acquired through a head-stage buffer amplifier to avoid signal loss in data transmission. Signals were sequentially filtered by an anti-aliasing filter in the preamplifier, digitized at a ~ 25-kHz sampling rate, and digitally band-pass filtered from 300 to 5000 Hz. Wideband signals were acquired to capture both spiking and local field potential (LFP) activity. Signals were continuously recorded for 3 seconds: a 1s at the initial off state, then a 1s during the drifting grating movie followed by a 1s long "black screen". Neural recording segments were analyzed offline using custom automated MATLAB (Mathworks Inc., MA) script.

5.4 Results and Discussion

The integration of Au NP nanocomposites and ANF/epoxy composites is essential for fabricating all composite electrodes. Therefore, we first evaluate the layer-by-layer (LBL) assembly of the Au NP composite on top of the ANF/epoxy composite. The LBL process relies on the charge interaction of material components. For Au NP nancomposites, we choose a biocompatible and positive polyelectrolyte, polydiallydimethylammonium chloride (PDDA), to pair with negative charged Au NP, which is stabilized with sodium citrate. The substrate for the LBL process should also have certain charge, in order to initiate the assembly process. We first create a six ANF/epoxy composite on a silicon wafer with 2 μm thermal oxide according to the established protocol. The epoxy resin in the ANF network would give the

composite negative charge on the surface. Therefore, we start our LBL process with PDDA as the first layer. The details of the LBL process is described in the Materials and Methods section. After 20 bilayers deposition, we first observe gold appearance on the ANF/epoxy substrate (Figure 6.1A). Four-point probe measurement shows electrical conductance of 10 Ohm. This result is very similar to previously reported values for Au NP nanocomposites.[42] To further confirm the successful deposition of the Au NP on the ANF/epoxy composite, the substrate is imaged by scanning electron microscopy. We observe a uniform and closely packed nanoparticle deposition on the substrate. This indicates that we can successfully deposit highly conductive Au NP composites on ANF/epoxy substrates.

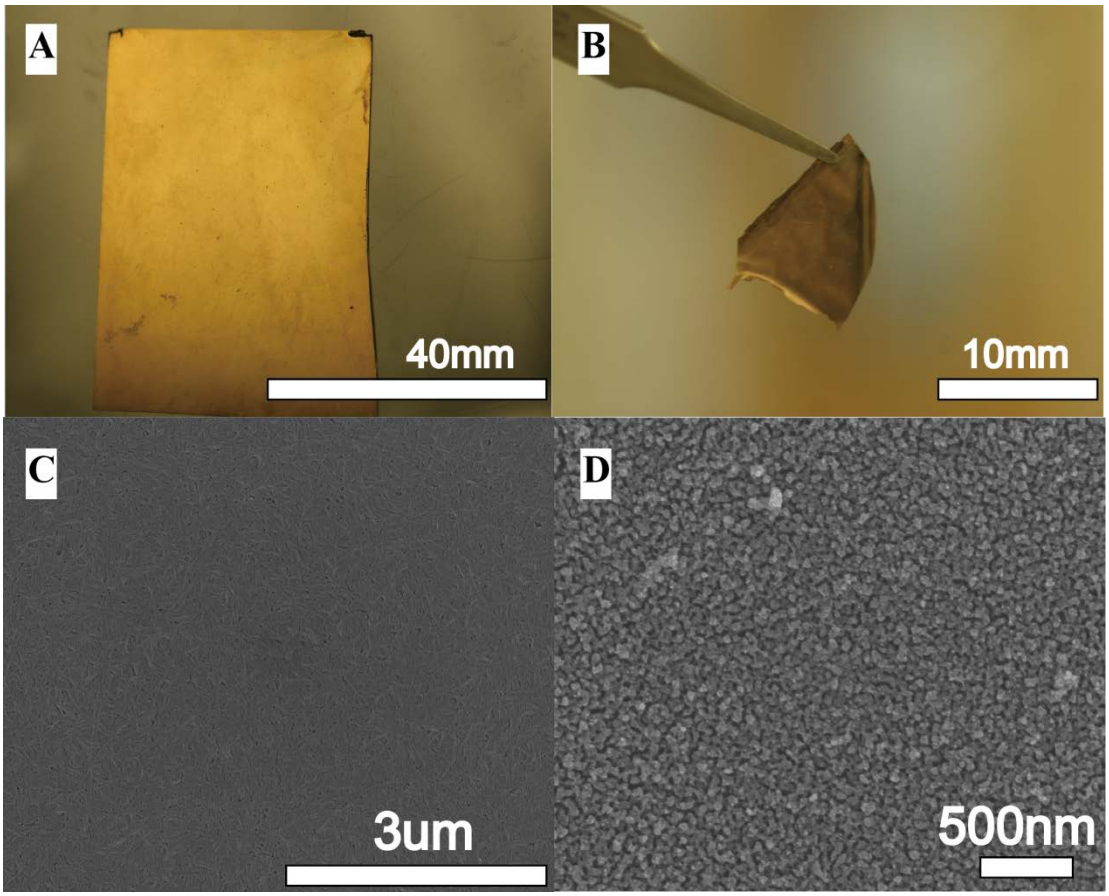

Figure 5.1 (A) Au NP LBL nanocomposites deposited on the ANF/epoxy layer (B) Free standing flexible composite material with ANF/epoxy and Au NP composite (C) SEM image of the ANF/epoxy composite prior to LBL assembly (D) SEM image of the ANF/epoxy composite after LBL assembly.

After confirming the successful deposition of the Au NP composites, we then consider the mechanical properties of the all-composite material. Mechanical properties of the electrode materials are important in preventing chronic tissue damage in the brain. In our previous mechanical force analysis,[36] we conclude that the Young's modulus of the electrode material should be below 3 GPa to mitigate the tissue damage induced by mechanical mismatch and brain micromotion. Therefore,

we should first assess the Young's modulus of the composite material. After deposition of gold nanocomposite, the entire substrate is soaked in 1% glutaraldyhyde for 1 hour to cross-link the Au NP composite. This process strengthens the interparticle connection in the composite, which is important for the microfabricaton process. After cross-linking, the entire ANF/epoxy composite with LBL-assembled nanoparticles is lifted off from the silicon substrate (Figure 6.1B). A mechanical tensile test is conducted to measure the Young's modulus of the composite (Figure 5.2). The Young's modulus of the composite is 2.8 GPa, which is suitable for electrode fabrication.

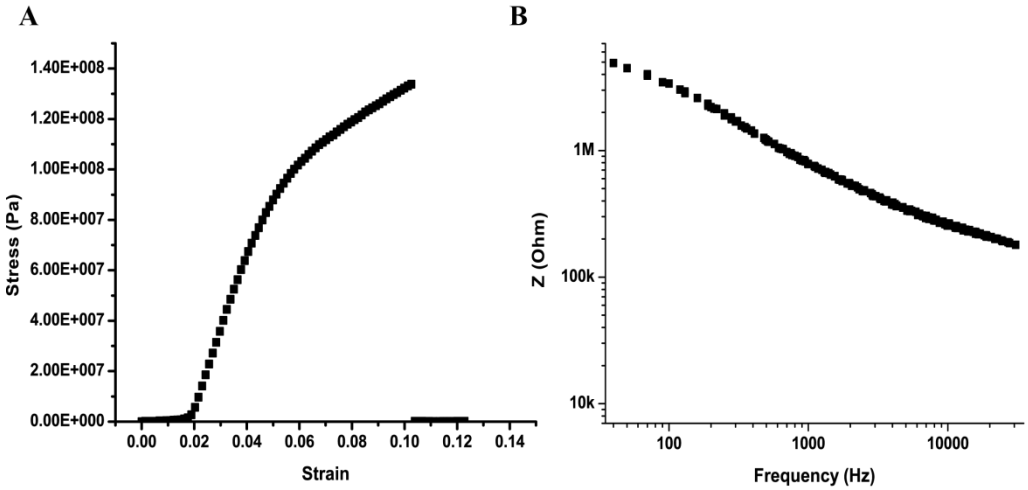

Figure 5.2 (A) Tensile test result of the all-composite electrode material (B) Magnitude of the impedance for typical as-fabricated electrodes.

The conductivity measurement and mechanical test demonstrate that this particular composite material is a promising platform to fabricate implantable electrodes. However, fabrication of this composite material requires special analysis to develop appropriate process protocol. First, both composite materials contain

organic components. ANF/epoxy composite is etched by oxygen plasma during the fabrication process. Regular gold film in traditional electrodes is not typically affected by the oxygen plasma process. In the case of composite electrodes, the electrically active material is the Au NP composite. Densely packed Au NPs are connected by thin polymer, which offers mechanical flexibility and high electrical conductivity. However, this Au NP composite will be affected by the high voltage oxygen plasma. We need to resolve the issue of non-selectivity during the oxygen plasma process. In this study, we applied a combination of etch stop and crosslink techniques to resolve this issue. The Au NP composite is first cross-linked to improve connectivity of the nanoparticle in the composite. Then we also use an additional layer of Cr to protect the nanocomposite from the oxygen plasma. The process protocol is described in detail in the Materials and Methods section.

By using this tailored fabrication process, we are able to produce high yield electrodes from the substrate. Figure 5.3B shows an all-composite electrode lifted off from the silicon substrate. In order to confirm the robustness of the Au NP composite, optical microscopy images are taken before and after the electrode liftoff process from the silicon substrate (Figure 5.3C and Figure 5.3D). Compare to both images, we can conclude that there is no delamination or cracking of the Au NP composite.

Prior to *in vivo* study, the electrochemical performance of the electrodes are evaluated to verify their functionality. Electrochemical impedance of the electrodes provides information related to the efficiency of the tissue/electrode interface. The typical impedance requirement for recording electrodes is about 1Mohm. The impedance of the as-fabricated electrodes is measured by a frequency analyzer from

10Hz to 32 kHz (Figure 5.2B). We observed the impedance value at 1kHz to be about 0.78 Mohm±0.2. This indicates that our electrodes have the appropriate electrochemical characteristics for *in vivo* recording.

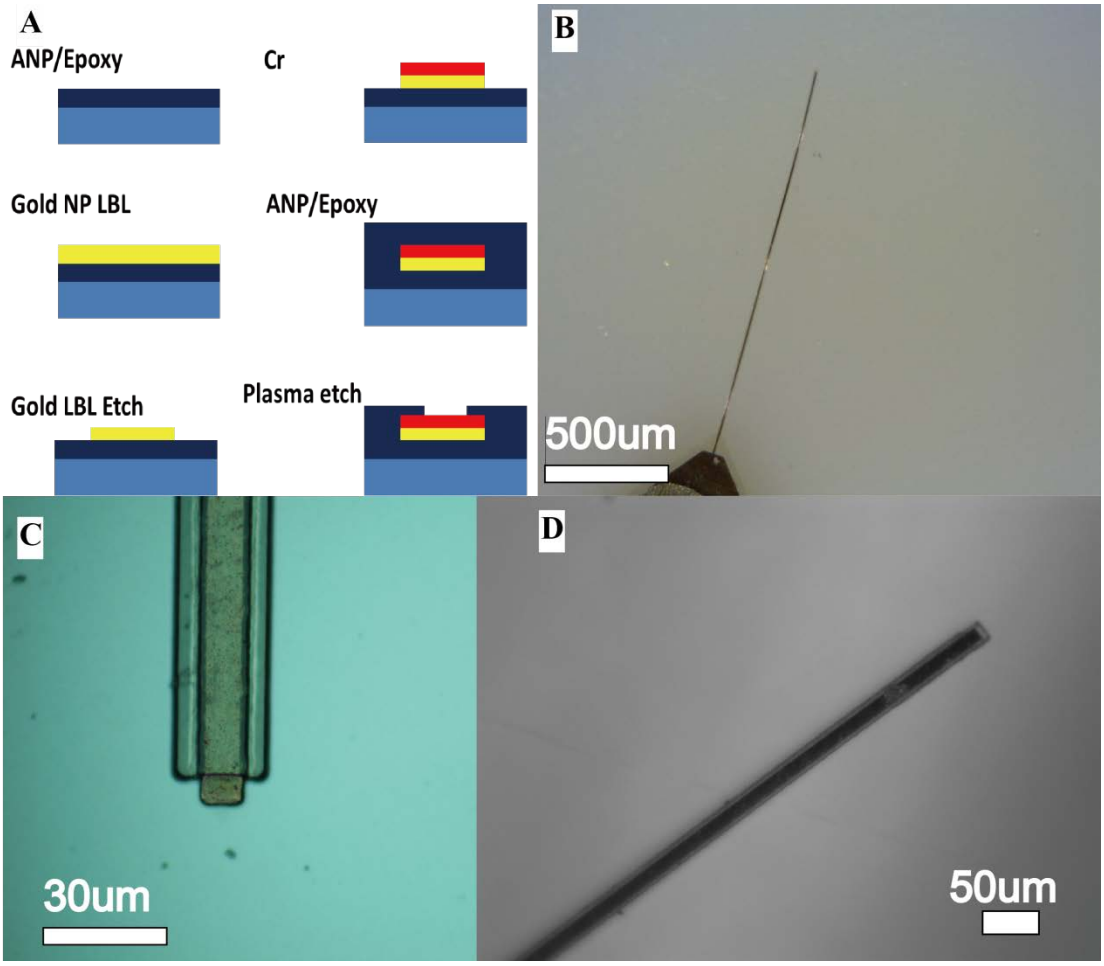

Figure 5.3 (A) Schematic of the fabrication process (B) Photography of an all-composite electrode (C) The tip of an all-composite electrode before liftoff (D) The tip of an all-composite electrode after liftoff , while suspended in water

After successful fabrication and characterization of all nanocomposite electrodes, we verify the electrode functionality *in vivo* The electrode is inserted by a shuttle method to the visual cortex described in previous work.[36] The electrode is

implanted in the right hemisphere. The stimulus is a drifting black and white grating movie. We first record 1s blank, then recorded while played 1s long drifting grating movie to stimulate the visual cortex (ON state), followed by 1s recording of the movie off (OFF state). The raw spike stream is shown in Figure 5.4A. We observe higher spike intensity during the ON state than the OFF state. In addition, we also plot a perstimulus time histogram to account the average threshold crossing during ON/OFF state. As shown in Figure 5.4B, we observe much higher average threshold crossing during the On state than the OFF state. These indicate that we indeed can utilize all composite electrodes to record neural signal.

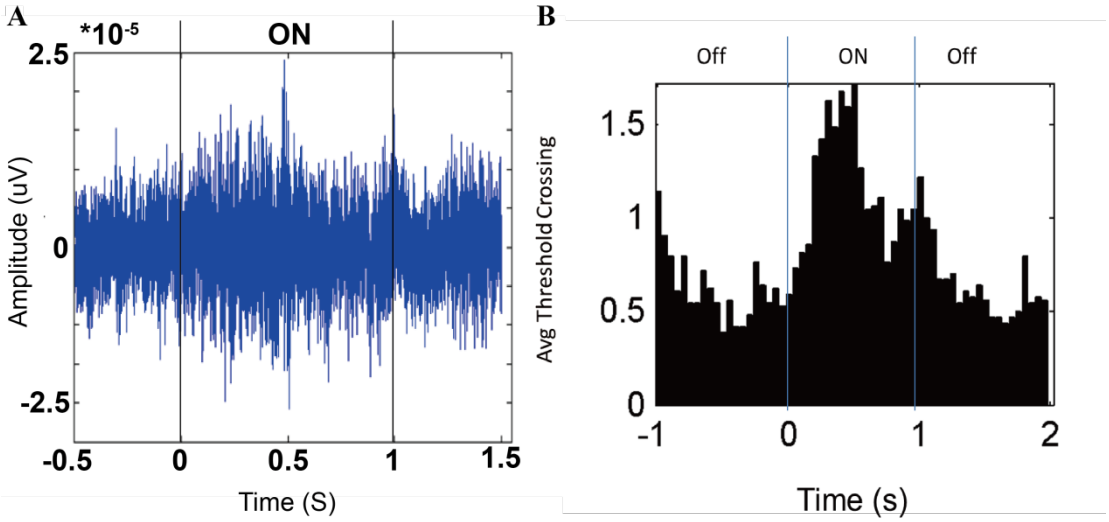

Figure 5.4 Visual cortex stimulus recording (A) Raw spike stream of on/off state, band pass filtered from 300 Hz to 5000 Hz (B) Peristimulus time histogram of the visual cortex during stimulus recording

5.5 Conclusion

The next generation of neural prosthetic devices requires mechanically flexible materials with outstanding electrochemical performance to mitigate chronic inflammation and tissue damage. Besides reduction of chronic inflammation, implantable devices also need biocompatible and strongly adhesive insulating material to maintain long term functionality under physiological conditions. This research combines two composite materials that have demonstratedthe appropriate properties necessary for neural prosthetic devices. We design a specific process to integrate these two materials. Due to the successful integration of these two nanocomposites, we can successfully fabricate functional electrodes with required electrochemical performance for neural recording. The functionality of the electrodes is further validated by *in vivo* acute recording experimentation. This study demonstrates the possibility to utilize nanocomposites for all aspects of neural electrodes. Further study related to chronic neural recording and histology are necessary to establish the efficacy of these new types of neural electrodes.

5.6 References

1. Banks, D., Neurotechnology. *Engineering Science and Education Journal* 1998, 7, 135-144.

2. Barinaga, M., Turning Thoughts into Actions. *Science* 1999, 286, 888-90.

3. Kotov, N. A.; Winter, J. O.; Clements, I. P.; Jan, E.; Timko, B. P.; Campidelli, S.; Pathak, S.; Mazzatenta, A.; Lieber, C. M.; Prato, M.; Bellamkonda, R. V.; Silva, G.

A.; Kam, N. W. S.; Patolsky, F.; Ballerini, L., Nanomaterials for Neural Interfaces. *Adv Mater* 2009, 21, 3970-4004.

4. Schwartz, A. B., Cortical Neural Prosthetics. *Annual review of neuroscience* 2004, 27, 487-507.

5. Cogan, S. F., Neural Stimulation and Recording Electrodes. *Annu. Rev. Biomed. Eng.* 2008, 10, 275-309.

6. Hatsopoulos, N. G.; Donoghue, J. P., The Science of Neural Interface Systems. *Annual review of neuroscience* 2009, 32, 249-66.

7. Velliste, M.; Perel, S.; Spalding, M. C.; Whitford, A. S.; Schwartz, A. B., Cortical Control of a Prosthetic Arm for Self-Feeding. *Nature* 2008, 453, 1098-101.

8. Collinger, J. L.; Wodlinger, B.; Downey, J. E.; Wang, W.; Tyler-Kabara, E. C.; Weber, D. J.; McMorland, A. J.; Velliste, M.; Boninger, M. L.; Schwartz, A. B., High-Performance Neuroprosthetic Control by an Individual with Tetraplegia. *Lancet* 2013, 381, 557-64.

9. Hochberg, L. R.; Serruya, M. D.; Friehs, G. M.; Mukand, J. A.; Saleh, M.; Caplan, A. H.; Branner, A.; Chen, D.; Penn, R. D.; Donoghue, J. P., Neuronal Ensemble Control of Prosthetic Devices by a Human with Tetraplegia. *Nature* 2006, 442, 164-71.

10. Polikov, V. S.; Tresco, P. A.; Reichert, W. M., Response of Brain Tissue to Chronically Implanted Neural Electrodes. *J Neurosci Meth* 2005, 148, 1-18.

11. Nicolelis, M. A.; Dimitrov, D.; Carmena, J. M.; Crist, R.; Lehew, G.; Kralik, J. D.; Wise, S. P., Chronic, Multisite, Multielectrode Recordings in Macaque Monkeys.

Proceedings of the National Academy of Sciences of the United States of America 2003, 100, 11041-6.

12. Wessberg, J.; Stambaugh, C. R.; Kralik, J. D.; Beck, P. D.; Laubach, M.; Chapin, J. K.; Kim, J.; Biggs, S. J.; Srinivasan, M. A.; Nicolelis, M. A., Real-Time Prediction of Hand Trajectory by Ensembles of Cortical Neurons in Primates. *Nature* 2000, 408, 361-5.

13. Laubach, M.; Wessberg, J.; Nicolelis, M. A. L., Cortical Ensemble Activity Increasingly Predicts Behaviour Outcomes During Learning of a Motor Task. *Nature* 2000, 405, 567-571.

14. Keefer, E. W.; Botternan, B.; Romero, M. I.; Rossi, A. F.; Gross, G. W., Carbon Nanotube Coating Improves Neuronal Recordings. *Nat Nanotechnol* 2008, 3, 434-439.

15. Wise, K. D.; Angell, J. B., A Low-Capacitance Multielectrode Probe for Use in Extracellular Neurophysiology. *Biomedical Engineering, IEEE Transactions on* 1975, BME-22, 212-219.

16. Wise, K. D.; Angell, J. B.; Starr, A., An Integrated-Circuit Approach to Extracellular Microelectrodes. *Biomedical Engineering, IEEE Transactions on* 1970, BME-17, 238-247.

17. Campbell, P. K.; Jones, K. E.; Huber, R. J.; Horch, K. W.; Normann, R. A., A Silicon-Based, Three-Dimensional Neural Interface: Manufacturing Processes for an Intracortical Electrode Array. *IEEE transactions on bio-medical engineering* 1991, 38, 758-68.

18. Maynard, E. M.; Nordhausen, C. T.; Normann, R. A., The Utah Intracortical Electrode Array: A Recording Structure for Potential Brain-Computer Interfaces. *Electroencephalography and clinical neurophysiology* 1997, 102, 228-39.

19. Wise, K. D.; Anderson, D. J.; Hetke, J. F.; Kipke, D. R.; Najafi, K., Wireless Implantable Microsystems: High-Density Electronic Interfaces to the Nervous System. *Proc. IEEE.* 2004, 92, 76-97.

20. Kim, S.; Bhandari, R.; Klein, M.; Negi, S.; Rieth, L.; Tathireddy, P.; Toepper, M.; Oppermann, H.; Solzbacher, F., Integrated Wireless Neural Interface Based on the Utah Electrode Array. *Biomedical microdevices* 2009, 11, 453-66.

21. Najafi, K.; Wise, K. D., An Implantable Multielectrode Array with on-Chip Signal-Processing. *Ieee J Solid-St Circ* 1986, 21, 1035-1044.

22. Subbaroyan, J.; Martin David, C.; Kipke Daryl, R., A Finite-Element Model of the Mechanical Effects of Implantable Microelectrodes in the Cerebral Cortex. *J Neural Eng.* 2005, 2, 103-13.

23. Gilletti, A.; Muthuswamy, J., Brain Micromotion around Implants in the Rodent Somatosensory Cortex. *Journal of neural engineering* 2006, 3, 189-95.

24. Lee, H.; Bellamkonda, R. V.; Sun, W.; Levenston, M. E., Biomechanical Analysis of Silicon Microelectrode-Induced Strain in the Brain. *Journal of neural engineering* 2005, 2, 81-9.

25. Subbaroyan, J.; Kipke, D. R., The Role of Flexible Polymer Interconnects in Chronic Tissue Response Induced by Intracortical Microelectrodes - a Modeling and an in Vivo Study. *2006 28th Annual International Conference of the IEEE Engineering in Medicine and Biology Society, Vols 1-15* 2006, 5782-5785.

26. Seymour, J. P.; Kipke, D. R., Neural Probe Design for Reduced Tissue Encapsulation in Cns. *Biomaterials* 2007, 28, 3594-3607.

27. Henze, D. A.; Borhegyi, Z.; Csicsvari, J.; Mamiya, A.; Harris, K. D.; Buzsaki, G., Intracellular Features Predicted by Extracellular Recordings in the Hippocampus in Vivo. *J Neurophysiol* 2000, 84, 390-400.

28. Boppart, S. A.; Wheeler, B. C.; Wallace, C. S., A Flexible Perforated Microelectrode Array for Extended Neural Recordings. *IEEE transactions on bio-medical engineering* 1992, 39, 37-42.

29. Fan, W.; Maesoon, I.; Euisik, Y. In *A Flexible Fish-Bone-Shaped Neural Probe Strengthened by Biodegradable Silk Coating for Enhanced Biocompatibility*, Solid-State Sensors, Actuators and Microsystems Conference (TRANSDUCERS), 2011 16th International, 5-9 June 2011; 2011; pp 966-969.

30. Greenberg, R. J.; Talbot, N. H.; Neysmith, J.; Little, J. S.; Mech, B. V.; Humayun, M.; Guven, D.; Ripley, A. M. D. M. Flexible Circuit Electrode Array for Neural Stimulation. 2006-413689

2006259112, 20060428., 2006.

31. Rousche, P. J.; Pellinen, D. S.; Pivin, D. P.; Williams, J. C.; Vetter, R. J.; Kipke, D. R., Flexible Polyimide-Based Intracortical Electrode Arrays with Bioactive Capability. *Ieee T Bio-Med Eng* 2001, 48, 361-371.

32. Seymour J., P.; Kipke D., R., Fabrication of Polymer Neural Probes with Sub-Cellular Features for Reduced Tissue Encapsulation. *Conference proceedings : ... Annual International Conference of the IEEE Engineering in Medicine and Biology*

Society. IEEE Engineering in Medicine and Biology Society. Conference 2006, 1, 4606-9.

33. Stieglitz, T., Hansjorg, B., Schuettler, M. and Meyer, J.-U, Micromachined, Polyimide-Based Devices for Flexible Neural Interfaces. *Biomedical microdevices* 2000, 2, 283-294.

34. Kim, Y.; Zhu, J.; Yeom, B.; Di Prima, M.; Su, X.; Kim, J. G.; Yoo, S. J.; Uher, C.; Kotov, N. A., Stretchable Nanoparticle Conductors with Self-Organized Conductive Pathways. *Nature* 2013, 500, 59-63.

35. Jan, E.; Hendricks, J. L.; Husaini, V.; Richardson-Burns, S. M.; Sereno, A.; Martin, D. C.; Kotov, N. A., Layered Carbon Nanotube-Polyelectrolyte Electrodes Outperform Traditional Neural Interface Materials. *Nano Lett* 2009, 9, 4012-8.

36. Zhang, H.; Patel, P. R.; Xie, Z.; Swanson, S. D.; Wang, X.; Kotov, N. A., Tissue-Compliant Neural Implants from Microfabricated Carbon Nanotube Multilayer Composite. *Acs Nano* 2013.

37. Zhang, H.; Shih, J.; Zhu, J.; Kotov, N. A., Layered Nanocomposites from Gold Nanoparticles for Neural Prosthetic Devices. *Nano Lett* 2012, 12, 3391-8.

38. Seymour, J. P.; Elkasabi, Y. M.; Chen, H. Y.; Lahann, J.; Kipke, D. R., The Insulation Performance of Reactive Parylene Films in Implantable Electronic Devices. *Biomaterials* 2009, 30, 6158-67.

39. Yasuda, H.; Yu, Q. S.; Chen, M., Interfacial Factors in Corrosion Protection: An Eis Study of Model Systems. *Prog Org Coat* 2001, 41, 273-279.

40. Yamagishi, F. G., Investigation of Plasma-Polymerized Films as Primers for Parylene-C Coatings on Neural Prosthesis Materials. *Thin Solid Films* 1991, 202, 39-50.

41. Sharma, A. K.; Yasuda, H., Effect of Glow-Discharge Treatment of Substrates on Parylene-Substrate Adhesion. *J Vac Sci Technol* 1982, 21, 994-998.

42. Zhang, H.; Shih, J.; Zhu, J.; Kotov, N. A., Layered Nanocomposites from Gold Nanoparticles for Neural Prosthetic Devices. *Nano Lett* 2012, 12, 3391-3398.

Chapter 6

Conclusion and Future Directions

6.1 Conclusion

Failure of the chronically implanted neural electrodes imposes tremendous challenges for the progress of brain computer interface. Designing neural electrodes with chronic functionality has been one of the important objectives in neural engineering. The current neural electrode materials contribute enormously to the device failure. This dissertation systematically evaluated different material aspects of the implantable neural electrodes, such as the electrical active components and insulation components. After careful evaluation, we rationally designed nanocomposite materials that have significant advantages over the traditional materials for implantable neural electrodes. This research focused on both the performance and the process ability of nanocomposites for neural interface

applicatons. These nanostructured materials are not only outperforming traditional materials in many benchmark evaluations, but also can be directly integrated into the established processing protocols. By investigating both material design and material processing, this dissertation demonstrated the feasibility of functional implantable neural electrodes based on nanocomposite. These developments in nanocomposite open new opportunities for chronic functional neural prosthetic devices.

In Chapter 2, we developed tissue compliant neural prosthetic devices based on carbon nanotube nanocomposite. We first assessed the material requirements for mechanically compliant neural electrodes. Based on our evaluation, we purposefully designed a flexible and conductive nanocomposite that is suitable for tissue compliant neural electrode. Furthermore, we established a process procedure for this carbon nanotube composite to construct neural electrodes by microfabrication technology. The functionality of the nanocomposite electrodes was validated *in vivo*

In Chapter 3, we examined the details of the electrode/tissue interface, specifically the interfacial electrochemical performance. Based on the existing knowledge on carbon nanotube nanocomposite, we designed gold nanoparticle nanocomposite that outperformed existing carbon nanotube composite in term of bulk electrical conductivity and interfacial electrochemical parameters (impedance and charge storage capacity). Additionally, the stability of the material is also comparable to carbon nanotube composite. This indicated that gold nanocomposite is a promising new material for the next generation neural prosthetic devices.

In Chapter 4, we investigated insulation material for implantable neural electrodes. Delamination of the insulation materials has been one of the major causes for device failure. Parylene, a commonly used insulation material has known issues with metal adhesion and interfacial adhesion. We developed a nanocomposite approach to create high adhesion material based on aramid nanofiber and Epoxy resin. The aramid nanofiber/Epoxy composite demonstrated superior adhesion and outstand biocompatibility.

Lastly, in Chapter 5, we designed and fabricated all nanocomposite electrodes based on our previous research on gold nanoparticle composite and aramind naofiber/epoxy composite. A specific microfabrication process was developed to tailor the specific process requirement for both composites. Our results showed that both composites can be integrated together to fabricate neural electrodes after fine tuning the process parameters. We demonstrated the possibility of combining both excellent electrochemical properties of gold nanoparticles composite and superior adhesion of ANF/Epoxy composite to fabricate tissue compliant and functional neural electrodes.

In conclusion, this dissertation is devoted to develop next generation neural prosthetic devices from nanocomposites. We first gain understanding of the material requirements for implantable neural electrodes. From the detailed material analysis, we utilized LbL assembly method to tailored the material properties of the nanocomposites, specifically for implantable neural prosthetic devices. After

material development, we also investigated the integration of these nanocomposites into fully functional devices.

6.2 Future Directions

In this dissertation, we established the concept of nanocomposite material design for neural prosthetic devices. The material design principles for nanocomposite based neural prosthetics in this dissertation are derived from the accumulative knowledge of many previous chronic inflammation studies. Chronic inflammation studies of brain tissue near implanted electrodes suggested that mechanically flexible and small footprint neural electrodes have the potential to establish a chronic neural interface. Additionally, studies also showed that better insulation adhesion improves the device lifetime. Therefore, the primary focus of this dissertation is design and fabrication of the nanocomposite materials for neural prosthetic devices from the existing knowledge. The advantages of these devices are demonstrated through material characterization techniques and quantitative benchmark tests. For the purpose of proof-of-concept, the device functionality was validated through *in vivo* acute recording studies. Based on this conceptual investigation, this dissertation built the foundation for numerous in-depth studies in the field of material and neural engineering.

Although we have created the design framework of the nanocomposite electrodes, many other aspects of the nanocomposite electrodes are still unexplored.

Frist of all, Chronic *in vivo* recording studies and histology studies are necessary to further demonstrate the clinical relevance of the nanocomposite devices. Chronic *in vivo* recording studies are essential to establish the recording ability of the nanocomposite. A comparison study of nanocomposite and silicon electrode can provide further support for the development of nanocomposite electrodes. Additionally, the biological response to nanocomposite electrodes has not yet been studied. Nanocomposite materials could have undiscovered tissue responses in the brain. Histology of chronically implanted nanocomposite are necessary to understand the tissue response of the nanocomposite electrodes. Furthermore, the inflammation reduction of the flexible nanocomposite electrode also should be validated by histology study of the inflammation process.

Besides further understanding of the chronic recording ability and tissue response, future developments in electrode design and fabrication would be important for nanocomposite multi-electrode array. In this dissertation, nanocomposites have only been fabricated into single electrode so far. Advanced applications for brain computer interface require multi-electrode arrays to record a large number of neurons in different regions of the neural tissue. The process protocol and design layout should be further refined to produce multi-electrode arrays. Fabrication of the nanocomposite arrays and validation of their functionality will be the next logic step for nanocomposite electrodes.

The major advantage of nanocmposite compared to traditional metal and silicon elecrodes is the mechanical compliance. According to previous histology study and mechanical analysis, mechanical compliance is the key factor to mitigate chronic tissue response to the electrodes. However, the mechanical compliance of the nanocomposite electrode imposes a significant challenge in term of the implantation techniques. Traditional rigid materials, like silicon can be directly inserted into the brain tissue. The mechanically compliant electrodes require additional strategies to assist the implantation. The versatility and robustness of the implantation techniques ultimately determines the clinical relevance of the tissue compliant neural electrodes. In this dissertation, we developed a shuttle method with interfacial water to deliver the nanocomposite electrodes to the brain. It is a robust technique for fundamental research. Nevertheless, further engineering development of the implantation system are needed to minimize the insertion injuries and increase the robustness of the implantation procedure.